THE PROPERTIES OF INTRINSICALLY LIGHT SENSITIVE RAT RETINAL GANGLION CELLS THAT PROJECT TO THE SUPRACHIASMATIC NUCLEUS

By Erin J. Warren

A DISSERTATION

Presented to the Neuroscience Graduate Program

and the Oregon Health & Science University

School Of Medicine

in partial fulfillment of the requirements for the degree of

Doctor of Philosophy

August 2005

School of Medicine

Oregon Health & Science University

CERTIFICATE OF APPROVAL

This is to certify that the Ph.D. dissertation of

Erin J. Warren

has been approved

(David W. Robinson)

Mentor

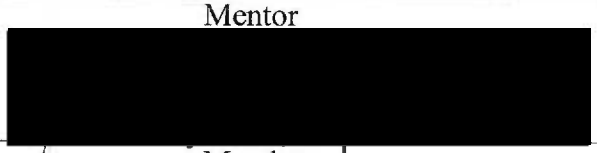

(Charles N. Allen)

Member

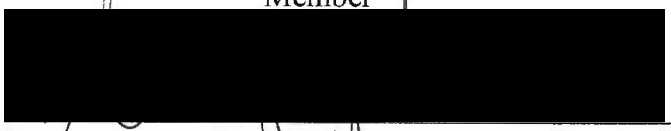

(Peter Gillespie)

Member

(Craig E. Jahr)

Member/Chairperson

(John T. Williams)

Member

TABLE OF CONTENTS

ACKNOWLEDGMENTS iii

WRITINGS INSPIRED BY SCN-PROJECTING RGCS v

LIST OF FIGURES vi

ABSTRACT viii

CHAPTER 1 General Introduction 1

Circadian rhythms 2

The SCN is the Site of the Clock 4

SCN connectivity 6

Molecular Clock Components 12

Entrainment 21

Cellular Mechanisms of Photoentrainment in the SCN 30

Photoreception: Visual and Circadian 37

Course of Thesis 50

CHAPTER 2 Intrinsic Light Responses of Retinal Ganglion Cells Projecting to the Circadian System 51

Abstract 53

Introduction 54

Methods 56

Stereotaxic Injection of Fluorescent Retrograde Tracers 56

Electrophysiology 57

Light Stimulation 58

Morphological Analysis 58

Statistical Analysis 61

Results 61

Morphology of SCN-Projecting RGCs 61

Intrinsic Membrane Properties of SCN-Projecting RGCs 63

Intrinsic Light Responses of SCN-Projecting RGCs 64

Characteristics of the light-activated current in SCN-Projecting RGCs 65

Discussion 67

CHAPTER 3 The Light-Activated Signaling Pathway in SCN-Projecting Retinal Ganglion Cells..... 80

Abstract..... 82

Introduction..... 83

Methods..... 84

Stereotaxic Injection of Fluorescent Retrograde Tracers..... 84

Electrophysiology..... 85

Light Stimulation..... 86

Statistics..... 86

Results..... 87

Light Response of SCN-Projecting RGCs in Voltage-Clamp..... 87

Role of G Proteins..... 88

Potential Role of CNG Channels..... 89

Role of Divalent Ions..... 91

Potential Role of TRP Channels..... 93

Discussion..... 95

CNG Channels do not Mediate the LAC..... 96

Sensitivity of the LAC to Cations..... 96

Evidence that TRP Channels Mediate the LAC..... 97

Closing Remarks..... 100

CHAPTER 4 Conclusions..... 108

A Unique Class of RGC..... 109

Physiology of SCN-Projecting RGCs..... 111

A Role for TRP Channels..... 115

REFERENCES 121

ACKNOWLEDGMENTS

There are many people (and creatures) to whom I am indebted for their academic guidance during the course of this project, for their encouragement when the technical challenges were frustrating, for their friendship during my stay in Portland, and for great humor that helped me keep my perspective (a couple examples of which are printed below).

Of course first to thank is Dr. David Robinson who has been an excellent advisor to me. In particular I am grateful for his patience and support, especially at the outset of this project when my progress was slow. I also thank Drs. Chuck Allen and Lane Brown whose suggestions and insights have helped direct this work. I thank Dr. Bill Cameron in whose lab space I worked for the first two years of my graduate studies, and whose equipment and expertise were used for the anatomical reconstructions of the cells that I studied. I also would like to thank all of the members of Dr. Allen's lab who graciously gave me bench and lab space for the last two years.

On a personal note, I would like to recognize Ret Beadnall, who was my neighbor and first true friend in Portland. I would also like to thank my dear friend Sally Aboelela who graduated from the lab two years before me, as well as fellow students Mary McKenzie and Court Hull, and postdoctoral fellows Tim Bailey, Ken Tovar, and Jorge Alberto Perez-Leon. I am grateful to the most recent addition to our lab, graduate student Linda Ruggiero, for her humor and friendship during the last few months.

I would like to thank my sister Michele who is my biggest supporter and best friend and her four terrific kids, the youngest of whom (Jordan) just wished me good luck on my "self-defense." My mom and dad deserve many thanks for their unconditional

support. While not human, I would nonetheless like to acknowledge two other members of my family, Bernard and Sophie, for their companionship. And I would like to acknowledge the animals that were used in these studies.

WRITINGS INSPIRED BY SCN-PROJECTING RGCS

There once was a cell in the eye,
Which was labeled with a dextran dye.
When I'd shine the light,
The cell would excite,
When it didn't I'd go home and cry.

There once was a girl named Erin,
Who spent half the day swearin'.
Oh how she hated to write,
Until one summer night,
She went home and finally stopped
Carin'!

Poems by Linda Ruggiero

A Translation and Transcription of an Intergenerational Oral Communication with Marked Periodicity of Vocal Formant and Peak Volume

By Eric Reid

A small sample (n<4) of retinally degenerate mutant *Mus musculus*,
A triad of enucleated diminutive domiciliary rodents,
Visually observe the manner in which they demonstrate their capacity for rapid quadrapedal kinesis,
Repeat observation of gait in subject group.

The entire sample population demonstrated capability of vigorous autolocomotion in pursuit of the spouse of a heterosexual male agriculturist. This married female performed a successful flagelectomy (removal of the caudal appendage) on the subject group using an instrument intended for the preparation of food (Goose et al., a long time ago).

Has the reader ever observed a phenomenon similar to a tripartite murine sample group with severe ocular impairment?

1. Goose, M., Grad Student A, Grad Student B. (a long time ago)
Pediatric insomnia treated with repetition of familiar word patterns.
J. Bedside Manner (123:456-789).

LIST OF FIGURES

CHAPTER 1:

Figure 1	Body temperature records of a golden hamster	3
Figure 2	Seasonal rhythms in leutenizing hormone surges in the ewe	4
Figure 3	The suprachiasmatic nuclei (SCN) of the hypothalamus	4
Figure 4	Pathways to/from the SCN	10
Figure 5	Properties of membrane potential oscillations in the SCN	12
Figure 6	Attached-X female *Drosophila* mating	13
Figure 7	*Per 2* message in the wild type mouse SCN displays a Diurnal rhythm with peak message at CT 16	14
Figure 8	A two-loop model for the *Drosophila* clock	17
Figure 9	Mammalian circadian clock-work model	20
Figure 10	Idealized actograph	23
Figure 11	Light pulses in the early and late subjective night induce phase delays and phase advances, respectively	25
Figure 12	Constructing a phase-response curve (PRC) for light	26
Figure 13	Phase-response curves for glutamate applied to the SCN and light in the rat	27
Figure 14	Phase-response curve for melatonin	28
Figure 15	Polysynaptic pathway regulating melatonin secretion from the retina to the pineal gland via the SCN	35
Figure 16	Adrenergic input to the pinealocyte induces melatonin synthesis	36
Figure 17	The photoreceptive net in the mouse inner retina	41
Figure 18	β-galactosidase and melanopsin expression in mice with *tau-lacZ* insertions into the melanopsin gene locus	42
Figure 19	Attenuated circadian light input in *Opn4 -/-* mice	46

Figure 20 Irradiance-response relations for the pupil reflex..... 47

Figure 21 Normal retinal morphology and presence and central connectivity of melanopsin-expressing RGCs in triple knockout (*Opn4 -/- Gnat -/- Cnga3 -/-*) mice..... 49

CHAPTER 2:

Figure 1 Retrograde labeling of RGCs following stereotaxic injection of the SCN..... 74

Figure 2 Morphology of SCN-projecting neurons..... 75

Figure 3 Spiking patterns of SCN-projecting RGCs..... 76

Figure 4 Intrinsic light responses of SCN-projecting RGCs..... 77

Figure 5 Current-voltage relation of the light-activated current..... 78

Figure 6 The light-activated current is insensitive to replacement of extracellular Na^+..... 79

CHAPTER 3:

Figure 1 Intrinsic and synaptically-driven light responses from RGCs held at -60 mV.....101

Figure 2 The intrinsic light response is G-protein dependent..... 102

Figure 3 Cyclic nucleotides modulate the light response but do not gate the light-activated channel..... 103

Figure 4 CNG channel blockers do not block the light-activated Channel..... 104

Figure 5 Divalent ions modulate the light-activated current..... 105

Figure 6 TRP channel antagonists block the intrinsic light response.. 106

Figure 7 OAG potentiated the intrinsic light response in a PKC-dependent manner..... 107

ABSTRACT

In mammals, circadian oscillations in metabolic, physiological and behavioral processes are driven by the central light-entrainable clock in the suprachiasmatic nuclei (SCN) of the hypothalamus. The sensory cells from which afferent photic input to the SCN arises are a minority of retinal ganglion cells (RGCs) referred to hereafter as SCN-projecting RGCs. Increased interest in their physiology and function followed after the recent discovery that a novel retinal photopigment, melanopsin, is expressed by them. As SCN-projecting RGCs gate the transmission of light input to the circadian clock, their physiology bears importantly on how general luminance information is coded and transmitted to the SCN.

The aim of this work was to investigate the intrinsic and excitable membrane properties of these neurons that might influence their response properties, and to characterize both the intrinsic light response and the signaling pathways underlying it. SCN-projecting RGCs were retrogradely-labeled by unilateral stereotaxic injection of a fluorescent dextran dye into the rat SCN. Whole-cell current-clamp, voltage-clamp, and perforated-patch recordings were made from labeled neurons in the retinal whole mount. I examined the intrinsic membrane properties of SCN-projecting RGCs and report their input resistance and resting potential are similar those of RGCs projecting to the visual system. Compared to type I and type II RGCs, however, they display strikingly few synaptic post-synaptic potentials and action potentials at rest. SCN-projecting RGCs respond to current injections with single or intermittent spikes that do not increase monotonically with steps in depolarization.

The first voltage-clamp recordings of the intrinsic light response are reported in this study. Light activates the opening of ion channels that conduct a nonselective cationic current, via a G-protein dependent pathway. The current-voltage relationship of the light-activated current is nonlinear, and displays no net current flow between ~ -10 mV and ~ +40 mV. In contrast to light responses reported in rod and cone photoreceptors, the light-activated current (LAC) in SCN-projecting RGC is slow to activate with a latency that is inversely proportional to the intensity of the light stimulus. While the current inactivates during prolonged light pulses, current-clamp recordings reveal that SCN-projecting RGCs can continue to fire low frequency action potentials for minutes after the light pulse.

To identify the ion channel(s) mediating the intrinsic light, I have conducted pharmacological studies focused on cyclic nucleotide gated (CNG) and transient receptor potential (TRP) channels, which mediate vertebrate and invertebrate rod phototransduction, respectively. The CNG channel antagonists pimozide, l-*cis*-diltiazem, and dichlorobenzamil failed to block the LAC in whole-cell voltage-clamp recordings. The nonspecific TRP channel blockers lanthanum, gadolinium, and ruthenium red either blocked or reduced the amplitude of the LAC. Several modulators of the LAC were identified, including intracellular magnesium and calcium, cyclic nucleotides, and1-oleoyl-2-acetyl-*sn*-glycerol (OAG), the potent analog of diacylglycerol that gates channels from the TRPC3/6/7 subfamily. Further study is required to determine which TRPC channel subtypes may mediate the intrinsic light response.

This work provides insight into how SCN-projecting RGCs transduce and code relevant photic input to the circadian system.

CHAPTER ONE

INTRODUCTION

INTRODUCTION

Circadian Rhythms

A diverse number of organisms - ranging from plants to primates - exhibit daily oscillations in physiological, metabolic, and behavioral processes. These oscillations are termed "circadian rhythms," derived from the Latin roots "circa" (about) and "dies" (day) because they are coordinated with the twenty-four hour period of the solar day. Just a few of the biological processes under the control of the circadian system include bioluminescence in cyanobacteria, photosynthetic respiration in plants, pupal eclosion in flies, and hormonal output in mammals (Dunlap 1999).

The circadian system has three key features that afford it the ability to keep time with the environment. The first is an endogenous clock that is capable of generating and maintaining rhythmic outputs to target tissues in the rest of the organism, even in the absence of external cues. The second is entrainability; external cues signaling the length and time of day set the clock so that its phase and the length of its period reflect those of the solar day. Entrainability affords the organism flexibility to dynamically synchronize its endogenous rhythms with changing environmental light cycles. The third feature is temperature compensation, which permits the clock to function reliably under varying thermal conditions. Temperature compensation is of particular importance for the maintenance of seasonal rhythms in hibernating animals that endure a wide range of temperatures throughout the year (Johnson et al., 2004).

There are different time scales by which the circadian system regulates the biological rhythms of an organism. In the short term, circadian clocks use daily environmental rhythms in photic cues (light) and nonphotic cues (for instance,

temperature) to fine-tune the period length and phase of the endogenous clock. Some of the overt circadian rhythms that cycle on such a scale in the mammal include plasma cortisol levels that surge in the morning, plasma melatonin levels that surge at night, and body temperature which peaks at night (Figure 1).

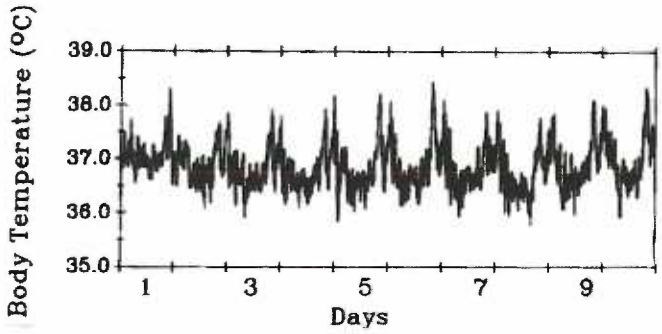

FIGURE 1

Body temperature records of a golden hamster.

Modified from Figure 5 (Refinetti 1995)

On a longer time scale, circadian clocks track seasonal changes in the environment to regulate rhythms in physiological processes over the course of a year. The best-studied examples of circannual rhythms are seasonal reproductive patterns in non-human mammals. When subjected to normal seasonal variation, estrous and breeding behaviors in hamsters will cycle such that females are fertile and receptive during the long warm days of summer while their reproductive axis is suppressed in the winter. The converse is true of sheep; short days of winter induce fertility and reproductive behaviors. Figure 2 shows the fluctuations in leutinizing hormone (LH) in untreated ewes over four years. The ewe is fertile during the winter months as evidenced by a rise in LH levels between September and February.

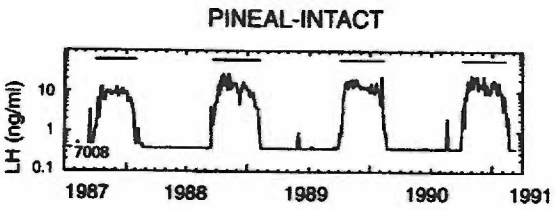

FIGURE 2

Seasonal Rhythms in leutenizing hormone surges in the ewe.

Representative patterns of serum leutenizing hormone (LH, on logarithmic scale) in a control ewe. High LH stages indicative of the breeding season began in September and lasted 4.5 mo, whereas low LH stages began in February and lasted -7.5 mo. Modified from Figure 3 (Woodfill et al., 1994) .

The SCN is the site of the clock

In the mammalian nervous system, the master circadian clock is contained in the bilateral suprachiasmatic nuclei (SCN) of the anteroventral hypothalamus. The pear shaped nuclei sit on either side of the third ventricle, dorsal to the optic chiasm (Figure 3). In the rat, each SCN is comprised of approximately 6,000-8,000 parvocellular neurons (Guldner 1983; van den Pol 1980).

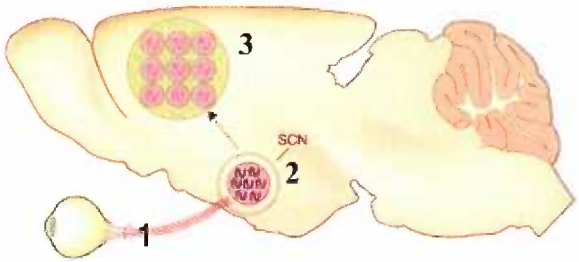

FIGURE 3

The Suprachiamatic Nuclei (SCN) of the hypothalamus.

(Left) A coronal section of rat brain through the rostral hypothalamus. The SCN lie on either side of the third ventricle dorsal to fibers of the optic chiasm. (Right) Saggital schematic of the mammalian brain emphasizing (1) direct retinal input to the SCN, (2) the intrinsic oscillatory behavior of SCN neurons, and (3) the ability of the SCN to drive rhythms in target tissues elsewhere in the CNS. Modified from Figure 1 (Reppert and Weaver 2002).

The discovery of a retinal projection to the SCN first focused attention on this locus as a potential site for the biological clock (Moore and Lenn 1972b). Subsequent lesion studies supported the hypothesis that the central clock was contained in the SCN by demonstrating arrhythmic locomotor and drinking behaviors in rats with SCN ablations (Moore and Eichler 1972; Stephan and Zucker 1972). An *in vivo* study carried out by Inouye and Kawamura (1979), in which the SCN was surgically isolated from the rest of the brain, lent further support to the notion that the SCN is the master clock. They recorded multiple unit activity from sites within, and outside of, the isolated SCN in behaving rats, and demonstrated that the SCN maintained its rhythmic firing while other brain regions became arrhythmic. Because many peripheral tissues are oscillatory *in vitro*, including liver, lung, and muscle (Yamazaki et al., 2000), it remained a possibility that the SCN was not the central pacemaker, but rather a slave oscillator to an as yet unidentified pacemaker. If the SCN were a pacemaker, then features of overt rhythms, such as phase or period, should be derived specifically from SCN cells (Ralph 1991). A series of transplantation studies in the rat and golden hamster confirmed that the SCN does indeed set the period of overt rhythms and is therefore a legitimate pacemaker.

Drucker-Colin et al. (1984) performed the first grafting experiments in which fetal SCN explants, transplanted into the floor of the third ventricle of arrhythmic SCN-lesioned rats, restored drinking rhythms. The limitation of this study was the difficulty in determining whether the overt rhythms measured following transplant resembled those of the donor or the recipient SCN. To more specifically address this question Ralph et al. took advantage of *tau*, a spontaneous mutation in the golden hamster, which manifests as a significantly shortened circadian period. The period length of wild type golden

hamsters is 24.2 hours, while that of *tau/+* heterozygotes and *tau/tau* homozygotes is 22.0 and 20.3 hours, respectively. Introducing fetal SCN tissue from any of the three genotypes into SCN-lesioned animals of another genotype rescued rhythmicity in the lesioned hamsters with the same period as that of the donor animal (Ralph et al., 1990). These experiments supplied definitive evidence that the SCN is a true pacemaker, driving and setting overt rhythms.

The identification of the central clock in the SCN begged two fundamental questions: **(1)** How does the SCN drive rhythms in target tissues? The complexity of its hypothalamic outputs and the shear number of systems that it regulates make the SCN a difficult brain region to study. However mapping its connectivity through labeling studies was a useful starting point in determining how the SCN exerts its effects on whole animal physiology, metabolism, and behavior. **(2)** What makes the SCN intrinsically oscillatory? This question remained difficult to address until components of the molecular clock were identified in the *Drosophila* circadian system.

(1) *SCN Connectivity*

Afferents

The SCN is a heterogeneous nucleus with respect to the neurochemistry and projections of its constituent neurons, but it can be divided roughly into two areas. The first is the dorsomedial SCN, which contains a large number of neurons expressing the neuropeptides arginine vasopressin (AVP) and somatostatin (SS). This portion of the SCN contains the majority of cells that project out of the SCN. In general, the

dorsomedial SCN receives most of its afferent inputs from the ventrolateral SCN, and significantly less input from the retina, the midbrain raphe nucleus, and the thalamus.

The second is the ventrolateral SCN, which is composed largely of vasoactive intestinal peptide (VIP)- and gastric releasing peptide (GRP)-containing neurons. The afferent input to the ventrolateral SCN includes projections from the retina via the retinohypothalamic tract (RHT) (Moore and Lenn 1972b), and a projection from the intergeniculate leaflet of the thalamus (IGL) via the geniculohypothalamic tract (GHT) (Hickey and Spear 1976). Photic information, therefore, takes two routes to the SCN; one arising directly from the retina, and another which is subjected to thalamic processing in the IGL. The neuroactive substances released by nerve terminals of the RHT include glutamate (Shibata et al., 1992), and pituitary adenylate cyclase-activating peptide (PACAP) (Hannibal et al., 1997). The major neuroactive substances released by the GHT onto the SCN are the inhibitory neurotransmitter gamma-aminobutyric acid (GABA) and neuropeptide Y (NPY) (Card and Moore 1982; Card and Moore 1989). Electron microscopic evidence suggests that individual neurons in the ventrolateral SCN receive multiple inputs from retinal ganglion cells (RGCs) and IGL neurons, indicating that this region of the SCN is a site of integration for primary and secondary visual inputs (Card and Moore 1982; Card and Moore 1989). Another significant afferent input to ventrolateral SCN is a serotonergic projection from the dorsal and medial raphe nuclei of the midbrain (Azmitia and Segal 1978).

Efferents

As the hypothalamus is a control center for many autonomic and neuroendocrine processes that display circadian rhythmicity, it is not surprising that it is a major target for

SCN efferent projections. It is estimated that the majority (70-80%) of SCN neurons give rise to local ipsilateral and contralateral SCN circuits and that the remaining SCN neurons project to various hypothalamic and extrahypothalamic nuclei. The most extensive projection extends dorsocaudally from the SCN to the subparaventricular zone of the hypothalamus (sPVHz), which is a region around the third ventricle that includes parts of the anterior periventricular, paraventricular, ventromedial, and anterior hypothalamic nuclei. There is segregation of inputs to the sPVHz so that the organization of the SCN is maintained. The sPVHz then sends overlapping projections to most of the other SCN targets, innervating them at a higher density than does the SCN.

Briefly, some additional efferent hypothalamic targets include smaller projections from the SCN to (1) the preoptic region, the most rostral part of the hypothalamus which is a control center for several rhythmic processes including drinking, thermoregulation, reproduction, and fluid balance, (2) the dorsal paraventricular nucleus which through its projections to sympathetic preganglionic neurons in the spinal cord, regulates pineal melatonin secretion, (3) the lateral hypothalamic area which is involved in feeding behavior, (4) and the dorsomedial and ventromedial nuclei which control ingestive and reproductive behavior. Extrahypothalamic targets include (1) the paraventricular nucleus of the thalamus, which receives input from both VIP and AVP neurons of the SCN, (2) the lateral septal nucleus, and (3) the IGL, which also receives direct retinal input and has a reciprocal connection to the SCN.

SCN neurons induce rhythms in target cells and tissues by synthesizing and releasing neuropeptide or neurotransmitter in a cyclic fashion, and by exhibiting rhythmic oscillations in action potential firing frequencies (Green and Gillette 1982; Inouye and

Kawamura 1979; Kalsbeek et al., 1995). For example, cyclic AVP release by SCN neurons underlies the circadian rhythm of adrenal corticosterone levels in the rat. *In vivo* microdialysis studies established that the SCN synthesizes AVP rhythmically with levels of the neuropeptide peaking during the subjective day (Kalsbeek et al., 1995). The SCN sends an inhibitory (AVP) projection to the dorsomedial hypothalamus (DMH). The DMH innervates the medial paraventricular hypothalamus (PVHm), which is the source of corticotropin-releasing hormone (CRH). CRH activates adrenocorticotropic hormone (ACTH) release by pituitary corticotrophs and eventually induces cortisol secretion by the adrenal glands. Low concentrations of AVP in cells of the SCN in early morning disinhibit the DMH and lead to adrenal release of cortisol just before the animal transitions to the day. Administering AVP receptor agonists or antagonists to the DMH of rats abolished corticosterone rhythms, demonstrating that the SCN AVP rhythm drives the corticosterone rhythm (Kalsbeek et al., 1996).

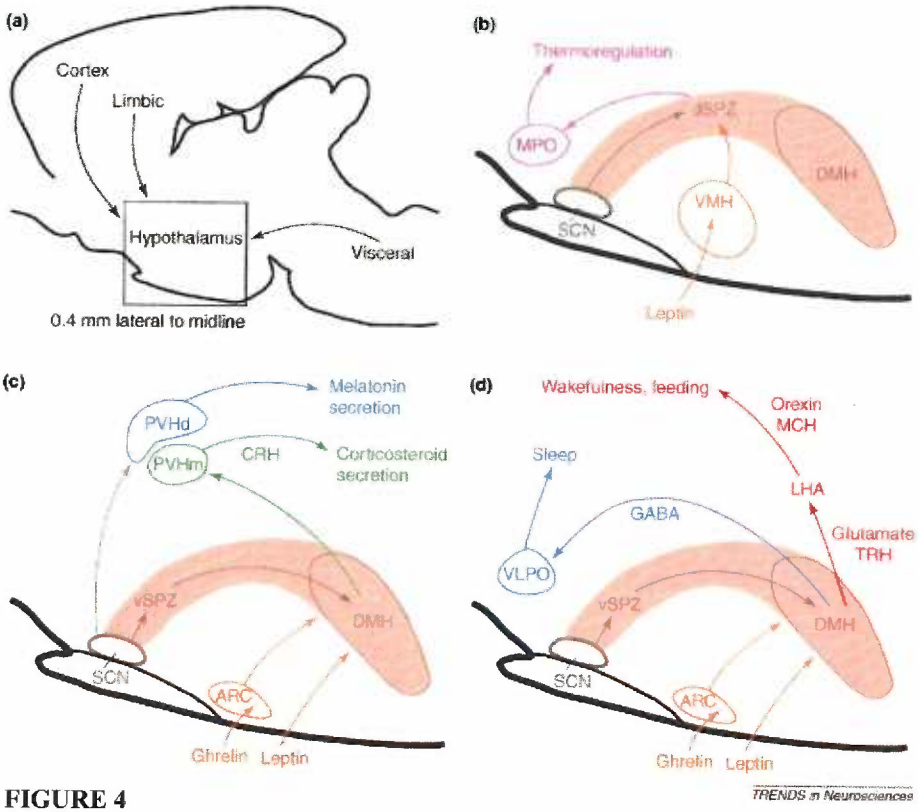

FIGURE 4

Pathways to/from the SCN.

(a)The SCN receives three types of non-photic input: cognitive input from cortex, emotional input from limbic system, and visceral input from the brainstem. (b) dSPZ is important for controlling body temperature through its projections through the MPO. Food cues from the hormones leptin and ghrelin are relayed by the VMH and ARC to the dSPZ and DMH. (c) the SCN projects to the PVHd neurons which project to preganglionic neurons in the spinal cord that control pineal melatonin secretion. The vSPZ sends a relay to the DMH which controls an array of circadian responses including corticosteroid secretion via a projection to the CRH cells of the PVHm and (d) sleep cycles via GABA projections to the VLPO and arousal and feeding cycles via glutamate and TRH projections to the LHA. Orexin and MCH-containing LHA neurons are important for wakefulness and feeding.

Abbreviations: d/vSPZ, dorsal/ventral subparaventricular zone; MPO, medial preoptic nucleus; VMH, ventral medial nucleus; ARC, arcuate nucleus; DMH, dorsal medial hypothalamus; PVHd/m, dorsal./medial paraventricular nucleus of hypothalamus; CRH, corticotrophin- releasing hormone; VLPO, ventrolateral preoptic nucleus; TRH, thyrotopin-releasing hormone; LHA, lateral hypothalamus; MCH, melanin-concentrating hormone. Modified from Figure 2 (Saper et al., 2005)

By modulating their own membrane excitability in a circadian fashion, SCN neurons can drive rhythms in target cells. Membrane excitability impacts action potential firing frequency and the release of neurotransmitter or neuropeptide at the nerve terminal. Pennartz et al. (2002) recorded from SCN neurons in the rat brain slice in current-clamp mode and reported that daytime firing frequencies were around 8 Hz, compared to irregular and infrequent spike firing at night. By blocking TTX-sensitive action potentials, they uncovered an underlying daytime 2-7 Hz oscillation in membrane potential that was absent during nighttime recordings (Pennartz et al., 2002).

Circadian rhythmicity in membrane excitability can be controlled by rhythmic expression of ion channels and/or proteins that modulate ion channel function. The cyclic firing rates exhibited by SCN neurons in rat brain slices can be accounted for, in part, by daytime increases in L-type calcium channel current (Pennartz et al., 2002). Daytime calcium influx both depolarizes the neuron which brings its resting potential closer to the threshold potential needed for voltage-gated sodium channel activation, and impacts calcium dependent intracellular signaling pathways. It is not yet known how SCN neurons reduce the L-type current during the subjective night, but possible mechanisms include reductions in channel expression, increases in channel degradation, alterations in channel trafficking, and perhaps the most economical for the cell, post translational modifications of existing channels.

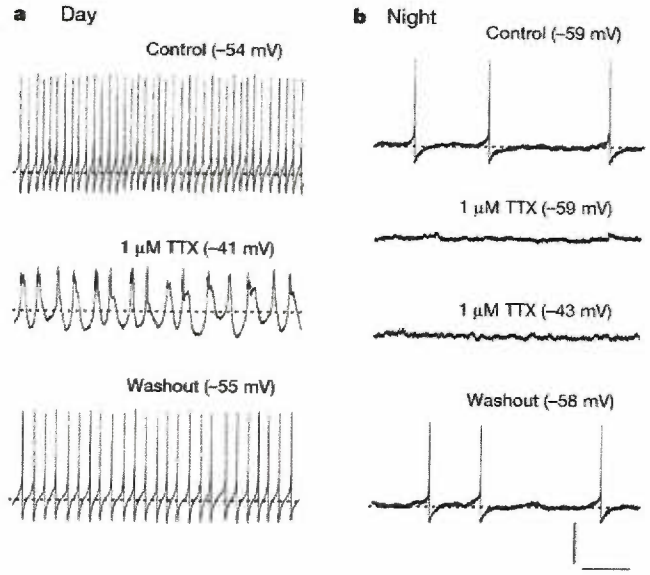

FIGURE 5

Properties of Membrane Potential Oscillations in SCN.

(a) Day:TTX revealed oscillations and tonically depolarized the membrane. Dotted lines: time-averaged membrane potential. (b) night: TTX failed to uncover oscillations or depolarize the cell. In 3rd trace from top, cell is depolarized with tonic current injection. Calibration bars: 40 mV, 500 ms, except middle trace in a, 20 mV, 500 ms. Modified from Figure 1 (Pennartz et al., 2002).

(2) ***Molecular Clock Components***

Interest in the intrinsic properties of SCN neurons grew after the lesion studies by Moore et al. (1972) and Stephan et al. (1972) established that overt circadian behavioral rhythms in the mammal required the intact SCN, and after Inouye et al. (1979) demonstrated that the SCN maintained rhythmic circadian firing when isolated from the rest of the brain. However the genes in circadian neurons that confer intrinsic rhythmicity, clock genes, were first identified in *Drosophila melanogaster*. It would take another twenty years for homologous genes in the mammal to be identified, cloned, and studied in the SCN.

The first molecular component of a circadian clock was discovered by Konopka and Benzer in *Drosophila* (Konopka and Benzer 1971). They mutagenized adult male flies using ethyl methane sulfonate and crossed them with attached-X chromosome females. As shown in Figure 6, by using female founders with two X chromosomes that

fail to segregate, all of the male progeny in the F1 generation are known to bear the X chromosome from the male parent.

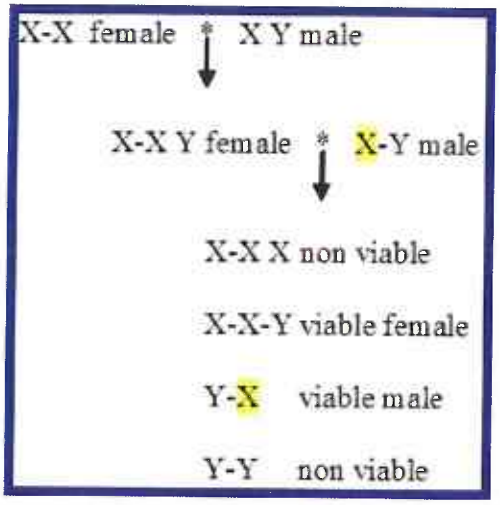

FIGURE 6

Attached-X Female *Drosophila* Mating.

Drosophila sex is determined not by the presence of a Y chromosome but by the ratio of X chromosomes to autosomes (A). A ratio of 2X:2A induces female development, and 1X:2A induces male development. Using an attached X female X-XY guarantees that all males in the F1 generation carry their father's mutagenized (yellow) X chromosome. This was desirable as the objective was to generate X chromosome rhythm mutations in the male parent fly that would be passed at high yield to progeny. This strategy also simplified subsequent gene mapping by limiting the genes of interest to the X chromosome.

Konopka and Benzer examined the males of the F1 generation to determine whether any exhibited altered pupal eclosion rhythms. The wild type fly has a normal eclosion rhythm in which the majority of flies eclose in the morning hours. From their studies Konopka and Benzer found three progeny with abnormal eclosion and locomotor rhythms in constant darkness (DD), indicating that the mutations were affecting the basic oscillator and not an input or output pathway. Genetic mapping demonstrated that the mutations underlying these three mutant phenotypes mapped to different regions within the same X chromosome-linked gene, *period* (*per*). The null mutation that gave rise to arrhythmic flies was named per^0, while missense mutations giving rise to the short period (~19 hr) and long period (~29 hr) mutants were named per^S and per^L, respectively.

Both *period* mRNA and PERIOD protein (PER) oscillate in a circadian fashion with the *per* transcript reaching peak levels in the early evening and PER reaching maximum levels in the nucleus 4-6 hours later during the late night and early morning (Hardin et al., 1990; Zerr et al., 1990). Moreover, *per* mRNA levels show altered phases in per^S and per^L mutants, supporting a role for PER in the circadian clock and also providing a molecular marker by which to detect circadian rhythms in individual cells and/or tissues (Hardin et al., 1990). Hardin et al. (1990) were the first to suggest that PER inhibits its own transcription and that a key strategy of the clock might be to use negative transcriptional feedback loops to generate oscillating rhythms in clock proteins .

Seghal et al. isolated another important *Drosophila* clock gene, *timeless* (*tim*) (Sehgal et al., 1994). *Tim* mutants, like per^0 mutants, are arrhythmic in DD and, unlike wild type flies, show no circadian rhythmicity in *per* mRNA transcripts. In a parallel

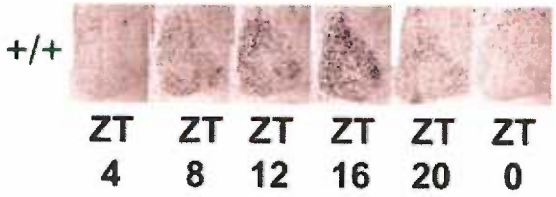

FIGURE 7

Per2 message in the wild type mouse SCN displays a diurnal rhythm with peak message at CT 16.

In situ hybridization of *Per2* mRNA in the SCN of mice held kept in 12:12 LD at different circadian times (ZT) (Masubuchi et al., 2005).

study by the same lab it was demonstrated that *tim* is required for the nuclear targeting of PER (Vosshall et al., 1994). It was subsequently shown that *tim* mRNA oscillates in phase with *per* mRNA in a PER and TIM-dependent manner (Sehgal et al., 1995). A autoregulatory feedback mechanism began to emerge in which the expression of two clock proteins whose mRNA oscillate in phase with each other also repress their own transcription.

More recent work has shown that the role of TIM is probably not to facilitate nuclear PER transport, but rather to stabilize cytoplasmic PER (Shafer et al., 2002). The effects that *tim* mutations have on nuclear PER are likely due to a reduction in the total levels of stable PER. Using immunocytochemistry, Shafer et al. showed that PER enters the nuclei of *Drosophila* ventrolateral neurons three hours before TIM does, demonstrating that PER does not require heterodimeric association with TIM for nuclear entry. A localization sequence that is sufficient for nuclear accumulation has since been found in the C-terminus of PER and is separate from the domain through which TIM and PER presumably interact (Chang and Reppert 2003).

Both the nuclear localization of PER as well as its role in regulating its own transcription (Hardin et al., 1992) suggested that it was a transcription factor. However, when PER was sequenced, no obvious DNA binding domains were observed. PER did, however, contain a roughly 270 residue region that would later be called the PAS (*per*-ARNT-*sim*) domain, named for *per* and the two other proteins in which it was found (subunits of the aromatic hydrocarbon nuclear receptor (ARNT) and the *Drosophila* gene product of *singleminded* (*sim*)). Three other transcription factors with basic helix-loop-helix (bHLH) DNA binding domains also contained a PAS domain. Huang et al. (1993) demonstrated that PAS-containing proteins could interact with PER and that PER could, through its PAS domain, interact with bHLH transcription factors to potentially regulate circadian gene transcription. Analysis of regions upstream of *per* identified an enhancer sequence that was sufficient to drive rhythmic gene transcription (Hao et al., 1997). Contained within that sequence was an E-box bHLH domain (CACGTG) necessary for the transcription of *per* and a number of other clock genes.

One feature of the *Drosophila* oscillator is a roughly 4 hour delay between peak *per* and *tim* transcript levels and peak nuclear PER and TIM levels. This critical delay permits the oscillator to continue functioning without damping over many cycles, but is longer than expected if nuclear translocation and translation are the only steps between transcription of *per* message and the eventual accumulation of nuclear PER (Zordan et al., 2001). Edery et al. (1994) showed that nuclear PER is phosphorylated at multiple sites compared to cytoplasmic PER . They inferred that PER phosphorylation is required for its nuclear translocation and suggested that the processes of phosphorylation and dephosphorylation in the cytoplasm may account for the delay in nuclear accumulation of PER. A recent study in *Drosophila* S2 cells challenges this prosposal by demonstrating that PER phosphorylation does not gate nuclear entry of PER, but rather increases its transcriptional repression, perhaps by affecting its chromatin-binding ability (Nawathean and Rosbash 2004). In their model, PER is in dynamic equilibrium between its hyperphosphorylated and hypophosphorylated states. Factors influencing the total amount of PER protein (TIM expression) and PER phosphorylation (by kinases and phosphatases which are themselves rhythmically expressed) would affect this equilibrium and thereby affect both nuclear levels and the phosphorylation status of PER. Whether post-translational phosphorylation of PER at multiple sites is required for PER nuclear entry, function, or both, the time required for modification by kinases and phosphatases may account for the 4 hour gap between peak *per* mRNA transcription and peak nuclear PER levels.

The discovery of a mutant mouse helped fill in the missing links in the *Drosophila* clock. A mutation in the *clock* gene gives rise to mice with long circadian

periods and who lack persistent rhythmicity (Vitaterna et al., 1994). CLOCK is a bHLH transcription factor with a PAS domain and therefore an obvious candidate binding partner for *per* and *tim*. A *Drosophila* homologue was identified and was shown to activate *per* and *tim* by binding to their E-BOX domains (Allada et al., 1998). CLOCK however, did not form homodimers as expected, but required another bHLH-PAS domain-containing transcription factor, CYCLE, to activate *per* and *tim* transcription (Rutila et al., 1998).

A second feedback loop is involved in the cycling of *clock* and *cycle* transcripts. In *Drosophila,* the transcription of *vrille* (*vri*) and *Par Domain Protein 1* (*Pdp1*), which encode two transcription factors, is activated by CLOCK/CYCLE heterodimers. VRI protein inhibits *clock* transcription and PDP1 protein activates it. VRI and PDP1 are not in perfect phase with one another, and can thereby drive oscillations in CLOCK protein levels (Cyran et al., 2003).

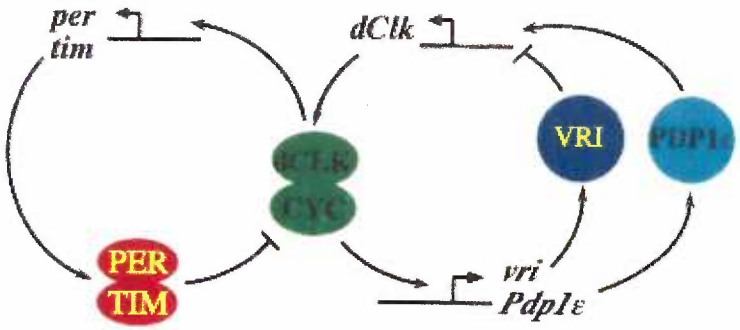

FIGURE 8

A Two-Loop Model for the *Drosophila* Clock.

Two interconnected transcription feedback loops lie at the core of the *Drosophila* molecular clock. In one loop, dCLK and CYC directly activate transcription of *per* and *tim* by binding their promoters. Inhibition of dCLK/CYC activity is mediated by TIM transporting PER into the nucleus. dCLK/CYC also directly activate *vri* and *Pdp1ε* transcription. *dClk* transcription is first repressed by VRI and then activated by PDP1ε. Repression and activation of *dClk* are separated by the different phases of VRI and PDP1ε proteins. Removal of PER in the early morning frees dCLK/CYC to resume transcription of *per, tim, vri*, and *Pdp1ε*, thus restarting both loops simultaneously. (Cyran et al., 2003)

Some of the circadian clock genes and proteins differ between *Drosophila* and murine models. First, there are three different *period* genes in the mouse, all of whose mRNA and proteins oscillate. Both *mPer1* and *mPer2* are considered core clock genes, as homozygous mutant mice for either gene display severe alterations in locomotor behavior during prolonged exposure to dark conditions. *mPer2* is required for clock gene transcript rhythms in the SCN, but mutations in *mPer1* seem to cause only subtle changes in period length and in the overall levels of other clock proteins (Bae et al., 2001). The authors conclude that mPER1 has a post translational function, and that mPER2 regulates rhythmic gene expression. mPER3 is suspected to play a role outside the core oscillator as mice homozygous for mPER3 mutations do not display altered locomotor rhythms (Bae et al., 2001). Another difference between clock cells in the mouse SCN and clock cells in the lateral brain of the fly is that instead of binding the protein TIM, mPER1 and mPER2 form heterodimers with the CRYPTOCHROME (CRY) proteins, CRY 1 and 2. Flies also express CRY, which appears to serve photoreceptive functions in their clock cells, and non-photoreceptive functions in other tissues. A role for CRYPTOCHROMES in the fly oscillator has not yet been proven. In mammals, CRYPTOCHROMES were considered potential circadian photopigments, but mounting evidence suggests that melanopsin, not CRYPTOCHROME, is the mammalian circadian photopigment. And finally, the homolog to CYCLE in the mouse is BMAL1. BMAL1 is repressed by REV-ERBα, a product of one of the genes BMAL1 transcriptionally activates, forming a second feedback loop, as is found in the fly.

The strategies of the circadian clock in the fly brain and in the mammalian SCN are similar: in part, the intrinsic oscillatory behavior of the SCN can be explained by a

transcription-translation negative feedback loops that drives rhythmic gene expression in individual SCN neurons. During the day, the transcription factors CLOCK and BMAL1 form heterodimeric complexes that bind to E-Box promoter regions on *Per1, Per2, Cry 1, Cry2,* and *Reverbα* genes and drive their transcription (Gekakis et al., 1998). Simultaneously, the Reverbα gene product inhibits *Bmal1* transcription generating a BMAL1 rhythm (Preitner et al., 2002; Ueda et al., 2002). During the night, after PER has been phosphorylated and sufficient levels of both PER and CRY have been translocated to the nucleus, they complex with CLOCK/BMAL heterodimers to inhibit *Per, Cry,* and *Reverbα* transcription. As REVERBα levels fall, *Bmal1* transcription increases so that by the beginning of the daytime, the cycle can begin anew with the transcription and translation of *Per, Cry,* and *Reverbα.* Similar to what is found in the *Drosophila* clock, the equilibrium and ubiquitization of mammlian clock proteins are determined in part by their degree of phosphorylation. Two kinases implicated in the regulatory phosphorylation of *Per1, Per2, Cry1, Cry2,* and *Bmal1* are Casein Kinase Iδ and Casein Kinase ε. (Lee et al., 2001; Lowrey et al., 2000). In summary, seven different genes involved in SCN pacemaking have been identified in mammals thus far and include *Per1, Per2, Cry1, Cry2, Clock, Bmal1* and *Reverbα* (Reppert and Weaver 2002). Variables in this model that may account for the long (approximately 24 hour) period of the endogenous clock include the time required for the synthesis, modification, accumulation, nuclear translocation, and degradation of key clock mRNAs and proteins.

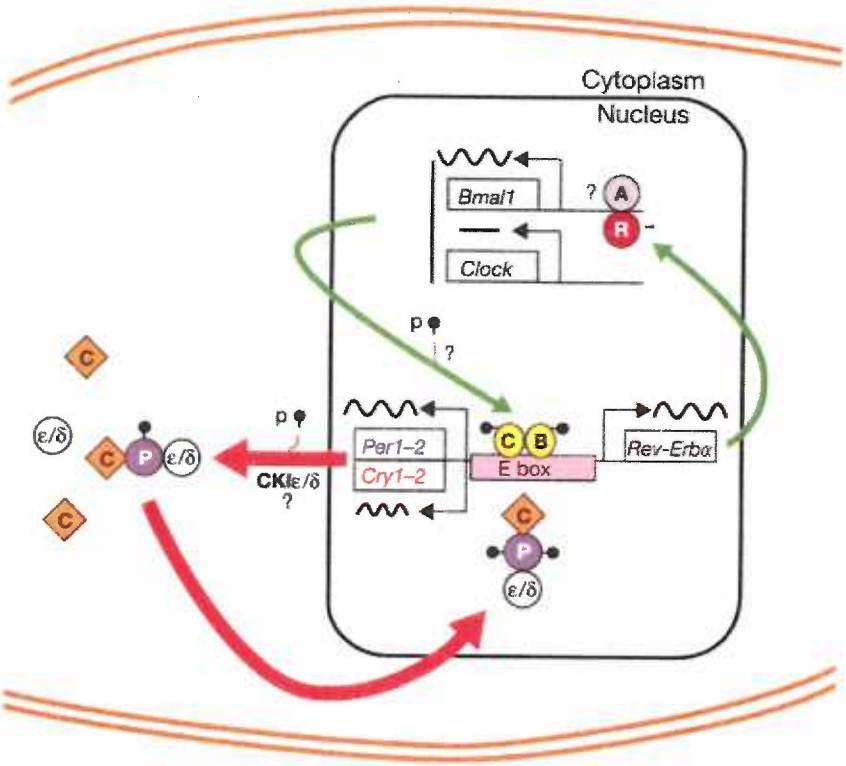

(Reppert and Weaver 2002)

FIGURE 9

Mammalian circadian clock -work model.

The clock mechanism comprises interactive positive (green) and negative (red) feedback loops. CLOCK (C, oval) and BMAL1 (B, oval) form heterodimers activate and transcription of the *Per*, *Cry* and *Rev-Erbα* genes through E-box enhancers. As the levels of PER proteins increase (P, blue circle), they complex with CRY proteins (C, diamond) and CKIε/CKIδ (ε/δ, circle), and are phosphorylated (p). In the nucleus, the CRY—PER– CKIε/CKIδ complexes associate with CLOCK–BMAL1 heterodimers to shut down transcription while the heterodimer remains bound to DNA, forming the negative feedback loop. For the positive that participate in phosphorylation of clock proteins. feedback loop, increasing REV-ERBα levels (R, circle) act through Rev-Erbα/ROR response elements in the Bmal1 promoter to repress (-) Bmal1 transcription. CRY-mediated inhibition of CLOCK–BMAL1-mediated transcription de-represses (activates) Bmal1 transcription, because REV-ERBα-mediated repression is inhibited. An activator (A, circle) may positively regulate Bmal1 transcription (?) alone or by interacting with mPER2. There are probably kinases (?) other than CKIε and CKIδ. Modified from Figure 2 (Reppert and Weaver 2002)

Entrainment

A critical feature of circadian clocks is their capacity to maintain a stable phase relationship, or phase angle, with environmental cues that signal the length of the solar day. When the oscillations of a circadian rhythm are in phase with an oscillating external cue (ie: light), the clock is "entrained" to that external cue. An environmental cue that can entrain a circadian clock is a "zeitgeber," meaning time giver.

Entrainment does not require perfect synchrony between a zeitgeber and a biological rhythm. To claim that a biological rhythm is entrained to a stimulus one must demonstrate that (1) the phase relationship between the output rhythm of the clock and the entraining stimulus rhythm is stable, (2) the period lengths of the output rhythm and the stimulus rhythm are, on average, equal, and (3) upon removing the stimulus, the clock continues oscillating at a phase that is consistent with the entraining stimulus (Johnson et al., 2003). A multitude of cues can serve as zeitgebers, including oscillations in temperature, arousal, muscular feedback following movement, and food availability. The most effective zeitgeber for entraining the mammalian circadian clock is light, and this particular type of entrainment is "photoentrainment."

Many non-mammalian species have extra-ocular photoreceptors located in the pineal gland and within deep brain regions. There is evidence supporting a role for pineal photoreception in photoentrainment in birds, reptiles, fish, and amphibians (Bertolucci and Foa 2004), and only one known case of a deep brain photoreceptor entraining circadian behavioral rhythms (the ruin lizard *Podarcis sicula*) (Pasqualetti et al., 2003). However the opacity of the mammalian skull has necessitated retinal input for mammalian photoentrainment. This was first shown by Wilson et al. (1976) who reported

that enucleation of adult female rats destabilized the phase relationship between their light/dark cycle and their pituitary adrenal output. It has since been shown that locomotor rhythms, other hormone rhythms, eating and drinking rhythms, and sleeping rhythms are decoupled from the light cycle following enucleation in the mammal (Ibuka et al., 1977; Stephan and Zucker 1972).

Phase-Shifting the Circadian Clock

The period of the endogenous un-entrained circadian clock is seldom exactly 24 hours. By convention, all circadian cycles are divided into 24 hours so that when a circadian period is longer than 24 hours, each circadian hour is slightly longer than 60 minutes, and when a circadian period is shorter than 24 hours, each circadian hour is slightly shorter than 60 minutes.

The block of time in a circadian cycle during which the animal is exposed to light is referred to as subjective day and its onset is denoted as circadian time (CT) 0. Subjective night refers to that time which the organism experiences darkness and in a light/dark (LD) 12:12 cycle its onset is denoted as CT 12. Nocturnal animals are inactive during the day and active at night, while the converse is true for diurnal animals. It is interesting that SCN neurons in both diurnal and nocturnal animals display a higher firing frequency during the day than at night. Their opposing behavioral responses to light must therefore result from a sign change either at or downstream of the SCN efferent signal to output pathways.

Actographs are used to plot and analyze the period, phase, and stability of a rhythmic output over many circadian cycles. This graphical depiction of activity

(locomotor, sexual, drinking, eating, etc.) is plotted with day on the ordinate axis and circadian time on the abscissa.

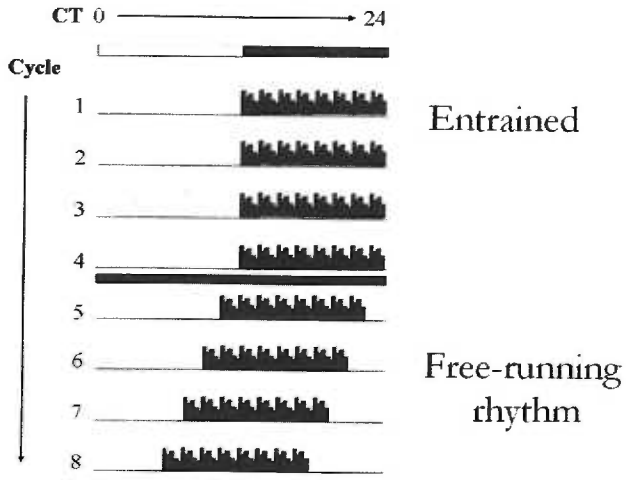

FIGURE 10

Idealized actograph.

Circadian time represented on the abscissa, cycle number represented on the ordinate axis, and lighting conditions represented as bars. Shows photoentrainment in LD 12:12 conditions, and free running rhythms in DD that have a period slightly longer than 24 hours. When plotted on a 24 hour actograph, the rhythms in DD begin at successively earlier circadian times.

The period of the endogenous clock in the absence of any zeitgeber is called the free-running period (FRP). To determine the FRP of a circadian clock, output rhythms are monitored for several days in darkness (DD) and in otherwise constant conditions (temperature, location, etc). With no external cues to which the animal can entrain, the period of the behavioral rhythm measured then directly reflects the period length of the endogenous clock. For example, when a hamster is exposed to a 14 hour light 10 hour dark schedule, (LD 14:10) locomotor activity reliably displays a 24 hour rhythm with a predictable surge in wheel running activity at CT 14 (light offset), and a consistent cessation at CT 0 (light onset.) This photoentrained rhythm has a stable phase relationship with the LD 14:10 schedule and its period is exactly 24 hours. If a hamster is then moved to DD for several days, there is a small incremental shift in the onset of activity with each cycle, because the FRP of the hamster's clock is slightly shorter or longer than 24 hours depending on the strain of animal.

A stimulus, such as a zeitgeber discussed above, has "phase-shifted" the circadian clock when its presentation alters the phase relationship between the phase of the entraining cue and the phase of the overt rhythm. The sensitivity and direction of phase shifting depend on the circadian time at which the stimulus is delivered. Consider again the hamster that is entrained to a LD 14:10 schedule. If a light pulse is delivered in the early subjective night, when the hamster is active, the animal will shift its phase toward the previous day. If the light pulse is delivered in the late subjective night toward the end of the active period, the animal will shift its phase toward the next day which is called a phase advance. Phase shifting is easily visible when overt rhythms are plotted on an actograph as in Figure 11.

The cellular events in SCN neurons that underly photoentrainment and phase-shifting occur rapidly in response to changing light schedules, and can stabilize within one circadian cycle. For instance, the induction of *Per1* by light occurs within 10 minutes of exposing mice to light (Shigeyoshi et al., 1997). However, the behavioral and physiological expressions of those cellular changes do not usually stablize for several circadian cycles. The transitional rhythms expressed before stabilization are called "transients," and are most dramatic in the case of phase-advancing and in organisms with complex circadian systems. The malaise associated with jetlag is thought to result from the temporary asynchrony between the phase of the central clock and the phase of overt rhythms, during transient rhythm expression (Johnson et al., 2004).

While the clock is differentially phase shifted by early and late night light pulses, it is insensitive to light pulses throughout the subjective day. The rhythms of hamsters in DD conditions are unaffected when light pulses are delivered during the inactive period

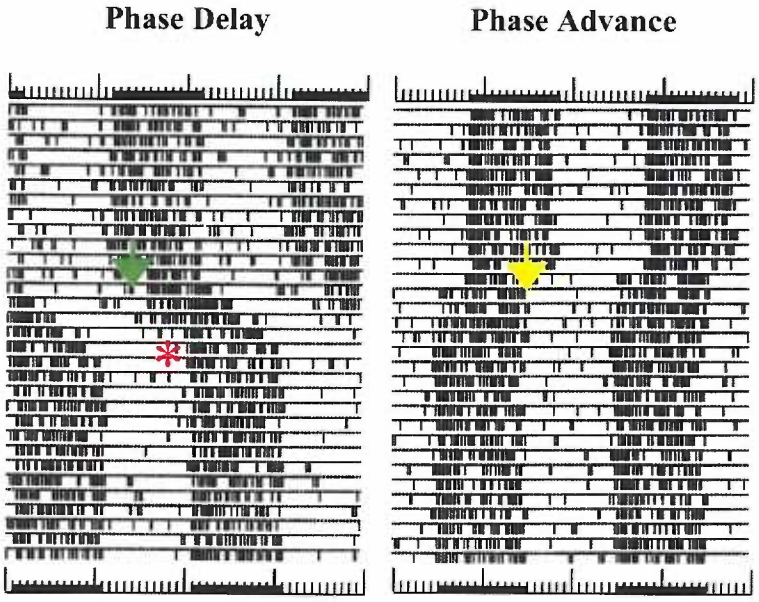

FIGURE 11

Light pulses in the early and late subjective night induce phase delays and phase advances, respectively.

(Left) A light pulse (green arrow) was given in the early subjective night, causing a phase delay. Subsequent bouts of locomotor activity began at later circadian times following the light pulse. (Right) A light pulse (yellow arrow) in the late subjective night caused a phase advance so that subsequent bouts of locomotor activity began at earlier circadian times. Data is displayed in double plotted actographs with 48 hours represented on the abscissa. Note the transient locomotor rhythms that persist for several cycles before a steady state phase (red asterisk) is reached. Provided by C.N. Allen.

of the hamster's free running rhythms, which corresponds to subjective daytime and is termed the "dead zone." This finding indicates that the core oscillator is sensitive to retinal input only during the subjective night when the presence of light is unexpected and behaviorally relevant.

Phase-Response Curve

For entrainment to be effective, the central clock must respond to phase-shifting stimuli differently at different phases of its cycle. Phase response curves (PRCs) depict

how the circadian timing of light pulse affects both the amplitude and direction of a phase shift. PRCs can be constructed for any phase-shifting stimulus and vary considerably depending on the stimulus. Photic information is transduced to the SCN via glutamatergic

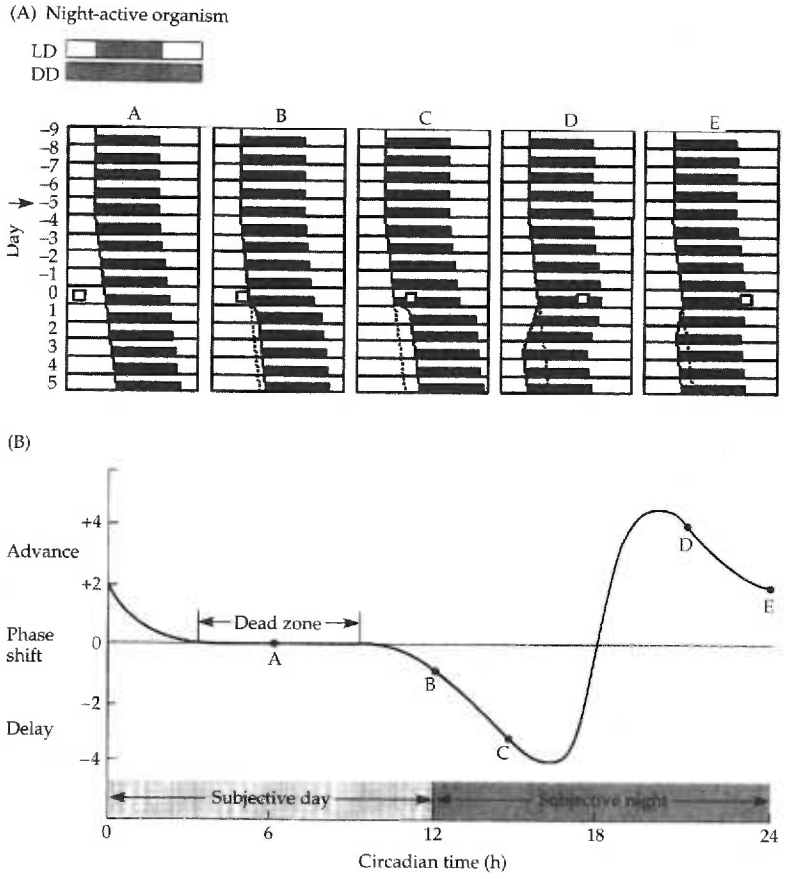

FIGURE 12
Constructing a Phase Response Curve (PRC) for light.

To construct a PRC, 5 nocturnal animals were first stably entrained to an LD cycle. The animals were then shifted to DD (black arrow) where they exhibited free-running rhythms. Light pulses (squares) were delivered at various times during the circadian cycle. The steady state phase shift (expressed as the number of hours the onset of an overt rhythm has shifted from its original value) is plotted against the circadian of light presentation. When the new overt rhythm begins at a later circadian time the value is expressed as a negative number by convention and is a phase-delay. If the new overt rhythm begins sooner, the shift is expressed as a positive number and is a phase advance. In this example, the animal was totally insensitive to light presented during CT3-CT9 for which this circadian time is called the "dead zone." Between about CT 9-10 and CT 18, light pulses induce phase delays, while between CT 18 and CT3, light pulses induce phase advances Modified from Figure 3-5(Johnson et al., 2004).

neurotransmission (Ding et al., 1994). As expected, the PRC for glutamate application to the SCN looks similar to the PRC for light. Both PRCs illustrate that the phase of the SCN is unperturbed when light and glutamate are presented during the subjective day. Beginning at CT 9, glutamate and light cause phase shifts in SCN firing rhythms and wheel running rhythms respectively. The peak phase delay occurs at CT 14 while the peak phase advance occurs at CT 20.

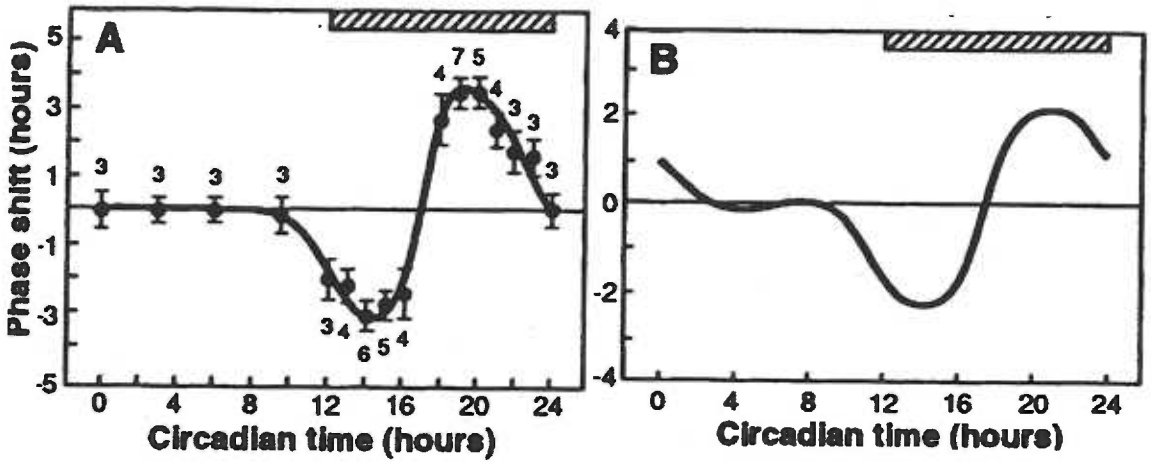

FIGURE 13

Phase-response curves for glutamate applied to the SCN (A) and light (B) in rat.

(A) The PRC for 10 mM glutamate applied to the SCN for 10 minutes derived from 63 experiments at 16 circadian time points. Hatched bars represent subjective night. Each point represents the mean ± SD of 3-7 experiments as indicated. (B) PRC for 1 hour pulses of light to rats in DD. Overt rhythm measured is wheel running. Modified from Figure 2 (Ding et al., 1994)

A number of neuropeptides arising from SCN afferents phase shift the oscillator during the day, including serotonin from the raphe (maximal effect at CT 7, phase advance), melatonin from the pineal (CT 10, phase advance), PACAP from the retina (CT 6, phase advance), and NPY from the GHT (CT 6-9, phase advance) (Hannibal et al., 1997; McArthur et al., 1991; Medanic and Gillette 1992; Shibata and Moore 1993). With the exception of PACAP, these neuropeptides are released from non photic afferent

pathways. Although the source of PACAP is retinal, PACAP is also considered to be a nonphotic phase shifting stimulus because the clock is sensitive to it during the dead zone when photic inputs are ineffective. A PRC for melatonin is shown in Figure 14 which depicts extracellular firing frequencies of rat SCN neurons recorded *in vitro*. Phase shifting is observed during the transition from day to night with a maximum around CT 10. In response to melatonin, the oscillator only exhibits phase advances.

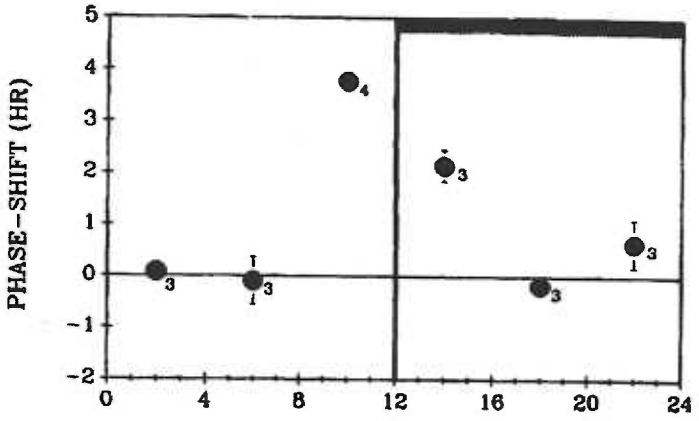

FIGURE 14

Phase-response curve for melatonin.

The effect of melatonin application at various circadian times (CT 2. 6, 10, 14, 18, 22) was tested in 3-4 experiments for each time point. Overt rhythm was electrical firing rhythm measured extracellularly in SCN of rat brain slices before and after melatonin application. (McArthur et al., 1991)

Several aspects of a light stimulus, besides the circadian timing of its presentation, affect the amplitude of the consequent phase-shift. These include the wavelength, intensity, and the duration of the light pulse presented. Takahashi et al. (1984) demonstrated that the wavelength of light by which hamster locomotor rhythms were maximally phase-shifted (λ_{max}) was around 500 nm . Estimates of λ_{max} values for both rat and mouse behavioral phase shifts are also near 500 nm. Rat pineal melatonin suppression was predicted by a Dartnall nomogram-based curve to have a λ_{max} of 495 nm.

Because the rat rod photoreceptor has a λ_{max} around 498 nm, photoentrainment was assumed to be mediated by rods. However, three pieces of evidence suggested otherwise. First retinally degenerate (*rd/rd*) mutant mice, whose retinas contained virtually no rods and very few cones, demonstrated behavioral phase-shifts to light with undiminished sensitivity compared to wild type mice (Foster et al., 1991). Second, when a spectral tuning analysis was done in the retinally degenerate *rd/rd* mutant mouse by two different groups, estimated λ_{max} values were better fit with middle wavelength and UV cone opsins than rod opsins. Using nomogram-based fits, Provencio et al. (1995) reported a λ_{max} of around 511 nm, and Yoshimura et al. (1996) a λ_{max} of 480 nm . Third, if the circadian system were detecting photons via the same subset of photoreceptors that mediate scotopic vision, one would expect the sensitivity thresholds of each to be similar. Instead, the circadian system is far less sensitive to light when compared to the visual system. Furthermore, there is an apparent divergence of light sensitivity amongst non-image forming pathways subserved by the SCN, as it requires roughly 25 times more light to phase shift the hamster locomotor rhythm than to suppress hamster pineal melatonin (Nelson and Takahashi 1991). In subsequent work, it was shown that there is also an optimum duration of light stimulation for maximal phase-shifting which is much longer than optimal durations of light for visual perception. When the total number of photons was kept constant by varying light intensity, hamster locomotor rhythms phase shifted best to 300 s stimulation compared to 30 s or 3000 s (Nelson and Takahashi 1991). Taken together, these observations demonstrate that while light is the salient stimulus for both circadian and visual photoreception, the two systems are optimized for the types of light stimuli most relevant to their functions.

Cellular Mechanisms of Photoentrainment in the SCN

Immediate Early Genes

Progress in understanding how light might induce changes in the mammalian molecular clock began with the discovery that light stimuli during the subjective night cause changes in SCN expression of the immediate-early gene (IEG) *c-fos* (Aronin et al., 1990). As immediate early genes couple transient stimuli to gene regulation in the cell nucleus, *c-fos* induction by light suggested a mechanism by which light could control nuclear events like gene expression in clock neurons. When a light pulse is given in the subjective night, Fos expression increases rapidly in parallel with the expression of another IEG, *jun*. Fos and Jun dimerize to make AP-1 transcriptional complexes which can then control the transcription of target genes.

C-fos mRNA reaches peak levels thirty minutes after light exposure, with peak Fos protein levels following 1-2 hours after light stimulation (Kornhauser et al., 1990; Rusak et al., 1990). Fos expression and light-induced phase-shifting of behavioral rhythms in the rodent are equally sensitive to light, suggesting that *c-fos* is an important molecular link between light input to the SCN and its subsequent regulation of circadian output rhythms (Kornhauser et al., 1990). Additionally, it was established that in hamster, *c-fos* is not induced by light during the dead zone, highlighting that it mediates phase-shifting during the night when the animal's circadian system is sensitive to light (Kornhauser et al., 1990). *C-fos* transcriptional rhythms are not only helpful in understanding the molecular underpinnings of the clock, but also supply scientists with a molecular immunohistochemical marker by which to measure the period and phase of circadian rhythms in the SCN.

Since the discovery that *c-fos* expression in the SCN is regulated by light, other upstream signaling molecules required for c-fos induction have been identified. There is a calcium/cAMP response element (CaCRE) 60 basepairs upstream of the transcription start site in the *c-fos* promoter. The CRE binding protein CREB binds to the CaCRE sequence and, when phosphorylated (P-CREB), initiates the transcription of *c-fos.* Because both the cAMP dependent kinase PKA as well as calcium-dependent calmodulin kinase (CaMK), can phosphorylate CREB, it can be said that both calcium and cAMP signaling pathways converge on CREB to regulate *c-fos* transcription.

Retinal Input: Calcium and cAMP pathways converge in SCN-projecting RGCs

The terminals of SCN-projecting RGCs release both glutamate and the neuropeptide PACAP, which activate calcium and cAMP signaling pathways, respectively (Hannibal et al., 1997). Evidence suggests that the two molecules are co-stored, and potentially co-released, from the same RHT terminals (Hannibal et al., 2000). Although glutamate and PACAP are released by SCN-projecting RGCs in response to light, they have different effects on their SCN targets. As deafferenting the SCN from both the raphe and the IGL does not affect entrainment, inputs from the RHT are alone sufficient for entrainment by glutamate and light.

Glutamatergic synaptic input is required for phase-shifting to light, as intraperitoneal injections of NMDA receptor antagonists abolished light-induced phase-shifting of wheel running rhythms in both wild type and *rd/rd* mice (Colwell et al., 1991). *In vitro* studies demonstrated that direct glutamate application to rat SCN slices phase shifted SCN neuronal firing rhythms during the subjective night, but not during the subjective day (Ding et al., 1994). And finally, application of glutamate receptor

antagonists (NMDA and non-NMDA) to the hamster SCN, *in vivo,* is sufficient to block light-induced phase shifts and to decrease Fos immunoreactivity by 50%. Moreover, the reduced SCN Fos immunoreactivity was distributed unevenly, with the dorsolateral SCN containing higher levels of Fos label compared to the retinorecipient region (Vindlacheruvu et al., 1992). These studies demonstrate that glutamatergic input from SCN-projecting RGCs is required for photic stimuli to (1) phase-shift behavioral rhythms, (2) phase-shift SCN firing rhythms, and (3) induce Fos expression specifically in retinorecipient SCN neurons. Additionally, the study by Ding et al. indicates that the dead zone during the subjective day is not caused by a change in retinal afferent signaling to the clock, but is due instead to insensitivity of the SCN to glutamatergic signaling.

When supplied at relevant circadian times, glutamate affects cyclic transcription and translation in SCN cells via the molecular events discussed previously. SCN-projecting RGCs release glutamate onto SCN neurons that contain both AMPA and NMDA receptors in their postsynaptic membranes. This glutamatergic input activates AMPA receptors, depolarizes the SCN cell membrane, and relieves the NMDA channel magnesium block. The influx of calcium through NMDA receptors is essential for CaM, CaMK, and P-CREB activation, and is required for the transcription of IEGs and of many clock genes. Following a pulse of glutamate in the subjective night, neurons in an SCN slice will express P-CREB within 15 minutes and Fos within an hour.

PACAP, which is also released by cells of the RHT, binds to adenylate cyclase (AC)- coupled VPAC2 and PAC1 receptors, increasing cAMP levels. PACAP, like cAMP phase advances the clock when applied during the subjective day. Phase advancement by PACAP is blocked by cAMP antagonists (Hannibal et al., 1997).

Additionally, PACAP modulates glutamate signaling during the subjective night. PACAP delivered to the SCN enhances the phase delays induced by glutamate pulses in the early subjective night and blocks phase advances induced by glutamate pulses in the late subjective night (Chen et al., 1999). The mechanism by which PACAP signaling modulates glutamatergic signaling in SCN neurons is not yet well understood. Calcium imaging studies by Dziema et al. suggest that PACAP potentiates the glutamate response of individual SCN neurons by enhancing L-type calcium currents through a MAP kinase pathway. Both nimodipine and the p42/44 MAP kinase inhibitors PD 98059 and U0126 blocked the potentiation of the glutamate response (Dziema and Obrietan 2002).

In summary, light input to the retina activates the release of glutamate and PACAP onto postsynaptic SCN neurons, to which the oscillator responds differently at different circadian times. These two types of inputs unleash a combination of calcium and cAMP signaling cascades that regulate the transcription of IEGs and clock genes. To date the "gate" in the SCN that causes the retinorecipient neurons to be cyclically sensitive to glutamate and PACAP is not well understood. However, the complex interactions of these two signaling pathways that converge on the same SCN neurons are made only more complex when one considers the breadth of afferent input arising from other hypothalamic and extrahypothalamic regions that also modulates retinorecipient SCN neurons.

Masking

There is a distinction between "entrainment," in which core components of the central clock are affected by the entraining stimulus – and "masking," in which the stimulus, independent of the clock, has a direct effect on the organism's physiology or

behavior. Examples of each can be discussed with respect to light and pineal melatonin secretion. SCN modulation of pineal melatonin output is the mechanism by which circannual reproductive rhythms discussed above are generated, as well as diurnal rhythms in the sleep/wake cycle.

Light input from the retina reaches the pineal gland via a polysynaptic pathway that first synapses in the SCN. SCN neurons containing GABA and AVP project to and inhibit AVP and oxytocin-containing neurons of the paraventricular nucleus (PVN). At this synapse sign inversion occurs so that high frequency firing in the SCN during the day leads to *inhibition* of pinealocytes and melatonin production. Neurons of the PVN then project to intermediolateral (IML) cells of the upper thoracic spinal cord. IML neurons innervate the superior cervical ganglia (SCG) whose neurons send a direct projection to the pineal gland. Studies have shown that the SCG-pinealocyte synapse is excitatory as SCG stimulation induces melatonin synthesis (Simonneaux and Ribelayga 2003).

Rhythmic SCN-driven noradrenergic input by the SCG drives rhythmic melatonin expression in the pinealocyte by modulating the transcription of N-acetyltransferase (AA-NAT), an enzyme required for melatonin synthesis. Noradrenergic input into the pineal activates β_1-adrenergic receptors (AR) which in turn activate G_s coupled adenylate and guanylate cyclases (AC,GC), increasing intracellular cAMP and cGMP, respectively. Pinealocytes also contain α-1 ARs whose stimulation by NE (1) potentiates the β-2 receptor-mediated response through a PKC/CaM dependent mechanism and (2) increases cGMP by nitric oxide synthetase activation, nitric oxide production, and stimulation of GC. The consequent 100-fold increase in cAMP and cGMP concentrations in addition to the parallel increase in intracellular calcium activate PKA and several transcription

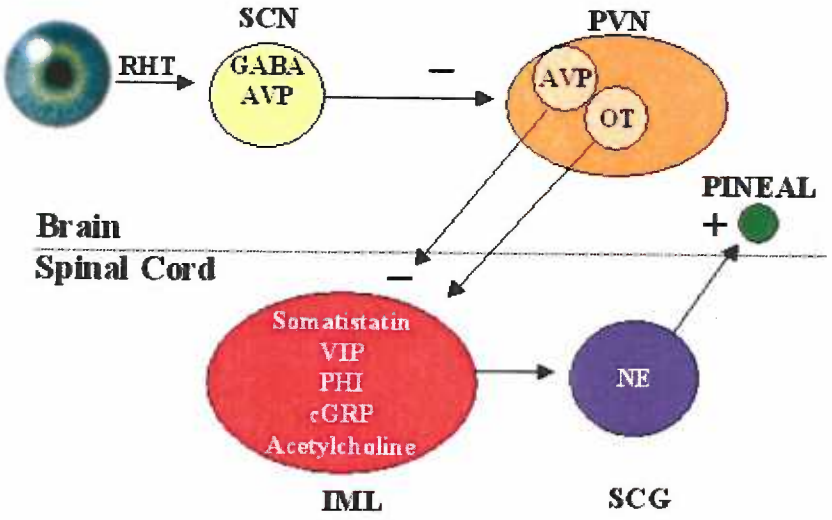

FIGURE 15

Polysynaptic pathway regulating melatonin secretion from the retina to the pineal gland via the SCN. Photic input from RGCs project to GABAergic and VIP-containing neurons in the SCN via the RHT. GABAergic and AVP-SCN neurons project to and inhibit (-) AVP and OT containing neurons in the PVN. These PVN neurons project to the IML cells in the spinal cord. Primarily, cholinergic IML neurons innervate the SCG, although neurons containing SST, VIP, PHI, cGRP might also innervate the SCG. Adrenergic SCG cells drive melatonin synthesis in target pinealocytes.

Abbreviations: PVN, paraventricular nucleus; OT, oxytocin; PHI, histidine isoleucine peptide; cGRP, calcitonin gene-related peptide; IML, intermediolateral; SCG, superior cervical ganglion; NE, norepinephrine.

factors, including CREB, that increase transcription of AA-NAT. The rhythmic transcription of AA-NAT is driven by the upstream rhythms in SCN synaptic input to the PVN that result from light-induced changes in SCN cell gene expression. The phase and period of the central clock in the SCN is therefore the pacemaker for the pineal melatonin rhythm.

While pineal melatonin secretion is under the control of the SCN, this control is overridden by nighttime light stimulation via the same pathway in Figure 15. Before any of the transcriptional events mediated by ARs in the pinealocyte occur, rodent pineal

melatonin secretion is acutely suppressed following a light flash at night. This immediate effect of light, known as masking, is independent of the core oscillator in the SCN. Acute melatonin suppression is thought to arise from the sudden cessation of norepinephrine (NE) input into the pineal with light stimulation. The consequent drop in cAMP levels reduces PKA activity. PKA not only stimulates the transcription of AA-NAT, but it also phosphorylates the enzyme which protects AA-NAT from cytosolic proteosome degredation (Gastel et al., 1998). The rapid turnover of AA-NAT mediates the acute reduction in melatonin synthesis that is seen within minutes of a light pulse during subjective night (Simonneaux and Ribelayga 2003). In summary, light has two effects on pineal circadian rhythms in the mammalian system: light entrains the oscillatory cells in the SCN that control rhythmic pineal melatonin synthesis, and through masking, light directly suppresses melatonin synthesis. Both of these effects of light are mediated by the RHT and are transduced by the same upstream population of retinal photoreceptors.

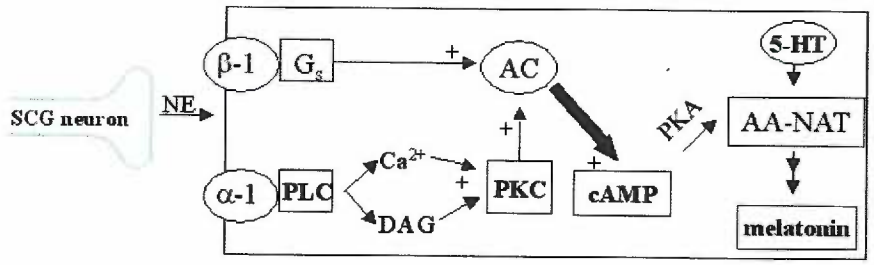

FIGURE 16

Adrenergic input to the pinealocyte induces melatonin synthesis.

Schematic of adrenergic signaling by SCG neurons in the pinealocyte. NE activates PLC-coupled–α-1 and Gs-coupled-β-1 metabotropic receptors. Stimulation of both receptor subtypes increases cAMP leading to PKA-dependent CREB phosphorylation and transcriptional activation of the melatonin biosynthetic enzyme AA-NAT.

Photoreception

In mammals light is detected in the eye and is transduced into an electrical signal for subsequent processing by two distinct systems. The visual system faithfully constructs a neural representation of the organism's physical environment so that it can find food, avoid predators, identify mates, and accomplish myriad other tasks that promote its survival. The circadian system generates physiological and behavioral rhythms in an organism, and synchronizes those rhythms with the solar cycle in order to promote the organism's survival. The visual and circadian systems differ in that the visual system is image-forming and requires high spatiotemportal acuity, while the circadian system is non-image forming, and primarily detects low acuity temporal changes in overall luminance. It is not surprising then that both the photoreceptors and photopigments used by each system are specialized for their respective functions.

Vertebrate Rod Photoreception

Vertebrate visual phototransduction occurs in the rod and cone photoreceptor cells in the outer nuclear layer of the retina (McNaughton 1990). Rhodopsin, the photopigment expressed by rod photoreceptors, is composed of the chromophore retinal and an opsin apoprotein. A single photon photoisomerizes one 11-*cis* retinal molecule to its all-*trans* isoform catalyzing the activation of a heterotrimeric G protein (transducin) by guanine nucleotide exchange of GTP for GDP. Transducin in turn activates a phosphodiesterase that induces the degradation of cyclic GMP (cGMP). Decreasing the concentration of intracellular cGMP results in the closure of non-selective, cation permeant, cyclic nucleotide gated (CNG) channels and hyperpolarizes the photoreceptor. The remaining

four classes of retinal neurons, including RGCs, serve to relay and process the signal generated by photoreceptors.

Circadian Photoreception

Melanopsin

Several observations within the circadian field challenged the long held assumption that the circadian system borrows the rod and cone photoreceptor pathways of the visual system to track time of day and year. First, a retinally degenerate mutant mouse, (*rd/rd*) that was visually blind based on electroretinogram and behavioral studies, phase-shifted to light as well as wild type mice. Due to a nonsense mutation in the β–subunit of the rod specific cGMP phosphodiesterase, rods in the *rd/rd* mouse undergo premature cell death that is complete by the age of 60-70 days, providing strong evidence that the rod photoreceptors in the rod-dominant mouse retina are not necessary for normal circadian function (Foster et al., 1991; Provencio et al., 1994). The murine retina contains two types of cone photoreceptors, those sensitive to UV light (λ_{max}= 359 nm) and those sensitive to green wavelength light (λ_{max}= 508 nm). To eliminate the possibility that surviving cone photoreceptors (which themselves are severely degenerated from the *rd/rd* mutation but are not completely eliminated) are not mediating the phase-shifting response, Freedman and colleagues constructed a second murine mutant carrying both of the trans-genes *rdta* and *cl.* The *rdta* mutation causes the specific ablation of rod photoreceptors while the *cl* gene causes selective ablation of all green cones and most UV cones. Mice that were *rdta/cl* showed no immunocytochemical or mRNA staining for opsin proteins or message, and still phase-shifted to 509 nm light normally. Enucleated

animals did not phase-shift (Freedman et al., 1999). With this study, it was confirmed that murine photoentrainment was not dependent on rod or cone photoreception, and that another ocular photoreceptor was sufficient to mediate phase-shifting behavior. These studies were consistent with observations of blind people in which the pathways mediating vision and circadian photoentrainment appeared to be separate. Some blind patients were still able to photoentrain and to suppress melatonin secretion normally, despite an apparently complete loss of visual function (Czeisler et al., 1995).

A second set of studies that began in 1998 revealed a candidate circadian photopigment in *rd/rd* and *rdta/cl* mice. The system studied was the *Xenopus* dermal melanophore which disperses its pigment granules, melanosomes, to the periphery of the melanophore when illuminated. By screening a *Xenopus* cDNA library, Provencio et al. identified a novel opsin which they named melanopsin. Melanopsin had structural similarities to other opsins including an extracellular amino terminus, seven transmembrane (TM) domains, a lysine in the 7^{th} TM domain for Schiff's base linkage to the chromophore, and 2 cysteines in the 2^{nd} and 3^{rd} TM loops for stabilization of the tertiary structure by disulfide bridge formation. *In situ* hybridization demonstrated that melanopsin transcripts were found in the tadpole eye, iris, preoptic area, and SCN (Provencio et al., 1998). They also determined based on sequence analysis that melanopsin more closely resembled invertebrate opsins than vertebrate opsins as (1) melanopsin shared 39% amino acid sequence with octopus rhodopsin compared to 30% with vertebrate opsins (2) melanopsin had an aromatic residue (Tyr-103) in its third TM helix thought to stabilize the Schiff's base (3) melanopsin had an insertion in its third cytoplasmic loop as invertebrate opsins do.

Provencio et al. next cloned human melanopsin and determined that it is expressed exclusively in the eye, and not in the pineal or in any other deep brain structures. They also cloned mouse melanopsin and generated an *in situ* hybridization probe that signaled melanopsin message in the mouse inner nuclear and ganglion cells layers of the retina. Using human melanopsin primers, they developed a probe that labeled monkey melanopsin mRNA in the inner nuclear layer of primate retina. No melanopsin transcript was found in the outer nuclear layer of the retina where the photoreceptors reside (Provencio et al., 2000). Based on the sites in which melanopsin was found in the tadpole eye and brain, and the layers in which it was expressed in the mammalian retina, they suggested that melanopsin might function as a circadian rather than a visual photopigment.

Several groups have since shown in more detail which retinal neurons express melanopsin and to what brain sites those neurons project. Using a combination of FluoroGold injections into the SCN and *in situ* hybridization of melanopsin probe in the retina, Gooley et al. (2001) were the first to demonstrate that the neurons in the murine retina which express melanopsin are the same cells that project to the SCN via the RHT. The PACAP containing RGCs from which the RHT arises also express melanopsin (Hannibal et al., 2002a). Immunofluorescent labeling of flat mount mouse retina by Provencio et al. (2002b) showed that the melanopsin-expressing RGCs had the same anatomical profile as the SCN-projecting RGCs that Moore et al. (1995) described in the rat retina and that Pu (1999) described in the cat retina. Because melanopsin immunoreactivity was found not only on the cell bodies of some RGCs, but also along their entire dendritic tree, the network of melanopsin positive cells was termed a

"photoreceptive net" (Provencio et al., 2002b). However, melanopsin expressing RGCs had not yet been shown to be intrinsic photoreceptors.

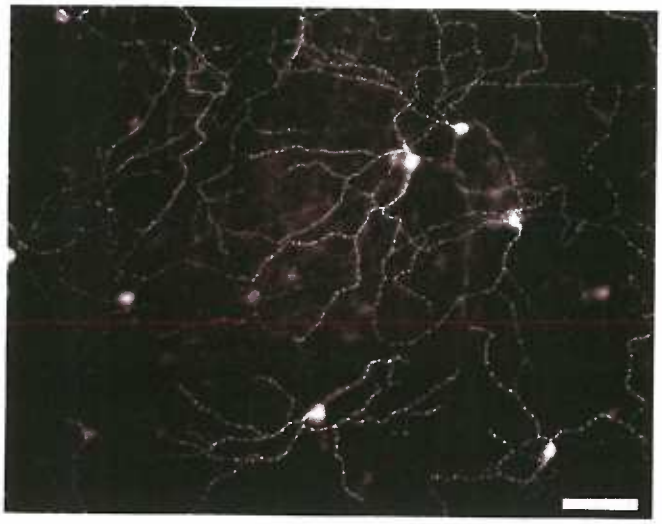

FIGURE 17

The photoreceptive net in the mouse inner retina. Immunofluorescent labelling of melanopsin containing retinal ganglion cells on a flat mount of mouse retina reveals an extensive network of immunopositive dendrites. Scale bar, 100 μm (Provencio et al., 2002b).

In a detailed study investigating the architecture and projections of melanopsin positive RGCs, Hattar et al. targeted *tau-lacZ* to the mouse melanopsin gene locus. This strategy allowed them to visualize the presynaptic terminals of melanopsin expressing RGCs and to elucidate their targets (Hattar et al., 2002). The translated fusion protein consisted of β-galactosidase fused to a signal sequence from the microtubule-associated protein tau. In heterozygous animals, cells that expressed melanopsin also expressed lacZ. The signal sequence permitted transport of the fusion protein down the axon into presynaptic terminals. Subsequent X Gal staining was used to visualize fusion protein distribution in the soma, axon, proximal dendrites, and synaptic terminals. Hattar et al. showed that melanopsin positive RGCs project to several areas including the SCN, the IGL, the ventral LGN, and the OPN in the pretectum. The discoveries that melanopsin was a good marker for SCN-projecting RGCs and that the RGCs bearing melanopsin projected to other brain sites involved in normal circadian rhythms, suggested that (1)

melanopsin bearing RGCs are the circadian photoreceptors in the inner retina that allow the *rd/rd* mouse to entrain and (2) melanopsin may be the surviving photopigment in the *rd/rd* mouse that mediates photoentrainment.

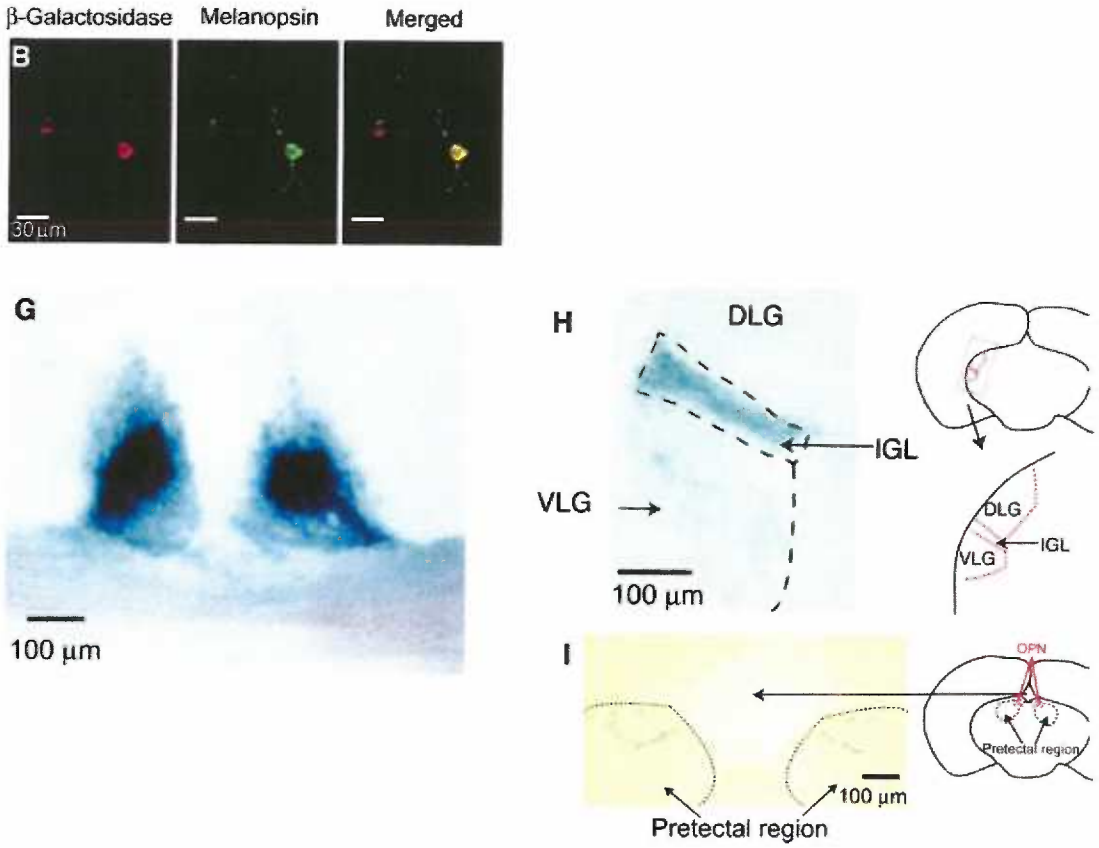

FIGURE 18

β–galactosidase and melanopsin expression in mice with *tau-lacZ* insertions into the melanopsin gene locus.

(**B**) Colocalization of β-galactosidase and melanopsin immunoreactivities in a flat-mounted retina from a +/- mouse. (Left) β-Galactosidase labeling. (Middle) Melanopsin labeling. (Right) Merged image. (**G**) Coronal section of the +/- brain showing blue optic nerve fibers converging to, and innervating, the SCN bilaterally. (**H**) Coronal section of the +/- brain showing uniform blue-labeled innervation of the left IGL and scattered innervation of the VLG. The DLG shows no labeling. (**I**) Coronal section of the +/_ brain showing innervation of the pretectal region. The blue staining corresponds approximately to the OPN, demarcated in red on the right. DLG, dorsal lateral geniculate; VGL, ventral lateral geniculate; IGL, intergeniculate leaflet; OPN, olivary pretectal nucleus. Modified from Figure 3 (Hattar et al., 2002)

RGCs from which the RHT arises

The first studies to examine the retinal ganglion cells (RGCs) that give rise to the RHT were undertaken in the hamster (Pickard 1980; Pickard 1982). After injecting the SCN with horseradish peroxidase to retrogradely label SCN-projecting ganglion cells, he reported that 0.1% of RGCs contribute to the RHT and that they were evenly distributed across the hamster retina. Subsequent work by Pu revealed that SCN-projecting RGCs in the cat retina are similar in morphology to cat γ RGCs, described first by Boycott and Wässle (Boycott and Wassle 1974; Pu 1999). Both SCN-projecting and γ RGCs have small cell bodies, only 3-4 primary dendrites, sparse dendritic branching, and dendritic trees that can span over 1 mm of retina.

In the rat, SCN-projecting RGCs correspond morphologically to a population designated "type III" by Perry (Berson et al., 2002; Moore et al., 1995a; Warren et al., 2003). Similar to the γ RGC in the cat, rat Type III RGCs are characterized by small cell bodies, 1-3 primary dendrites that stratify in the inner aspect of the inner plexiform layer, and large dendritic spreads (Perry 1979). SCN-projecting RGCs are more numerous in the rat retina than in the mouse or hamster, and are estimated to comprise between 1 and 2% of the total RGC population. They are relatively evenly distributed, with a slightly higher density in the superior temporal quadrant (Moore et al., 1995b). With the exception of total number which seems to vary with species, the descriptions of SCN-projecting RGCs, both in terms of distribution and anatomy, align nicely with the those of melanopsin positive cells reported in the mouse, rat, cat, primate, and blind subterranean mole rat (Berson et al., 2002; Hannibal et al., 2002b; Provencio et al., 2000; Pu 1999).

Prior to investigation of the intrinsic light sensitivity of SCN-projecting RGCs in the Berson laboratory, little was known about the physiology of these neurons. The only study which specifically addressed the physiology of SCN-projecting RGCs was carried out by M. Pu. In these experiments, SCN-projecting RGCs in young adult cats were retrogradely labeled by injecting fluorescent microspheres into the SCN (Pu 2000). Using an extracellular recording electrode, he successfully recorded light responses from nine cells, and all of them displayed sustained firing throughout the duration of the light stimulus. Eight of nine cells showed ON-center receptive field properties, and one showed ON-OFF-center receptive field properties. The numbers of each receptive field type were unexpected as morphological data suggested that the majority (45%) of SCN-projecting RGCs stratify in the ON layer, only 15% stratify in the OFF layer, and 40% stratify in the both the ON and OFF layers (Pu 1999). It is not clear why ON-surround cells were overrepresented, but the small sample size may have played a role. Pu also reported that of the five cells that underwent spectral tuning analysis, 3 of them exhibited a λ_{max} at 500 nm, while the other two maximally responded at 560 nm and 575 nm. As photoreceptor input was not blocked in this study, it was unclear whether rods, cones, or a different photoreceptor containing the putative photopigment melanopsin might be driving the light responses.

Berson et al. were the first to show that SCN-projecting RGCs are intrinsically sensitive to light (Berson et al., 2002). In the presence of a cocktail of antagonists to a variety of receptors (GABA, NMDA, AMPA/Kainate, metabotropic glutamatergic, nicotinic, glycinergic), bright white light elicited a depolarization in SCN-projecting RGCs that was sufficient to drive low frequency action potentials. The latency between

stimulus and response onsets was long, on average several seconds to one minute. The latency between stimulus onset and peak response varied between 10-20 seconds and was inversely proportional to the intensity of light used. Most striking in contrast to light responses of rod and cone photoreceptors, was that the light responses of SCN-projecting RGCs did not bleach. A plateau depolarization above baseline was maintained for the entirety of a 20 minute light stimulus. Furthermore, a single cell could respond to multiple sequential light stimulations without replenishment of the chromophore by the experimenter.

Several reports examining the role that melanopsin plays in photoentrainment, the pupillary light reflex, and behavioral phase-shifting followed. Using melanopsin knockout mice (*Opn4* -/-) generated in the lab of Provencio, Panda et al. (2002) demonstrated that *Opn4* -/- mice have normal free running rhythms, entrain to a light/dark cycle, and exhibit normal masking responses to light delivered during subjective night, but have significantly smaller phase shifts than wild type mice to a light pulse delivered during subjective night. Furthermore, the FRP of wild type mice was indistinguishable from that of *Opn4* -/- mice in constant darkness, but significantly longer in constant light (see Figure 19). FRP in constant light is considered to reflect both the period of the intrinsic oscillator and the influence that light input pathways have on the oscillator. In constant light, FRPs are always longer than they are in constant darkness. The finding that the *Opn4* -/- mice had a shorter FRP in constant light indicates that melanopsin is indeed impacting a light input pathway. These data suggested that there are either compensatory or complementary photoreceptive systems in place that cannot entirely accommodate for the loss of melanopsin in the *Opn4* -/- mouse.

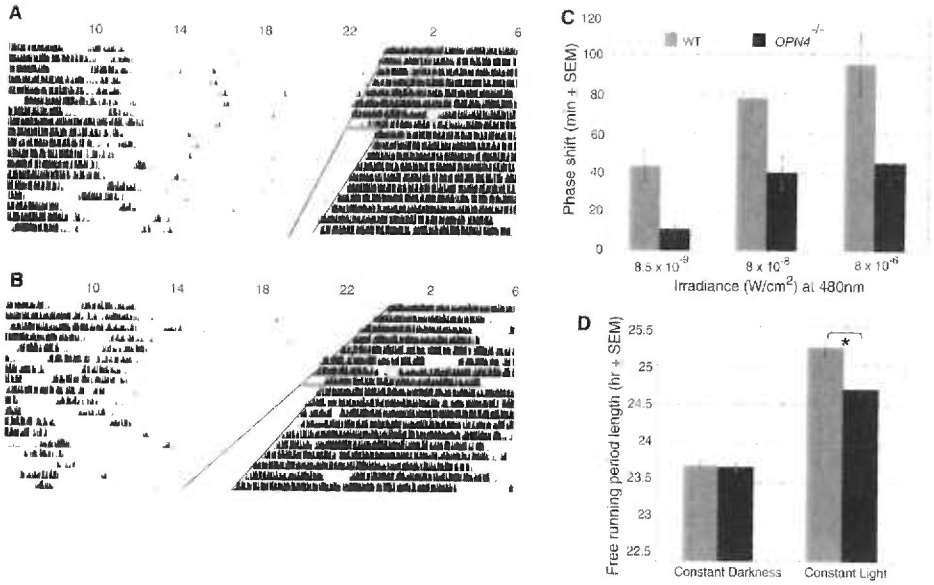

FIGURE 19

Attenuated circadian light input in *Opn4* $^{-/-}$ mice.

A single 15-min pulse of monochromatic light of 480 nm (circle) was administered 3 hours after the onset of activity, which produced a smaller phase shift in the activity rhythm of the *Opn4* $^{-/-}$ animal (**B**) than in the wild-type littermate (**A**). (**C**) The light-induced phase-shift defect in the null mice is evident at all irradiance levels tested. Means (±SEM) of phase-shift measurements for the *Opn4* $^{-/-}$ mice (black) and the littermate wild-type mice (gray) are shown (n = 5 to 17 mice per group).(**D**) An attenuated lengthening of period was observed in *Opn4* $^{-/-}$ mice (black) relative to wild-type mice housed in constant light but not in constant darkness. Asterisk indicates a statistically significant difference ($P < 0.05$). Modified Figure 2 (Panda et al., 2002)

The pupillary light reflex was also functional, but attenuated, in melanopsin knockout mice. Using the tau-LacZ mouse developed by Hattar and colleagues, Lucas et al. (2003) demonstrated that the pupillary light reflex in the melanopsin homozygous knockouts were normal at low irradiances, and attenuated at high irradiances. They confirmed that pupillary constriction by carbachol application was normal in the knockout mice. By adding the irradiance response relations for the pupillary reflex among melanopsin homozygous knockouts and rodless coneless mice (*rd/rd cl*) they

showed that the full complement of all three classes of photoreceptors accounts for a wild type pupillary reflex (Lucas et al., 2003).

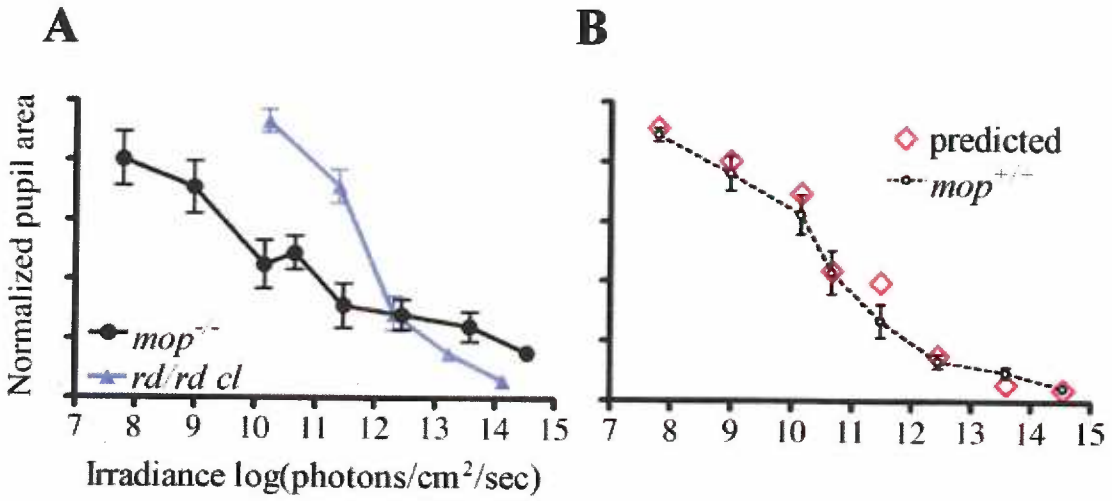

FIGURE 20

Irradiance-response relations for the pupil reflex for melanopsin knockout mice and rodless coneless mice summate to predict the wild type irradiance response relation.

The minimum pupil area (mean +/- SEM; normalized with respect to with respect to dark-adapted value) attained during exposure to 1-min 480-nm monochromatic light is plotted against irradiance. (A) Comparison of relations for *mop* -/- and *rd/rd/cl* mice (4-6 animals each irradiance). (B) The wild-type irradiance-response relation can be well predicted by summing the relations from *mop-/-* and *rd/rd cl* mice Modified Figure 3 (Lucas et al., 2003).

Panda et al. (2003) went on to show that an *Opn4* -/- mouse on an *rd/rd* background eliminated all photoentrainment, pupillary light reflexes, photic suppression of the AANAT transcript, and masking of locomotor activity by light.

That rods and cones contribute to the circadian system's responsiveness to light helped explain some discrepancies between the behavioral and *in vitro* literature. A spectral tuning analysis of individual SCN-projecting RGC responses to various wavelengths of light indicated that the λ_{max} was 484 nm and that the photopigment responsible for the intrinsic light response was most likely a retinaldehyde-based opsin,

like melanopsin (Berson et al., 2002). The λ_{max} of 484 nm was 15-25 nm blue-shifted from the λ_{max} values obtained by behavioral phase-shifting experiments already described (Provencio and Foster 1995; Takahashi et al., 1984). The studies by Panda and Lucas suggested that rod and cone input to the circadian system might explain residual circadian function in the absence of melanopsin, and might also account for a shifted action spectra in the whole animal. To resolve this issue, Hattar et al. (2003) constructed action spectra for rodless coneless (*rd/rd/ cl*) mice, with an intact melanopsin system. The λ_{max} at which rodless coneless mice phase-shifted their locomotor activity was 481 nm, quite close to the λ_{max} of 484 nm at which SCN-projecting RGCs maximally responded to light. Hattar and colleagues inserted the previously described tau-LacZ construct into the melanopsin gene to confirm that the melanopsin system was the only photoreceptor system mediating the surviving phase-shifting response. By generating a triple homozygous knockout mouse lacking rods, cones, and melanopsin, (*Gnat1 -/-, Cnga3 -/-, Opn4 -/-*), the pupillary light reflex and photoentrainment were completely eliminated, in spite of normal RGC development, normal targeting of Xgal stained cells to the SCN, IGL, and OPN (see Figure 21), and normal pupillary response to carbachol. This study confirmed that together, rods, cones, and intrinsically sensitive RGCs containing melanopsin account for all of the circadian photoreception in mice.

Recent work demonstrating that SCN-projecting RGCs express a novel photopigment melanopsin and are intrinsically sensitive to light suggest that they are not merely retinal neurons borrowed by the circadian system, but circadian photoreceptors evolved specifically for photoentrainment. The purpose of the work undertaken in this thesis was to gain a better understanding of the physiological properties and intrinsic light

responses of SCN-projecting RGCs.

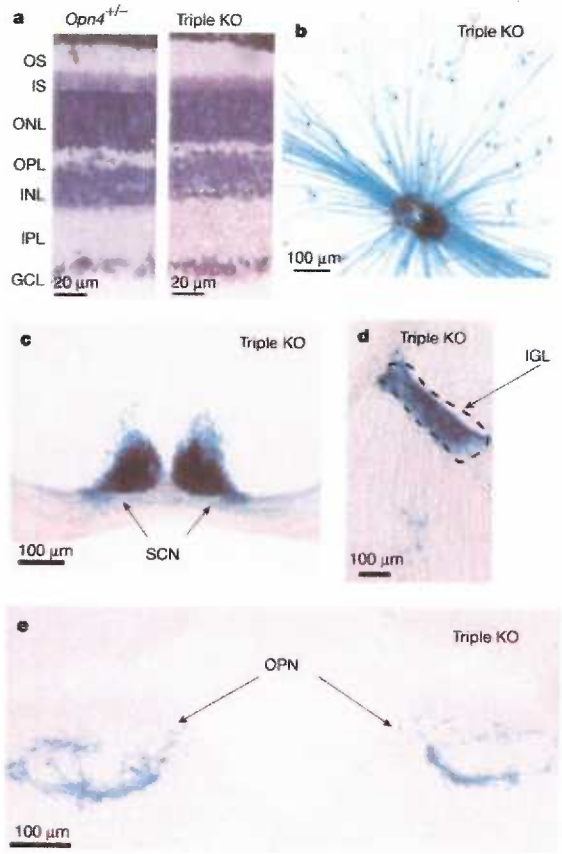

FIGURE 21

Normal retinal morphology and presence and central connectivity of melanopsin-expressing RGCs in triple-knockout (*Opn4 -/- Gnat 1-/- Cnga3 -/-*) mice.

a. Retinal cross-sections from *Opn4* +/- and triple knockout (KO) mice. Glemsa stain shows the various layers. Both are similar in morphology and thickness to wild type. GCL, ganglion cell layer; INL, inner nuclear layer; IPL, inner plexiform layer; IS, inner segment layer; ONL, outer nuclear layer; OPL, outer plexiform layer **b**. Flat-mount view of a triple KO retina stained with X-gal (blue). **c-e**, coronal sections of triple KO mouse brain showing normal innervation of the SCN, IGL and OPN byX-gal labeled axons (Hattar et al., 2003).

Course of Thesis

This thesis is divided into two parts. In the first, the properties of individual SCN-projecting RGCs are examined with the aim of determining if they are intrinsically sensitive to light and if they constitute a novel class of RGC in the mammalian retina based on their intrinsic membrane properties. In the second part, the identities of the signaling pathways and ion channels involved in the intrinsic light response are considered in more detail.

CHAPTER TWO

Intrinsic Light Responses of Retinal Ganglion Cells Projecting to the Circadian System

INTRINSIC LIGHT RESPONSES OF RETINAL GANGLION CELLS PROJECTING TO THE CIRCADIAN SYSTEM

Erin J. Warren[1, 2], Charles N. Allen[3], R. Lane Brown[4], and David W. Robinson[1]

Department of Physiology and Pharmacology[1], Neuroscience Graduate Program[2],

Center for Research on Occupational and Environmental Toxicology[3],

Neurological Sciences Institute[4],

Oregon Health & Science University, Portland OR 97239 U.S.A.

European Journal of Neuroscience 2003. 17: 1727-1735

ABSTRACT

In mammals, light entrainment of the circadian clock, located in the suprachiasmatic nuclei (SCN), requires retinal input. Traditional rod and cone photoreceptors, however, are not required. Instead, the SCN-projecting retinal ganglion cells (RGCs) function as autonomous photoreceptors and exhibit light responses independent of rod- and cone-driven input. Using whole-cell patch-clamp recording techniques, we have investigated the morphological and electrophysiological properties of this unique class of RGCs. Although SCN-projecting RGCs resemble Type III cells in form, they display strikingly different physiological properties from these neurons. First, in response to the injection of a sustained depolarizing current, SCN-projecting cells fired in a transient fashion, in contrast to most RGCs, which fired robust trains of action potentials. Second, in response to light, SCN-projecting RGCs exhibited an intensity-dependent transient depolarization in the absence of rod and cone input. This depolarization reached a peak within 5 seconds and generated increased spiking activity before decaying to a plateau. Voltage-clamp recordings were used to characterize the light-activated conductance that generated this depolarization. In response to varying light intensities, SCN-projecting RGCs exhibited a graded transient inward current that peaked within 5 seconds and decayed to a plateau. The voltage dependence of the light-activated current was obtained by subtracting currents elicited by a voltage ramp before and during illumination. The light-activated current displayed both inward and outward rectification and was unaffected by substitution of extracellular Na^+ with choline. In both respects, the intrinsic light-activated current observed in SCN-projecting RGCs resembles currents carried by ion channels of the transient receptor potential (TRP) family, which are known to mediate the light response of invertebrate photoreceptors.

INTRODUCTION

In mammals, light entrainment of the circadian clock in the suprachiasmatic nuclei (SCN) requires input from the retina (Johnson et al., 1988; Moore et al., 1995). However, traditional rod and cone photoreceptors are not required (Foster et al., 1991; Freedman et al., 1999). Instead, the retinal ganglion cells (RGCs) that project to the SCN seem to function as autonomous circadian photoreceptors. In striking contrast to their counterparts projecting to the primary visual targets (the dorsal lateral geniculate nucleus and the superior colliculus), SCN-projecting RGCs exhibit light responses independent of rod- and cone-driven synaptic input (Berson et al., 2002). Furthermore, the majority of these neurons express the novel photopigment, melanopsin (Provencio et al., 2000; Hattar et al., 2002; Gooley et al., 2001; Hannibal et al., 2002). As an obligate part of the neural pathway from the retina to the SCN, these RGCs play a critical role in generating and shaping retinal output to the circadian system.

The primary neural pathway from the retina to the SCN is the retinohypothalamic tract (RHT), which arises from a small subset (1-2 %) of RGCs (Moore et al., 1995; Pickard, 1985). In rats and cats, these SCN-projecting ganglion cells morphologically resemble the Type III or gamma RGCs (Boycott & Wassle, 1974; Fukuda, 1977, Perry, 1979; Pu 1999; Berson et al., 2002). Type III neurons are characterized by relatively small cell bodies and expansive dendritic fields (Perry, 1979; Wassle & Boycott, 1991). This morphology would seem ideal for the circadian system because it could survey the light intensity over a large sector of the retina. The most striking and novel property of SCN-projecting RGCs is an intrinsic sensitivity to light (Berson et al., 2002; Hattar et al., 2002). Using whole-cell patch-clamp techniques, Berson et al. (2002) recorded intrinsic

light responses from RGCs that were labeled with retrograde tracers following stereotaxic injection of the SCN. In response to light, SCN-projecting RGCs depolarized slowly, and generated increased spiking activity. The light response persisted in the presence of a formidable cocktail of synaptic blockers and in isolated cells, suggesting that it does not require synaptic input derived from excitation of classical rod and cone photoreceptors. Furthermore, the long response latency suggested that the depolarization was mediated by an intracellular signaling pathway. Under the same conditions, RGCs that were not labeled by the retrograde tracer from the SCN did not respond to light.

Due to their distinct functional role, RGCs mediating entrainment might be expected to have physiological properties that are markedly different from those mediating vision. While little is known about the intrinsic membrane properties of the RGCs that project to the SCN, the spiking properties and ionic conductances of enzymatically-dispersed rat RGCs projecting to the visual system have been examined using patch-clamp techniques (Lipton & Tauck, 1987; Karschin & Lipton, 1989). Typically, these neurons have a relatively high input resistance and a resting membrane potential around –60 mV. In the adult rat, all three types of RGCs produce trains of TTX-sensitive spikes in response to maintained depolarizing currents (Wang et al., 1997; Schmid & Guenther, 1999).

In the current study, we have examined unique aspects of the morphology and physiology of SCN-projecting RGCs that enable them to generate and propagate intrinsic light responses. While these neurons bear morphological resemblance to Type III neurons of the visual system, we show that they have markedly different physiological properties. Specifically, in addition to their previously reported intrinsic light sensitivity, SCN-

projecting neurons exhibit transient spiking patterns to maintained depolarizing currents and little synaptic input at their resting membrane potential. Most significantly, we show that the depolarization observed in response to light is mediated by the activation of an inward current with biophysical characteristics similar to those reported for members of the TRP family of ion channels.

METHODS

Stereotaxic Injection of Fluorescent Retrograde Tracers

Surgical procedures were carried out in compliance with guidelines from the National Institutes of Health, and in accordance with protocols approved by the Institutional Animal Care and Use Committee (IACUC) of Oregon Health & Science University. Because retinas from younger rats were more amenable to patch-clamp recording, we used six week old rats, weighing between 120 and 170 g. Fluorescent retrograde tracers (0.04 μm red Fluospheres, Molecular Probes, Eugene, OR) were injected into the SCN using a stereotaxic apparatus (Cartesian Designs, Inc., Sandy, OR) to enable unequivocal identification of RGCs projecting to the circadian system. Between two and ten days after injection, animals were killed by cervical dislocation following deep anesthesia with ether. After the eyes had been removed for electrophysiological recordings, the brain was removed and fixed by immersion in 4% paraformaldehyde for 24 hrs. The brain was subsequently sectioned on a Vibratome, and each section (200 μm) was carefully inspected to insure against possible injection of the optic chiasm, which lies directly below the SCN.

Electrophysiology and Light Stimulation of Retinal Wholemounts:

The anterior chamber of each eye was removed, and the retinas were gently peeled from the eyecup and stored in oxygenated EMEM (Hepes modification) at room temperature. To prepare a wholemount, a small piece of retina was cut from the whole and mounted on a piece of nitrocellulose filter paper with a 2-mm hole to provide access for the recording electrode. This preparation was placed in the recording chamber with the ganglion cell layer facing up. SCN-projecting RGCs were identified by the presence of fluorescent beads using epifluorescent illumination, and the membrane potential and light-activated currents were recorded using whole-cell patch-clamp techniques. Recordings were made at 22°C with an Axopatch 1D amplifier controlled by pClamp8 software via a Digidata 1320 interface (Axon Instruments). Data were low-pass filtered at rates between 1 (voltage-clamp) and 5 (current-clamp) kHz and digitized at rates between 2.5 and 10 kHz. Patch pipettes with tip resistances between 3 and 8 MΩ were pulled from borosilicate glass (Sutter Instruments). For current-clamp recordings, electrodes were filled with a solution containing (in mM): 5 NaCl, 110 KCl, 1 $CaCl_2$, 1 $MgCl_2$, 10 Hepes, 11 EGTA, 3 ATP, Lucifer Yellow (0.1%) and biocytin (2%), pH 7.4. The bath solution, continuously bubbled with oxygen, consisted of (in mM): 120 NaCl, 5 KCl, 3 $CaCl_2$, 2 $MgCl_2$ and 10 Hepes, 5 D-glucose, pH 7.4 (290-300 mOsm).

For voltage-clamp recordings, electrodes were filled with a cesium-based intracellular solution containing (in mM): 117 CsCl, 4 Mg-ATP, 0.3 Na_3GTP, 2 creatine phosphate (Na^+ salt); 10 Hepes, 5 K_4BAPTA, pH 7.4. The typical external solution contained (in mM): 120 NaCl, 6 KCl, 0.5 $CaCl_2$, and 10 Hepes, pH 7.4, and 500 nM TTX. The series resistance and cell capacitance were electronically compensated prior to

each recording. During light stimulation, cells were held at –60 mV unless otherwise noted. To determine the voltage-dependence of the light-activated current, a voltage ramp was applied from –100 to +100 mV over 1 s prior to light stimulation and during the peak response. All voltage-clamp data have been corrected for the junction potential.

Light Stimulation

Illumination was provided by a 100 W tungsten-halogen light source, and the intensity was reduced using a variety of neutral density filters. The intensity was determined using a radiometer (International Light) with a detector that had a flat response between 400 nm and 1000 nm. All light intensities are given in W/cm^2. For a point of reference, detector readings are given for a number of lighting environments: a well-lit room in a laboratory, 1.7×10^{-6} W/cm^2; an overcast December day in Oregon, 1.1×10^{-6} W/cm^2; a sunny December day in Oregon, 1.8×10^{-4} W/cm^2. All recordings were conducted in a dimly lit room with an average total irradiance of 2.3×10^{-9} W/cm^2. By using a calibrated thermocouple (Fluke) we determined that the broad-spectrum light used in the present study had no thermal effects on the recording chamber or the bath solution.

Morphological Analysis

At the end of each recording, a –200 mV hyperpolarizing potential was applied to facilitate diffusion of Lucifer Yellow and biocytin into the cell. Once adequate filling was achieved, the retina was fixed in 4% paraformaldehyde for 6-8 hours at 4°C. Following fixation, retinas were processed using a standard diaminobenzidine reaction (Vectastain ABC kit). SCN-projecting RGCs judged to be fully stained by the DAB reaction were analyzed using the Neurolucida neuronal reconstruction system

(MicroBrightField). The dendritic field areas (areas of influence) were calculated using the area of a complex polygon that encompasses the ends of the dendrites. The software application ImageJ (http: //rsb.info.nih.gov/ij/) was used to calculate the area of this polygon as well as its circularity (4π * [area of influence/perimeter^2]).

In-house software routines were used to convert the 2D structure of the neuron into polar coordinates to assess dendritic extent, dendritic distribution index, and the dendritic polarity index. These routines analyzed a black and white 2D image of a neuron (1600 x 1200 pixels) and calculated the polar coordinates for each black pixel that made up the soma and dendrites using the center of the soma as the origin (0,0). Therefore, thicker dendrites had a larger number of polar coordinates per unit length of dendrite than did finer ones. The dendritic extent was determined by summing the lengths of the longest dendrites in symmetrically opposite 30° (π/6 radians) regions of the dendritic field.

The dendritic distribution index was calculated by dividing the polar plot into 16 equal regions (π/8 radians), determining the number of black pixels contained in each region, and normalizing these values by the total number of pixels in the whole neuronal structure. The distribution index is the minimum number of whole regions required to account for 80% of the total dendritic structure. A value close to 1 indicates that the dendritic mass of a cell is evenly distributed around the soma, while a value close to 0 indicates that the majority of dendrites are restricted to single region. This value does not account for the distance of a particular part of the dendritic field from the soma, or the relationship between the dendritic masses of neighboring regions, but merely gives an indication of how tightly clumped dendrites are in regions of space around the soma.

The dendritic polarity index provides a quantitative analysis of how symmetrically distributed the dendritic tree is around the soma. In contrast to the distribution index, the polarity index takes into account both the location and the distance of each dendrite with respect to the soma. However, the polarity index does not give any information regarding the degree of dendritic clumping that may exist within the whole arbor. To calculate the polarity index, the polar coordinate of each pixel that comprises the dendritic tree was converted into a vector, with a distance and angle relative to the center of the soma. The vector angle was defined as the angle formed by a line connecting the point in the dendritic tree and the center of the soma with an arbitrarily oriented axis. A vector sum was then calculated to determine the resultant vector length and angle. This method cancels symmetrically opposed parts of the dendritic tree and the resultant vector length indicates the degree of polarity within the dendritic arbor. The resultant angle indicates the direction of polarization. By normalizing the resultant vector length by the sum of the lengths of all the vectors, it was possible to compare the degree of polarity across cells with different sizes of dendritic arbor. A neuron with a symmetrical dendritic tree, such as a starburst amacrine cell, would have a polarity index close to 0, whereas a very polarized cell, such as a cortical pyramidal neuron, would have a polarity index closer to 1. While the resultant angle provides information regarding the direction of polarity, the orientation of each neuron analyzed, and its location within the retina, was unknown. Therefore, in the present study a comparison of resultant vector angles across neurons was not meaningful.

Statistical Analysis

All values are given as the mean ± standard deviation. Significance was determined using the permutation test for paired differences.

RESULTS

Morphology of SCN-projecting RGCs

Figure 1A illustrates a successful injection of the SCN with fluorescent polystyrene beads. The site of injection showed a focal area of fluorescence that was entirely contained within 1-2 sections, consistent with a diameter of ~ 400 μm. Furthermore, there was no visible labeling in the optic chiasm (OX) or nerves. Figure 1C displays a retinal wholemount showing clear labeling of RGCs following injection of the SCN. Following a typical injection, we observed of 20 - 50 labeled cells per retina. This number represents only a fraction of the neurons reported to project to the SCN and probably reflects poor bead uptake. In addition, the injection site never encompassed the entire SCN, which also reduced the total number of labeled neurons one would expect to observe in the retina.

In contrast, control experiments were performed in which beads were injected directly into the optic chiasm (Fig. 1B). In these experiments, fluorescent beads were clearly visible in transit along the optic nerve, and the density of labeled cells found in the retina was substantially higher (Fig 1D). In all experiments the injection site was closely examined to confirm that the optic chiasm had not been injected with fluorescent beads.

Following recording, SCN-projecting RGCs were filled with biocytin, and the retina was processed using a standard DAB reaction. Figure 2A shows a photomicrograph of an SCN-projecting RGC from which a recording was made. A two-dimensional representation of a detailed reconstruction of this neuron by Neurolucida is shown in Figure 2B. The morphology exhibits many characteristics similar to those reported for Type III rat RGCs (Perry, 1979). The somal area of the cell was 204 $\square m^2$, and it had 2 sparsely branched primary dendrites with 17 branch points. The dendritic field covered a relatively large area of retina (extent: 587 μm; area: 132,057 μm^2). Similar detailed reconstructions were conducted on 5 fully filled SCN-projecting RGCs. On average, SCN-projecting RGCs had somal areas of 195 ± 5 μm^2 and 2.6 ± 0.6 primary dendrites with 14.0 ± 8.5 branch points. The area of influence ranged from 45,758 μm^2 to 457,640 μm^2. In addition, the dendrites of SCN-projecting RGCs were found to stratify in several different regions of the inner plexiform layer. Of the five reconstructed neurons one stratified in the inner lamina and two in the outer lamina of the inner plexiform layer (IPL) exclusively, while two others were found to be bi-stratified in both inner and outer lamina (Figure 2C). The average dendritic depths in the inner and outer laminas were 20.8 ± 3 μm and 9.8 ± 1 μm, respectively.

By plotting the 2D representation of each reconstructed neuron on polar coordinates relative to the center of the cell soma (Figure 2D), it was possible to determine the degree of symmetry by calculating the polarity index (c.f. Methods). In this neuron, the resultant vector had a non-zero resultant angle (red line) and a polarity index of 0.21, indicating that its dendritic arbor was biased towards an angle of 54 degrees relative to an arbitrarily chosen zero degree axis orientation (Figure 2D). The

average polarity index was 0.49 ± 0.3. The distribution of dendritic mass within the arbor was also assessed by determining the distribution index for each neuron (c.f. Methods). The average distribution index for SCN projecting RGCs was 0.5 ± 0.08 indicating that the dendrites were not evenly distributed around the soma but tended to be clumped together.

Intrinsic Membrane Properties of SCN-projecting RGCs

Successful current-clamp recordings were made from 18 SCN-projecting RGCs. The average resting potential was – 44.5 ± 6 mV. At the resting membrane potential, these neurons exhibited no spontaneous spiking activity (c.f. Figure 5), although small and infrequent spontaneous postsynaptic potentials (PSPs) were observed. Application of 400 ms maintained hyperpolarizing current pulses was used to assess the input resistance of SCN-projecting RGCs. The average input resistance was 860 ± 300 MΩ, determined by fitting a plot of the maximum change in membrane potential against the magnitude of injected current with a straight line. The membrane time constant for each neuron was calculated by fitting a single exponential function to the change in membrane potential resulting from a step hyperpolarizing current injection. The average membrane time constant recorded in response to a 45 pA hyperpolarizing maintained current injection was 40.5 ± 21 ms.

In response to injections of maintained depolarizing currents, SCN-projecting RGCs responded with either a single spike (29%) at stimulus onset or with sporadic firing (71%) throughout the stimulus irrespective of its magnitude (Figure 3A and 3B, respectively). The number of spikes elicited by a 900 ms maintained depolarization ranged from 1 to 6. While subsequently larger current injections initially increased the

number of spike elicited, above 35 pA of injected depolarizing current no further increases in spike number were observed. Analysis of individual spikes showed that action potentials generated by SCN-projecting neurons have a half-width of 1.12 ± 0.22 ms and maximum rates of rise and decay 97.86 ± 38.6 mV/ms and -78.12 ± 42.4 mV/ms, respectively.

In contrast to RGCs that project to the SCN, unlabeled RGCs exhibited markedly different spiking patterns in response to injection of a maintained depolarizing current. As shown by the typical recordings from Type I (Figure 3C) and Type II (Figure 3D) rat RGCs, neurons not projecting to the SCN responded in a sustained manner, with up to 10 spikes being elicited in response to a 900 ms maintained depolarization. In contrast to SCN-projecting RGCs, no response saturation was observed over the range of depolarizing current magnitudes used. Also, unlike SCN-projecting RGCs, Type I and II RGCs often exhibited robust spiking activity at their resting membrane potential as well as higher rates of PSPs (c.f Figure 5B).

Intrinsic Light Responses of SCN-Projecting RGCs

Current-clamp recording in combination with full-field illumination of the retina with a tungsten-halogen lamp was used to examine the intrinsic light sensitivity of SCN-projecting RGCs. The light responses exhibited by these neurons were characterized by a transient depolarization that reached a peak within 5 seconds and decayed steadily towards a plateau during illumination (n = 9 cells; Figure 4A). In response to the highest intensity light stimulus (5.8×10^{-5} W/cm^2), the amplitude of the light-induced depolarization was 14.44 ± 5.5 mV (n=9). The level of the plateau depolarization, measured 24 seconds into the light stimulus, varied between 20-80% of the peak

depolarization. RGCs selected at random did not respond to light under the same conditions (n = 13; Figure 4B), presumably due to bleaching of the rod and cone photoreceptors resulting from the extensive exposure to bright light during the dissection and epifluorescent scanning of the retina. This insensitivity to light was observed in all randomly selected RGCs whether they exhibited high levels of spontaneous activity or were quiescent at their resting membrane potential.

The magnitude of the depolarization and the number of resulting spikes were dependent on the intensity of the light stimulus (Figure 4C). In response to the lowest intensity used (2.6×10^{-6} W/cm^2), the cell exhibited a peak depolarization of 5.9 mV, which elicited 2 spikes. Increasing the light intensity 18-fold caused a peak depolarization of 10.2 mV, which elicited 38 spikes during the 25 s light exposure. We were unable to accurately determine threshold for the light response or demonstrate response saturation because the current experimental setup had a limited range of attainable light intensities (Figure 4D).

Characteristics of the Light-Activated Current in SCN-Projecting RGCs

To characterize the light-activated current that underlies the membrane depolarization, we made voltage-clamp recordings from SCN-projecting RGCs. In response to light, these neurons exhibited a transient inward current (Figure 5A, lower panel). Using maximal illumination (5.8×10^{-5} W/cm^2), the light-activated current developed slowly, with a time to peak of 5.35 ± 2.7 s and an average peak amplitude of -135.3 ± 100 pA (n = 8). After the peak, the current declined with a time constant of 10.9 ± 4 s (n = 6) to a plateau that was typically 20 – 80 % of the maximum. After the step of illumination was terminated, the current returned to its original resting level. The time

course of the light-activated current is similar to the membrane depolarization elicited in response to the same light intensity (Figure 5A, upper panel).

The voltage-dependence of the light-activated current was obtained by subtracting the currents elicited by a voltage ramp before and during light stimulation in the presence of 500 nM TTX (Figure 5B). The resulting light-activated current (Figure 5C) was inward and linear between -100 mV and -30 mV with a slope conductance of 1.85 ± 1.2 nS (n = 8). As shown by the typical cell in Figure 5C, there was little net current flow between –10 mV and +40 mV, however outward current was observed above +40 mV.

The contribution of Na^+ to the light-activated current was examined by substituting the extracellular Na^+ with choline to obtain solutions containing either 0 mM or 20 mM Na^+. In Figure 6A, the amplitude of the light-activated current recorded at –60 mV in reduced Na^+, is plotted as a percentage of the current amplitude recorded in 120 mM Na^+. The gray bars show data gathered where the amplitude of the light-activated current was first determined in 120 mM Na^+ before the extracellular Na^+ was lowered to 20 mM. The hashed bars represent data in which the amplitude of the light-activated current was first measured in 0 mM Na^+ and then in 120 mM Na^+. These data indicate that substitution of extracellular Na^+ did not dramatically reduce the amplitude of the light-activated current (184 ± 64%). The differences in current amplitude shown in Figure 6A can be attributed to run down of the light-activated current during the course of the experiment. In 8 of 9 cells recorded, the amplitude of the light-activated current recorded first were greater than that recorded subsequently, regardless of the solution. Moreover, the permutation test for paired differences indicated that the amplitude of the

light-sensitive current in low Na^+ was not significantly different ($p = 0.125$) from its amplitude in a normal extracellular solution (120 mM Na^+).

Figure 6B shows the I-V characteristics of the light-activated current obtained first in 0 mM Na^+ (red trace) and then in 120 mM Na^+ (black trace). As discussed above, there was an appreciable rundown in the amplitude of the light-activated current over time. Therefore, to facilitate comparison, the I-V obtained in 0 mM Na^+ has been scaled so that its amplitude at +100 mV matches that obtained at +100 mV in 120 mM Na^+. Despite this dramatic reduction in extracellular Na^+, the I-V characteristics of the light-activated current was relatively unchanged in this and all other cells examined ($n = 4$).

DISCUSSION

The photic information required for vision and circadian entrainment are quite different, and they may require different mechanisms for generation and propagation of signals to these systems. These differences are manifest in the distinct physiological responses of RGCs that serve these functions. In this study, we present the first characterization of the light-activated current that underlies the intrinsic light sensitivity of rat SCN-projecting RGCs. Furthermore, we describe the intrinsic membrane properties and morphology of these neurons.

Morphological characteristics, as revealed by Golgi staining, have been used to classify rat RGCs into three groups (I – III) (Fukuda, 1977; Perry, 1979). A number of studies have provided strong evidence to suggest that the neurons projecting to the SCN exhibited morphological characteristics similar to those ascribed to Type III RGCs: somal diameters of ~12 μm, 3-5 primary dendrites with relatively few branches, and a dendritic

extent of around 340 µm (Moore et al., 1995; Pu, 1999; Berson et al., 2002). All of our reconstructed neurons fit these parameters very closely. In addition, examination of cells not included in the detailed morphometric analysis revealed similar morphologies. It should be noted that we observed a large range in the areas of influence of SCN-projecting RGCs. A possible explanation for this result could be that the neurons with larger dendritic fields were located in more peripheral retina than those with smaller ones. In the present study retinal location was not noted. Another explanation could be that there are different sub-groups of SCN-projecting RGCs. The recent observation that between 20% and 30% of SCN projecting RGCs do not contain melanopsin (Gooley and Saper, 2002; Sollars et al., 2002) supports this idea, although we have yet to observe any distinct groups based on functional criteria.

The similarity between the morphology of SCN-projecting RGCs and Type III RGCs is in agreement with the results obtained by Berson and colleagues (2002). However, our observation that their dendritic arbors are either mono-stratified in the inner or outer laminas of the IPL, or bi-stratified is in contrast to this previous study, which reported that SCN-projecting neurons were observed predominantly extending to the outer lamina alone. Our results, however, do support the immunocytochemical analysis of Provencio and colleagues, who demonstrated that the dendritic arbors of melanopsin-containing RGCs were bi-stratified in both the inner and outer laminae of the inner plexiform layer (Provencio et al., 2002a; Provencio et al., 2002b). Our results are also consistent with physiological studies in cats where SCN-projecting RGCs exhibit ON and ON-OFF receptive field properties (Pu 1999).

The functional significance of the large dendritic tree and the different levels of stratification have yet to be addressed in any detail. At least some SCN-projecting RGCs appear to receive stimulatory input from rod and/or cone photoreceptors (Dunn and Berson 2002). This input has been proposed to arise from synaptic contacts onto the proximal dendrites in the ON lamina of the IPL. In addition, our preliminary data show that these neurons express receptors for both inhibitory and excitatory neurotransmitters, including GABA and glutamate. Together, these findings strongly suggest that conventional retinal circuitry, in addition to the intrinsic light sensitivity, may modulate the activity of SCN-projecting RGCs. Indeed, this is in agreement with the reported sensitivity and action spectrum for the excitation of SCN neurons (Aggelopoulos and Meissl 2000).

Although the SCN-projecting RGCs are similar in form to Type III cells, they display a markedly different and unique physiology from RGCs that project to the visual system (Wang et al., 1997). In response to injection of depolarizing current, SCN-projecting RGCs generated only transient or sporadic patterns of spiking activity. Such patterns are in contrast to those previously reported for Type I, II and III RGCs, which respond with sustained patterns of activity (Wang et al., 1997). Instead, the responses we observed from SCN-projecting RGCs resembled those reported for immature rat ganglion cells (Skaliora et al., 1993; Wang et al., 1997). During development, the primary determinant of spike pattern is reported to be the rate of recovery from sodium channel inactivation (Wang et al., 1997). The possibility that slow recovery from sodium channel inactivation is responsible for the sporadic firing patterns we observed in SCN-projecting RGCs remains to be determined.

Perhaps the most striking property of SCN-projecting RGCs is their intrinsic sensitivity to light. In agreement with previously published work (Berson et al., 2002), we found that these cells respond to light with a slow depolarization that triggers an intensity-dependent sporadic firing of action potentials. In contrast, RGCs selected at random did not respond to light, presumably because the photopigment in rods and cones was totally bleached during dissection and epifluorescent identification of labeled neurons. Under similar conditions, Berson et al. (2002) also reported that control RGCs did not exhibit intrinsic light responses. The close similarity of our results from photobleached retina with those obtained by Berson et al (2002) from retina bathed in a cocktail of blockers designed to preclude any residual photoreceptor-driven synaptic input indicates that these blockers are not necessary to isolate the intrinsic light response of SCN-projecting RGCs. We therefore chose not to use them in our experiments due to the uncharacterized pharmacology of the light-activated channel. The ability of SCN-projecting RGCs to respond to light when the photopigment in both rods and cones has presumably been photoisomerized into the all-*trans* isoform, suggests that the photopigment in these neurons may be similar to those found in invertebrates, which are resistant to bleaching.

The light intensities used in the present study ($2.6 \times 10^{-6} - 5.8 \times 10^{-5}$ W/cm^2) are within the range observed in the environment during the day (c.f. Methods) but are somewhat brighter than the intensities observed at dusk (2×10^{-8} W/cm^2) or a dimly lit location (2.3×10^{-9} W/cm^2). In mice lacking rod and cone photoreceptors, circadian entrainment was observed using light intensities ($1 \times 10^{-9} - 1 \times 10^{-5}$ W/cm^2) lower than those used in the present study (Freedman et al., 1999). This inconsistency suggests that

the sensitivity of the light-activated pathway may have been reduced, possibly by adaptation, during the dissection and epifluorescent scanning of the retina. Another explanation could be that the sensitivity is regulated in a circadian fashion. In this study retinas were isolated during the animals' day and it would be interesting in future experiments to examine whether SCN-projecting RGCs in retinas isolated during the animals' night exhibit a higher sensitivity to light.

Compared to the light responses reported previously, the majority of those in the present study appear more transient in nature, with the underlying depolarization returning to almost baseline levels within 15 s, even in the continued presence of light. The time course of this transient depolarization was also closely matched by the time course of the light-activated current recorded in voltage-clamp mode with the membrane being held at –60 mV. The differences between our results and those published previously (Berson et al., 2002) cannot be easily explained. However, both the internal and external solutions are quite different. Until much more is known about the ion channel and intracellular signaling pathway that mediate the intrinsic light response, the reasons why our responses are more transient than those reported by Berson et al. (2002), remain unknown.

By recording from SCN-projecting RGCs in the whole-cell voltage-clamp mode, we were able to directly observe the light-activated current that underlies the depolarizing response. The light-activated current was inward and relatively linear between –100 mV and –30 mV and was outward at potentials greater than +40 mV. However, there was little to no net current flow between –10 mV and +40 mV. In this respect, the light-activated current in SCN-projecting RGCs resembles currents carried by certain ion

channels of the transient receptor potential (TRP) family (Freichel et al., 2001). Specifically, the I-V characteristics closely resemble those reported for the TRPC6 channel in A7r5 smooth muscle cells (Jung et al., 2002), the mTRP6 channel in vascular smooth muscle (Inoue et al., 2001), and the TRPC4 and TRPC5 channels expressed in embryonic kidney cells (Shaefer et al., 2000). Furthermore, the I-V characteristics and amplitude of the light-activated current at –60 mV were largely unaffected by total replacement of extracellular Na^+ with choline. While these results do not unequivocally identify the light-activated channel as being a member of the trp family, it does seem to rule out other candidates. For example, inward current carried by the cyclic nucleotide-activated channels found in rod photoreceptors would be nearly abolished under these conditions (Hodgkin et al., 1985).

While further genetic and pharmacological experiments are needed to confirm the identity of the light-activated channel, it is interesting to note that TRP channels mediate the light response of invertebrate photoreceptors (Hardie and Minke 1992; Montell and Rubin 1989). Moreover, octopus rhodopsin bears an evolutionary similarity to melanopsin (Oshima 2001), which is expressed in SCN-projecting RGCs in the rat (Provencio et al., 2000). Melanopsin is thought to form a retinal-based photopigment, and its sequence displays several hallmarks of invertebrate opsins, including a tyrosine counter-ion for the retinal Schiff's base, instead of the glutamate that is characteristic of vertebrate opsins (Provencio et al., 2000). A tenable hypothesis is that photoexcited melanopsin activates an intracellular signaling pathway similar to that found in invertebrate photoreceptors, leading to the opening of TRP channels and membrane depolarization.

The transient light-induced depolarization seen at stimulus onset, in addition to the apparent transient nature of the spike generating machinery, raises a myriad of questions regarding how such a system could signal the SCN about general luminance information over long periods of time. If one were to design such a system, one might select a non-adapting mechanism, in which the retinal input to the circadian clock faithfully follows the light intensity of the environment. Clearly much work is needed to elucidate how a system that appears to respond best to the onset of illumination rather than its duration can result in circadian entrainment.

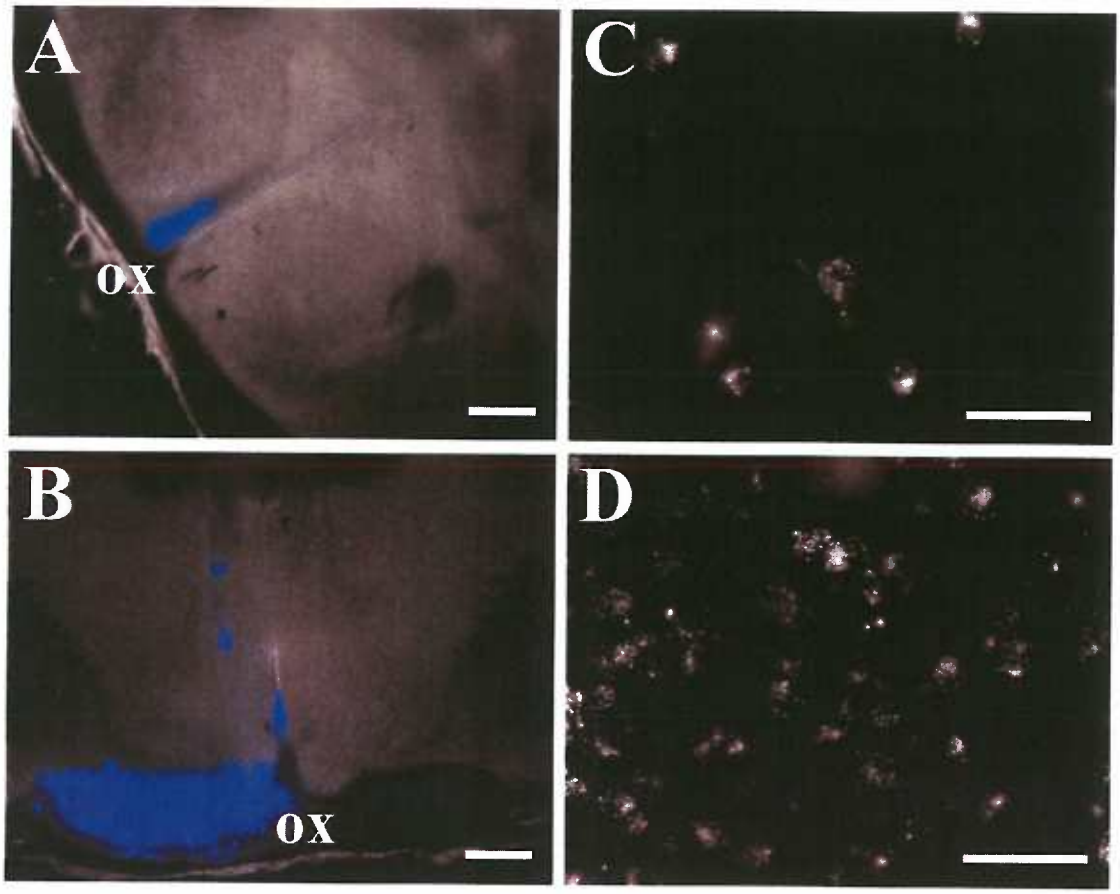

Figure 1: Retrograde labeling of RGCs following stereotaxic injection of the SCN. (A) 200 μm brain slice containing the central SCN was imaged using DIC optics and overlaid with a fluorescence image (blue) showing the location of the fluorescent beads. Scale bar = 500 μm. (B) Similar overlay showing an injection into the optic nerve. (C & D) Photomicrographs of retinal wholemounts showing the distribution of labeled neurons resulting from injection of the SCN (A) and the optic nerve (B), respectively. Scale bars = 25 μm.

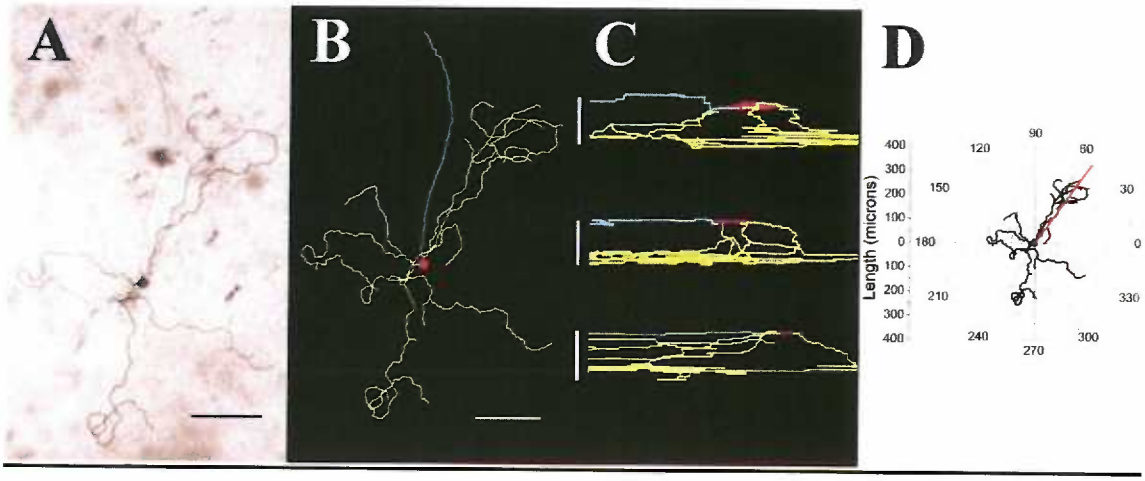

Figure 2: Morphology of SCN-projecting neurons. (A) Photomicrograph showing the typical morphology of SCN-projecting RGCs. Filled cell was visualized with a DAB reaction and photographed (Scale bar: 100 μm). (B) A two-dimensional representation of the same neuron using the Neurolucida software (Scale bar: 100 μm). (C) Cross-sectional representations of three Neurolucida reconstructed neurons to show the variety of stratification observed in SCN-projecting RGCs. From top to bottom, the scale bars are 12.5 μm, 20 μm and 25 μm, respectively. (D) A polar plot of the neuron from A and B, used to determine dendritic polarity index and dendritic distribution index.

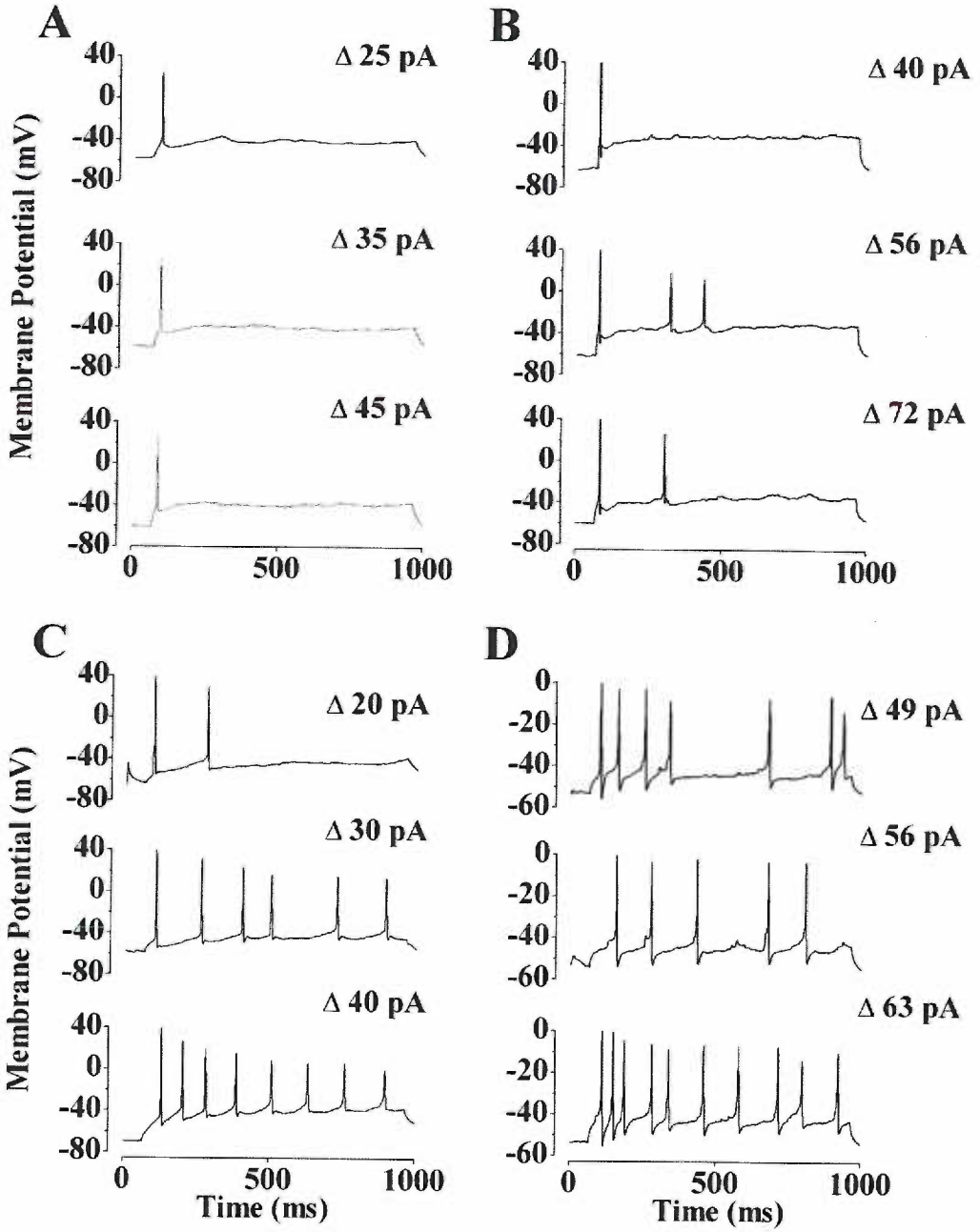

Figure 3: Spiking patterns of SCN-projecting RGCs. (A & B) Current-clamp recordings from 2 SCN-projecting RGCs. The response of each cell to increasing depolarization is shown from bottom to top. The magnitude of the depolarization is shown on the right. (C & D) For comparison, the spiking patterns elicited from a similar stimulus protocol are shown for a Type I (C) and Type II (D) neuron.

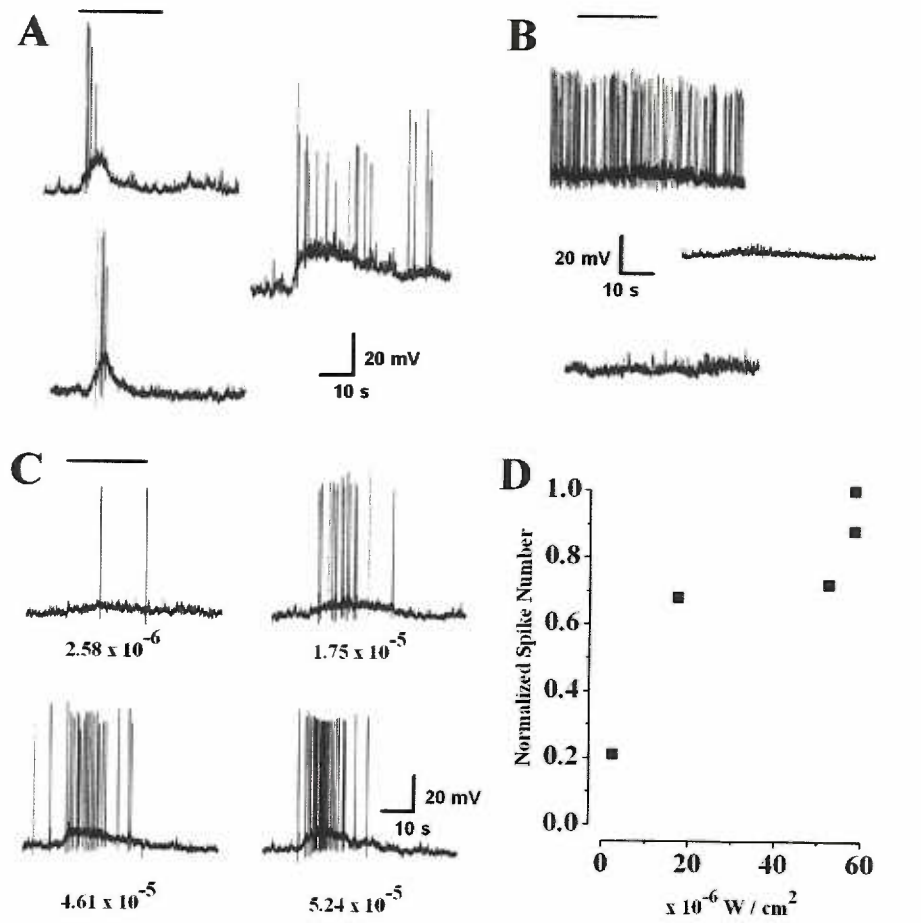

Figure 4: Intrinsic light responses of SCN-projecting RGCs. During recordings, cells were exposed to a 20 s step of white light from a tungsten-halogen lamp (*bar*). In current-clamp (A), the cells responded to light (5.8×10^{-5} W/cm^2) with a slow depolarization that generated increased spiking activity. (B) In contrast the resting membrane activity of un-labeled ganglion cells, chosen at random, did not show any response to the same light stimulus (top two traces). No light responses were observed from RGCs labeled by an optic nerve hit (lower panel). (C) The responses of an SCN-projecting RGC to increasingly brighter illumination. The numbers below each trace represent the light intensity of the stimulus in W/cm^2. (D) The relationship between stimulus intensity and spike frequency was approximately linear over the range of light intensities used.

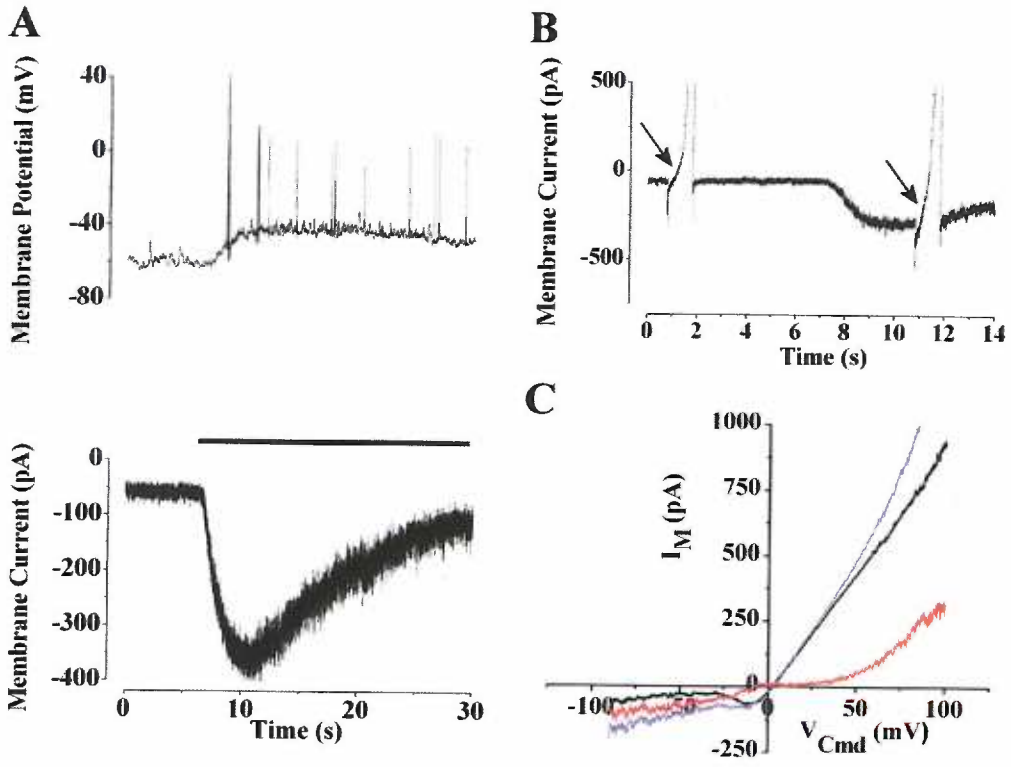

Figure 5: Current-voltage relation of the light-activated current. (A) The lower panel shows the light response (black bar; irradiance 5.8 x 10^{-5} W/cm^2) of an SCN-projecting RGC recorded in voltage-clamp mode. To illustrate the similar time courses, a light responserecorded in current-clamp mode is shown in the upper panel. (B) To determine the voltage dependence of the light-activated current, voltage ramps (-100 to +100 mV over 1 sec) were applied before and during illumination. (C) The light-activated current (*red*) was determined by subtracting currents elicited by the voltage ramp before (*black*) and during (*blue*) illumination.

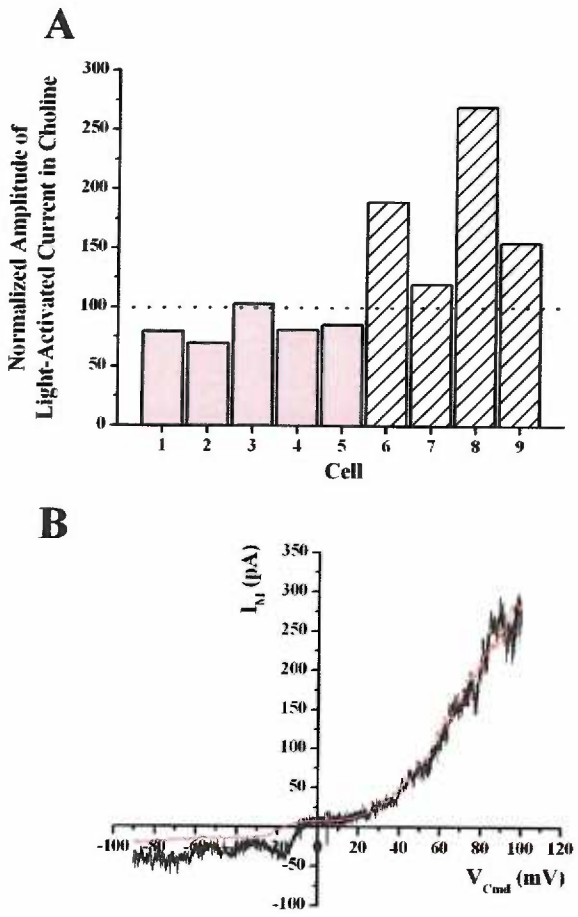

Figure 6: The light-activated current is insensitive to replacement of extracellular Na^+. (A) The bars represent the amplitude of the light-activated current recorded in an external solution containing 20 mM (gray) or 0 mM (hashed) Na^+. The amplitudes in low Na^+ were normalized to the amplitude of the current recorded in 120 mM Na^+ extracellular solution. The permutation test for paired differences indicates that the amplitude of the light sensitive current in low Na^+ is not significantly different ($p=0.125$) from that measured normal Na^+ extracellular solution. (B) I-V Characteristics of the light-activated current in 120 mM Na^+ (*black*) and 0 Na^+ (*red*). The I-V in 0 Na^+ was obtained first and, to permit comparison, has been scaled to match the amplitude of the current obtained at +100 mV in 120 Na^+.

CHAPTER THREE

THE LIGHT-ACTIVATED SIGNALING PATHWAY IN SCN-PROJECTING RETINAL GANGLION CELLS

THE LIGHT-ACTIVATED SIGNALING PATHWAY IN SCN-PROJECTING RETINAL GANGLION CELLS

Erin J. Warren[1,2], Charles N. Allen[1], R. Lane Brown[3],

David W. Robinson[1]

Center for Research on Occupational and Environmental Toxicology [1],

Neuroscience Graduate Program [2], Neurological Sciences Institute [3],

Oregon Health & Science University, Portland, OR 97239 U.S.A.

ABSTRACT

In mammals, the master circadian clock resides in the suprachiasmatic nuclei (SCN) of the hypothalamus. The period and phase of the circadian pacemaker are calibrated by direct photic input from a subset of retinal ganglion cells (RGCs). SCN-projecting RGCs respond to light in the absence of rod and cone-driven synaptic input, a property for which they are termed intrinsically photosensitive. In SCN-projecting RGCs, light activates a nonselective cationic current that displays inward and outward rectification. The goal of the present study was to investigate the identity of the light-activated ion channel and the intracellular signaling pathway leading to its activation. We considered two candidate channels, cyclic nucleotide gated (CNG) channels and transient receptor potential (TRP) channels, which mediate vertebrate and invertebrate phototransduction, respectively. We report that the intrinsic light response relies upon a G-protein dependent process. Although our data indicate that cyclic nucleotides modulate the signaling pathway, CNG channels do not appear to conduct the light-activated current (LAC) because (1) cyclic nucleotides in the pipette solution do not activate a conductance or occlude the light response (2) CNG channel blockers fail to inhibit the light response (3) the effects of internal and external divalent cations are inconsistent with their effects on CNG channels. Finally, we show that the pharmacology of the light-activated channel (LACh) resembles that of some TRPC channel family members; the response is blocked by lanthanides and ruthenium red, and is enhanced by flufenamic acid and 1-oleoyl-2-acetyl-*sn*-glycerol (OAG). Our data suggest a role for TRPC3, TRPC6, or TRPC7 in the intrinsic light response.

INTRODUCTION

In mammals, the master circadian clock resides in the suprachiasmatic nuclei (SCN) of the hypothalamus (Moore 1983; Moore and Eichler 1972). The period and phase of the circadian pacemaker are calibrated by direct photic input from a subset of retinal ganglion cells (RGCs) that comprise 1-2% of the total RGC population (Johnson et al., 1988; Moore et al., 1995a; Moore and Lenn 1972a). SCN-projecting RGCs respond to light in the absence of rod and cone driven synaptic input, a property for which they are termed intrinsically photosensitive (Berson et al., 2002; Hattar et al., 2002). In previous work, we have shown that light stimulation triggers a slowly-activating inward current in these neurons (Warren et al., 2003). The response is coincident with an increase in membrane noise fluctuations, suggesting that light causes ion channels to open. Current-clamp recordings reveal that a slow depolarization, which drives low frequency action potentials, underlies the intrinsic light response.

The goal of this study was to investigate the identity of the light-activated ion channel and the intracellular signaling pathway that leads to its activation in SCN-projecting RGCs. Cyclic nucleotide gated (CNG) channels and transient receptor potential (TRP) channels have been considered candidates for the light-activated channel (LACh). CNG channels mediate a hyperpolarizing light response in the vertebrate rod and cone photoreceptors (Baylor 1987; Fesenko et al., 1985). Via activation of the G-protein transducin (G_T) and a cGMP-dependent phosphodiesterase, light causes a decrease in the cytosolic concentration of cyclic GMP. In response, CNG channels in the plasma membrane close causing a reduction in the tonic inward cationic current and a decrease in the open channel noise (McNaughton 1990). In contrast, the TRP channel

family which was first identified in the *Drosophila* photoreceptor, mediates sensory transduction in several invertebrate species (Bandyopadhyay and Payne 2004; Hardie and Minke 1992; Montell 2003). In *Drosophila* photoreceptors, light increases internal concentrations of diacylglycerol (DAG) and inositol 1,4,5-trisphosphate (IP_3) through a $G_{q/11}$–PLC coupled cascade. The consequent activation of an inward cationic current mediated by TRP channels causes an increase in channel noise and depolarization of the photoreceptor cell membrane (Hardie 2001). Our data support a role for TRP channels, but not CNG channels, in the intrinsic light response of SCN-projecting RGCs.

METHODS

Stereotaxic Injection of Fluorescent Retrograde Tracers

Surgical procedures were carried out in compliance with guidelines from the National Institutes of Health, and in accordance with protocols approved by the Institutional Animal Care and Use Committee (IACUC) of Oregon Health & Science University. Because retinas from younger rats were more amenable to patch-clamp recording, we used six week old Sprague-Dawley rats, weighing between 120 and 170 g. Tetramethylrhodamine (TMR) -dextran (3000 M.W.; 10mg/ml); Molecular Probes, Eugene, OR) was injected into the SCN using a stereotaxic apparatus (Cartesian Designs, Inc., Sandy, OR) to enable unequivocal identification of RGCs projecting to the circadian system. Between two and ten days after injection, animals were killed by cervical dislocation following deep anesthesia with ether.

Electrophysiology

The anterior chamber of each eye was removed, and the retinas were gently peeled from the eyecup under a Leica GZ4 dissection scope and stored in oxygenated EMEM (HEPES modification) at room temperature. A small piece of retina was mounted on nitrocellulose filter paper containing a 2-mm hole that provided access for the recording electrode. This preparation was placed in the recording chamber with the ganglion cell layer facing up. SCN-projecting RGCs were identified by the presence of fluorescent TMR-dextran using epifluorescent illumination.

Patch pipettes with tip resistances between 3 and 8 MΩ were fabricated from filamented borosilicate glass (O.D.:1.5 mm, I.D.:0.86 mm using a P-97 electrode puller (Sutter Instruments, Novato, CA). Recordings were made at 22°C with a Multiclamp 700A amplifier controlled by pClamp9 software via a Digidata 1320 interface (Axon Instruments, Hayward, CA). During voltage-clamp recordings, cells were held at – 60 mV. Series resistance was noted but uncompensated. Data were low-pass filtered at rates between 2 (voltage-clamp) and 5 (current-clamp) kHz and digitized at rates between 2.5 and 10 kHz.

For voltage-clamp whole-cell recordings, recording electrodes were filled with an intracellular solution containing (in mM): 121 KCl, 1 $MgCl_2$, 10 HEPES, 10 EGTA, 4 Mg-ATP, 0.3 Na_3-GTP, 2 Creatine Phosphate (Na salt), Lucifer Yellow (0.1%) at pH 7.35 (290 mosm). When 18 mM K-BAPTA was used in calcium buffering experiments, KCl was reduced to 77 mM. For current-clamp perforated-patch recordings, electrodes were filled with an intracellular solution containing (in mM): 117 KCl, 10 HEPES, 10 EGTA, 4.0 Mg-ATP, 0.3 Na_3-GTP, 2 Creatine Phosphate (Na salt), Lucifer Yellow,

0.1%, Nystatin, 3 mg/ml, pH 7.35, osmolarity, 290 mOsm. Adequate perforation was determined by monitoring input resistance throughout the experiment. In all experiments, the bath solution consisted of (in mM): 127 NaCl, 7 KCl, 3 $CaCl_2$, 1 $MgCl_2$ and 10 HEPES, 10 D-glucose, pH 7.4 (290-300 mOsm), and was continuously bubbled with oxygen.

Light Stimulation

Illumination was provided by a 250 W tungsten-halogen light source through the transmitted light path of a Zeiss Axioscope 2 FS microscope, and the intensity was reduced using a variety of neutral density filters. Light intensities were determined using a radiometer (International Light, Newburyport, MA). All recordings were conducted in a dimly lit room exposing the retina to 5.0×10^{-7} W/cm^2 of background illumination. The initial dissection of the retina was done under about 1.0×10^{-4} W/cm^2 white light. Intrinsic responses were elicited by exposure to 1.40×10^{-4} W/cm^2 white light. Infrared illumination was used to visualize the tissue during electrode placement.

Statistics

Averages are reported as the mean ± SE. Significance was determined using the student's t test. Variance between groups was determined using One-Way ANOVA.

RESULTS

Light Response of SCN-Projecting RGCs in Voltage-Clamp

All responses recorded in voltage-clamp to date were similar to the response shown in Figure 1A: light (*bar*) stimulation triggers a slowly-activating inward cationic current in the ganglion cell. The increase in membrane noise during the response suggests that ion channels are opening rather than closing. The rate at which the response decays to baseline and the extent of decay during the light stimulus depended upon the length of the light stimulus and on the individual cell. Differences exist, both in time course and in shape, between the light responses of SCN-projecting RGCs (Figure 1A) and the synaptically-driven light responses of other ganglion cells (Figure 1B). For example, the Type I ganglion cell in Figure 1B exhibited a transient burst of synaptic activity with a latency of 200-300 ms following light stimulation. In contrast, the interval between the light flash and the beginning of the intrinsic response in SCN-projecting RGCs depends on the light intensity, and can be as long as 2 seconds. Also noteworthy is the relative quiescence of SCN-projecting RGCs, which exhibit very little synaptic activity at rest.

Rundown of the LAC in SCN-projecting RGCs can be quite marked during whole-cell patch-clamp recordings, and internal solutions were selected which maximize and stabilize the amplitude of the LAC. Average rundown of the LAC within the first twenty minutes of recording was 45.4% ± 7 (n=5). The response amplitude did not rundown to zero, but instead reached a steady-state amplitude. Bath-delivered drugs were applied only after a steady-state response was obtained to ensure that subsequent current reduction was an effect of drug application and not rundown.

Role of G Proteins

The slow activation and subsequent rundown of the light-induced current in SCN-projecting RGCs during whole-cell recordings suggest that channel activation lies downstream of an intracellular second messenger system. Phototransduction via CNG channels in vertebrates, and TRP channels in invertebrates, is coupled to transducin (G_T) and $G_{q/11}$, respectively. We first asked if the intrinsic light response is G-protein dependent. If so, we hypothesized that inclusion of the nonhydrolyzable stimulatory GTP analog, GTPγS (300 μM), in the pipette solution would constitutively activate the ion channel in question and occlude subsequent light responses. In one SCN-projecting RGC, GTPγS caused a 55% reduction in the amplitude of the light response between the first light stimulus and a second light stimulus delivered 4 minutes later (Figure 2A). The amplitudes of responses elicited by subsequent steps of light were reduced by 91%. Our finding that the baseline membrane current did not shift to that of the initial light response amplitude indicates that constitutive activation of G-proteins leads to channel inactivation or desensitization. On average, GTPγS decreased the light response by 92 % ± 6 (n=4, p=0.008) and the average time required for maximal effect was 20 ± 4 min. Within the first four minutes of recording, the average reduction in response amplitude was 50 % ± 10.

Substituting GDPβS, a competitive inhibitor of GTP binding, for intracellular GTP inhibits G-protein dependent processes. If the intrinsic light response is G-protein dependent, infusion of GDPβS in the pipette should block the light response. In one SCN-projecting RGC, 1 mM GDPβS reduced the light response by 96% (Figure 2B). The average decrease in amplitude was 89 ± 5% (n=4, p=0.006) and the average time required

for maximal effect was 25 ± 4 min. Within the first four minutes of recording, the average reduction in response amplitude was 48% ± 18.

The reduction of the light response by GTPγS and GDPβS is quantitatively different than that caused by rundown (Figure 2C). Firstly, the light response did not reach a steady state level as seen with rundown, but was nearly abolished with GTPγS and GDPβS in the pipette. Secondly, the reduction in the light response amplitude occurred faster in the presence of GTP analogs. On average, the amplitude of the light response in control cells declined to 50% of the initial value in 20 minutes, while the amplitude reached the same level in only 4 minutes in the presence of GTPγS and GDPβS.

Potential Role of CNG Channels

CNG channels were considered as possible mediators of the LAC because of their central role in vertebrate rod and cone phototransduction. If cyclic nucleotides directly gate the light-activated ion channel, then their inclusion in the pipette solution should have two consequences: an inward current should develop as CNG channels open, and eventually the light response should be occluded after all the CNG channels are constitutively opened.

To investigate whether cyclic nucleotides gate a conductance in SCN-projecting RGCs, either 500 μM cAMP (n=5) or 500 μM cGMP (n=6) was included in the recording pipette during whole-cell voltage-clamp recordings. Baseline currents were monitored immediately upon break-in and for up to 90 minutes. Neither cAMP nor cGMP activated an inward current (Figure 3A; cAMP, One-Way ANOVA $p=0.954$, $F=0.212$; cGMP, One-Way ANOVA $p=0.836$, $F=0.412$). To control for the possibility that endogenous

phosphodiesterases were degrading cAMP or cGMP, we applied 500 μM IBMX, a broad-spectrum phosphodiesterase inhibitor, via the bath. IBMX had no effect on baseline membrane currents (Figure 3B and 3C).

Although inclusion of cyclic nucleotides in the intracellular solution did not directly activate any currents in SCN-projecting RGCs, cyclic nucleotides are known to activate a number of enzymes that can modulate signaling cascades and ion channels. Therefore, we next addressed whether light responses were blocked by intracellular cyclic nucleotides. Light responses were evoked every four minutes during whole-cell voltage-clamp recordings with either 500 μM cAMP or cGMP in the recording pipette. To distinguish between pharmacological block and rundown, IBMX (500 μM) was applied only after the light responses of each cell reached a steady-state amplitude. Light responses could still be elicited after intracellular perfusion of cAMP and cGMP and fifteen minutes of IBMX application (Figures 3B and 3C). The persistence of the light response despite high internal concentrations of cyclic nucleotides indicates that a molecule other than cAMP or cGMP is gating the LACh. However, cyclic nucleotides did modulate the amplitude of the light response. In five cells with pipette solutions containing cAMP, IBMX reduced the light response by 23.0 ± 4 % (Figure 3D, left; student's paired T-test, $p<0.002$). Similarly, IBMX reduced the light response by 37.8 ± 5 % in five cells containing cGMP (Figure 3C, right; student's paired T-test, $p<0.012$). In 8 of 10 cells, the effect of IBMX was reversible following washout (n=5 cGMP, n=3 cAMP).

To further rule out a role for CNG channels in the intrinsic light response, we applied known blockers of CNG channels during light stimulation of SCN-projecting RGCs.

Light responses evoked in whole-cell voltage-clamp conditions were compared before and after the application of CNG channel blockers. Bath application of the CNG channel blocker pimozide (50 μM) did not significantly reduce the amplitude of the light response (Figure 4A; n=5, student's paired T-test, $p>0.187$). The light response was similarly unaffected when a cocktail of CNG channel blockers including pimozide (50 μM), l-*cis*-diltiazem (30 μM), and dichlorobenzamil (30 μM) was bath applied to three cells (Haynes 1992; Nicol et al., 1987; Nicol 1993). To complement these findings in the absence of current rundown, a representative trace recorded from a cell in the perforated-patch current-clamp configuration is shown in which the CNG blocker cocktail did not attenuate the amplitude of the light-induced depolarization (Figure 4B).

Role of Divalent Ions

The conductance of CNG channels is dramatically reduced by the presence of divalent cations, which act as voltage-dependent permeant blockers (Haynes 1995; Kleene 1995; Zimmerman and Baylor 1992). At negative potentials, extracellular divalents are particularly effective at reducing the inward cation current. Therefore, if the intrinsic light response were mediated by CNG channels, removal of extracellular divalents would be expected to dramatically enhance the light response between 20- and 500-fold, depending upon the CNG channel isoform. Although removal of extracellular divalents caused the recordings to become unstable, there was no marked increase the magnitude of the light response (data not shown).

Intracellular divalent cations have also been shown to reduce the conductance of CNG channels, although their effects would be moderate at a holding potential of -60 mV. Intracellular calcium is also known to modulate the affinity of CNG channels in a

calmodulin-dependent manner. Therefore, we compared the amplitude of the light response and the time to peak in the presence of increasing amounts of divalent buffering: 0.1 mM EGTA, 10 mM EGTA, and 18 mM BAPTA. The intracellular concentrations of free Mg^{2+} and Mg-ATP were estimated using the web-based Max Chelator program (http://www.stanford.edu/~cpatton/webmaxc/webmaxcS.htm), and were found to change only moderately, within a range of 0.83 – 1.27 mM for free Mg^{2+}, and 3.58 – 3.88 mM for Mg-ATP. From these estimations, we conclude that the effects seen in Figures 5A and 5B are due primarily to differences in calcium buffering.

As shown in Figure 5A (Upper), light responses evoked in whole-cell voltage-clamp from cells containing 10 mM EGTA had an average amplitude of 72.63 ± 9.2 pA (n=7). In the presence of 18 mM of intracellular BAPTA, the amplitude of the light response was significantly reduced by almost 70 % to -22.48 ± 4.0 pA (n=4; One Way ANOVA, $p<0.003$). In weakly buffered solutions containing 0.1 mM EGTA, the amplitude of the light response was only slightly reduced (63.29 ± 6.7 pA, n=7). The degree of calcium buffering also altered the kinetics of the intrinsic light response. In the presence of 0.1 mM EGTA, the light response peaked after a delay of 2.91 ± 0.3 s (n=7); in the presence of 18 mM BAPTA, the light response peaked only after a delay of 6.2 ± 2s (Figure 5A, lower; n=4). This was significantly slower than the average time to peak measured in cells containing 0.1 mM EGTA (One-Way ANOVA $p<0.025$).

In addition to its affect on light response amplitude and rate, increased calcium buffering also reduced the rate of LAC rundown. In Figure 5B (upper), the normalized light responses from each cell in the three buffering conditions are plotted and fit with a single exponential. The average time constant of rundown for 0.1 mM EGTA (n=6) was

212 ± 75 s and for 10 mM EGTA (n=6) was 592 ± 153 s (Figure 5B, lower). In cells containing 18 mM BAPTA (n=4), rundown did not fit a single exponential decay. Three of the four cells in which BAPTA was used as a buffer showed small initial light responses that dropped to an even smaller steady state amplitude immediately. The fourth cell showed a steady linear decay in amplitude. Because cells containing 10 mM EGTA responded with maximal amplitudes, faster times to peak, and finally minimal rundown, 10 mM EGTA became the standard pipette solution buffer for all subsequent experiments.

To assess the role of internal magnesium in modulating the LAC (Figure 5C), the concentration of intracellular Mg^{2+} was changed while the divalent buffering was kept constant (10 mM EGTA). Although the differences in light response amplitude (p=0.078) and time to peak (p=0.081) were not statistically significant between cells containing 1 mM $MgCl_2$ (n=7) and 4 mM $MgCl_2$ (n=5), a trend emerged in which higher Mg^{2+} reduced the amplitude and slowed the light response.

Potential Role of TRPC Channels

TRP channels were considered as possible candidates for the LACh because TRP and TRPL channels mediate a depolarizing light response in *Drosophila* photoreceptors. We first determined if ruthenium red (RR), a nonselective ryanodine receptor and potent TRPV channel antagonist that also blocks TRPC channels, inhibited the light response. In whole-cell voltage-clamp and perforated-patch current-clamp recordings, application of 20 μM RR reduced the intrinsic light response by 94 ± 1% (n=3) and 86 ± 12% (n=3), respectively (Figure 6A).

The nonselective TRPC channel blockers lanthanum and gadolinium were bath applied to SCN-projecting RGCs to determine their effects on the LAC. Lanthanum effectively blocked the light response at 100 μM in perforated-patch current-clamp recordings (n=2, Figure 6B), and reduced the light response amplitude at 500 μM in whole-cell voltage-clamp recordings by 60 ± 17% (n=3). Gadolinium also reduced the amplitude of the LAC by 72.9 ± 8% in whole-cell voltage-clamp recordings (n=3, Figure 6C).

The nonselective cation channel blocker flufenamic acid (FFA) is useful for distinguishing channels within the TRPC3/6/7 subfamily, as it blocks currents through TRPC3 and TRPC7 channels and potentiates currents through TRPC6 channels. Bath application of FFA to SCN-projecting RGCs in the perforated-patch configuration did not block the light response, but caused a 9.9 ± 4% increase in the light-activated depolarization (n=3, Figure 6B).

We studied the effects of the TRPC3/6/7 channel activator, OAG, on the intrinsic light response because of the similarities between the I-V curve of the LAC and those published for currents through TRPC6 channels (Hofmann et al., 1999; Jung et al., 2002; Okada et al., 1999). OAG, a membrane permeant analogue of DAG, was applied at 100 μM to 18 SCN-projecting neurons during perforated-patch current-clamp recordings. While OAG did not induce a depolarization in the absence of light stimulation, it did induce a 28.4 ± 10% potentiation of the light-activated depolarization (p=0.008, Figure 7). One downstream effect of DAG is stimulation of PKC. To determine if the potentiating effects that OAG had on the intrinsic light response were mediated through PKC, we applied the PKC antagonist sphingosine (20 μM) (Hannun et al., 1991). When

applied alone, sphingosine had no effect on the light induced depolarization (n=5). When co-applied with OAG, sphingosine blocked OAG induced potentiation (n=4) suggesting that OAG enhanced the LAC via activation of PKC.

DISCUSSION

Our previous work characterized the intrinsic light response of SCN-projecting RGCs in whole-cell patch-clamp recordings (Warren et al., 2003). In the present study, we use pharmacology to investigate the identity of the light-activated channel and the underlying intracellular signaling pathway leading to its activation.

Approximately 80% of rat SCN-projecting RGCs express melanopsin, a novel invertebrate-like opsin first described in *Xenopus* dermal melanophores and found in the inner nuclear and ganglion cell layers of primate retina (Provencio et al., 1998; Provencio et al., 2000; Sollars et al., 2003). Its predicted structure is that of a seven transmembrane G-protein coupled receptor (Provencio et al., 1998). Melanophores respond to light by dispersing pigment granules in PLC/PKC/calcium dependent manner (Isoldi et al., 2005). In heterologous systems, melanopsin forms a functional G-protein coupled photopigment that can activate a TRPC3 current in response to light (Panda et al., 2005; Qiu et al., 2005). Melanopsin has also been shown to effectively couple to other G-proteins (Newman et al., 2003) and native ion channels in the mouse Neuro-2A cell line (Melyan et al., 2005). In the present study we establish an essential role for G-proteins in generating the intrinsic light response of SCN-projecting RGCs by demonstrating that stimulatory and inhibitory analogs of GTP abolish the LAC. The G-protein dependence

of the light-activated pathway is consistent with that of melanopsin-based signal transduction reported in other systems.

CNG Channels Do Not Mediate the LAC

Several lines of evidence suggest that the intrinsic light response in SCN-projecting RGCs is not mediated by CNG channels. First, inclusion of cAMP and cGMP in the intracellular pipette solution at a concentration at least 20-fold greater than the $K_{½}$, did not activate inward currents or occlude the light response, even after co-application of IBMX (Fesenko et al., 1985; Kaupp and Seifert 2002). Second, bath application of CNG channel antagonists did not block the light response. Pimozide is a voltage-independent blocker of rod CNG channels with a $K_{½}$ of ~ 1 μM (Nicol, 1993), and would be expected to eliminate > 95 % of rod channel current at the concentration used in this study. Dichlorobenzamil is a potent inhibitor of both the rod and olfactory CNG channels ($K_{½}$ of ~ 1 and 4 μM, respectively) and should block 90 - 95 % of CNG current under the conditions used in this study (Nicol, et al., 1987; Kolesnikov, 1993). L-*cis*-diltiazem is a potent inhibitor of all three isoforms of CNG channel with $K_{½}$ values of 2.6, 47, and 49 μM at – 30 mV for the rod, olfactory, and cone channels, respectively (Haynes, 92; Kolesnikov, 1990). Finally, as discussed below, the effects of divalent cations and intracellular calcium buffering on the light response are not consistent with a role of CNG channels as the LACh.

Sensitivity of the LAC to Cations

Extracellular divalent cations function as voltage-dependent permeant blockers of CNG channels by impeding the passage of monovalent cations. In the presence of physiological concentrations of Ca^{2+} and Mg^{2+}, the conductance of CNG channels is

dramatically reduced (Haynes 1995; Kleene 1995; Zufall and Firestein 1993). For example, at a holding potential of -60 mV, the conductance of the retinal rod is most profoundly affected, being reduced from 24 pS in the absence of divalent cations to < 0.1 pS under physiological conditions (Gray and Attwell 1985). However, the intrinsic light response in SCN-projecting RGCs persists in external solutions containing 3 mM Ca^{2+} and 1 mM Mg^{2+}, sometimes attaining a magnitude of 100 pA, which is several times larger than the photoresponse of retinal rods.

While the light response was not blocked by external or internal divalent ions, intracellular calcium and magnesium levels seemed to regulate both the amplitude and kinetics of the LAC. Addition of 18 mM BAPTA to the pipette solution caused a dramatic reduction in the amplitude of the light response, compared to that seen in 0.1 and 10 mM EGTA. Once again, this behavior is inconsistent with the known behavior of CNG channels. For all native CNG channels, the cyclic nucleotide sensitivity is reduced by binding of the Ca^{2+}-calmodulin complex, although this effect is most pronounced in the olfactory channel (Hsu and Molday 1993; Wei et al., 1998). Therefore, in contrast to our experimental findings, we would predict that increased buffering of intracellular Ca^{2+} might enhance the light response if it were mediated by CNG channels.

Evidence that TRP Channels Mediate the LAC

The TRP superfamily is composed of three families of ion channels (TRPC, TRPV, TRPM) whose members share sequence homology with TRP and TRPL channels first described in the *Drosophila* photoreceptor. We considered members of the TRPC family specifically because they have the most sequence homology with *Drosophila* TRP channels and are widely expressed in mammalian nervous systems. While TRPC channel

gating depends on the particular cell type in which a channel is expressed, all TRPC channel proteins lie downstream of G_q and PLC activation. TRPC channel activators include calcium store depletion and products of PLC activation (Hofmann et al., 1999; Inoue et al., 2001; Minke and Cook 2002; Okada et al., 1999).

Both cAMP and cGMP, in concert with IBMX, reduced the size of the inward current evoked by light suggesting a role for the cyclic nucleotide-dependent kinases, PKA and PKG, in modulating the LAC. Consensus phosphorylation sites have been described for all 7 TRPC channel proteins, however the effects of phosphorylation by PKA and PKG have, to date, only been studied on TRPC3 and TRPC6 channels (Kwan et al., 2004). Currents through TRPC3 are blocked by PKG activation, while currents through TRPC6 are unaffected after phosphorylation by both PKA and PKG, (Hassock et al., 2002; Kwan et al., 2004).

The results from our pharmacological experiments also provide further support for the hypothesis that the LAC is conducted through a TRPC channel. Lanthanum (0.1-4.0 mM) (Halaszovich et al., 2000; Zhu et al., 1998) and gadolinium (150-200 mM) (Trebak et al., 2002) block TRPC3 and TRPC6 channels and potentiate currents through TRPC4 and TRPC5 channels (Jung et al., 2003). Our observations that these ions block the LACh would seem to eliminate TRPC4 and TRPC5 as candidates. Moreover, FFA did not inhibit the light response in SCN-projecting RGCs, suggesting that the LACh is not a homomeric TRPC3 or TRPC7 channel but may contain a TRPC6 subunit (Inoue et al., 2001). The high concentration required for lanthanide block in our study may reflect a site of action on the intracellular side of the LACh, or it may be a feature of the specific

subunit composition of channels in the native SCN-projecting RGC (Halaszovich et al., 2000).

Currents mediated by TRPC channels exhibit a complex dependence on calcium. Both their activation and inactivation are modulated by a variety of calcium-dependent processes including internal store depletion, CaM binding, and phosphorylation by calcium-dependent kinases, including both CaMKII and PKC. Binding sites for the IP_3 receptors and CaM exist on all 7 TRPC proteins, and these domains interact in a calcium-dependent way to inhibit channel activity (Tang et al., 2001). Considering the TRPC3/6/7 subfamily specifically, internal calcium (Ca^{2+}_i) differentially regulates TRPC6 and TRPC7. Low Ca^{2+}_i (80 nM) enhances the amplitude and kinetics of current through TRPC6 channels, but inhibits current through TRPC7 channels, while higher concentrations of Ca^{2+}_i (2 mM) inhibit currents through both channel subtypes (Shi et al., 2004). While we cannot quantify the $[Ca^{2+}_i]$ in SCN-projecting RGCs from which we recorded, our results indicate that some amount of Ca^{2+}_i is required to elicit larger and faster intrinsic light responses. The dependence of the light response on Ca^{2+}_i is consistent with the reported potentiation of TRPC6 mediated currents by Ca^{2+}_i.

Although much of our evidence points towards TRPC6 as being the best candidate for the LACh, the effects of OAG on the light response in SCN-projecting RGCs complicates this interpretation. OAG has been shown to directly gate TRPC3/6/7 channels (Hofmann et al., 1999) and its failure to gate a current in SCN-projecting RGCs would tend to rule out these channels as LACh candidates. In addition, the block of OAG-induced potentiation by sphingosine suggests that OAG is modulating the light response via PKC activation. While TRPC channels contain PKC binding sites near their

C termini, PKC stimulation by OAG or phorbal ester has previously been reported to inactivate, rather than enhance, TRPC mediated currents (Trebak et al., 2005; Venkatachalam et al., 2003).

However, OAG has been shown to potentiate receptor-stimulated currents elicited by carbachol in HEK 293 cells expressing TRPC6 channels (Estacion et al., 2004). The authors of this study concluded that the TRPC6 channels were being synergistically regulated by multiple signaling pathways, both of which need to be activated to elicit a maximal response. Our observation that OAG enhances the amplitude of the light response is somewhat consistent with these findings and provides support for to the hypothesis that the LACh in SCN-projecting RGCs is a TRPC6 channel.

CLOSING REMARKS

From these studies, we conclude that the intrinsic light response in SCN-projecting RGCs lies downstream of a G-protein mediated signaling cascade. We provide strong evidence against a role for CNG channels and strengthen the case for TRPC channels by demonstrating that several pharmacological agents that target TRPC channels block the intrinsic light response. Future studies will focus on the specific subtype of TRP channel(s) involved in the intrinsic light response, with particular attention focused on TRPC3, TRPC6, and TRPC7.

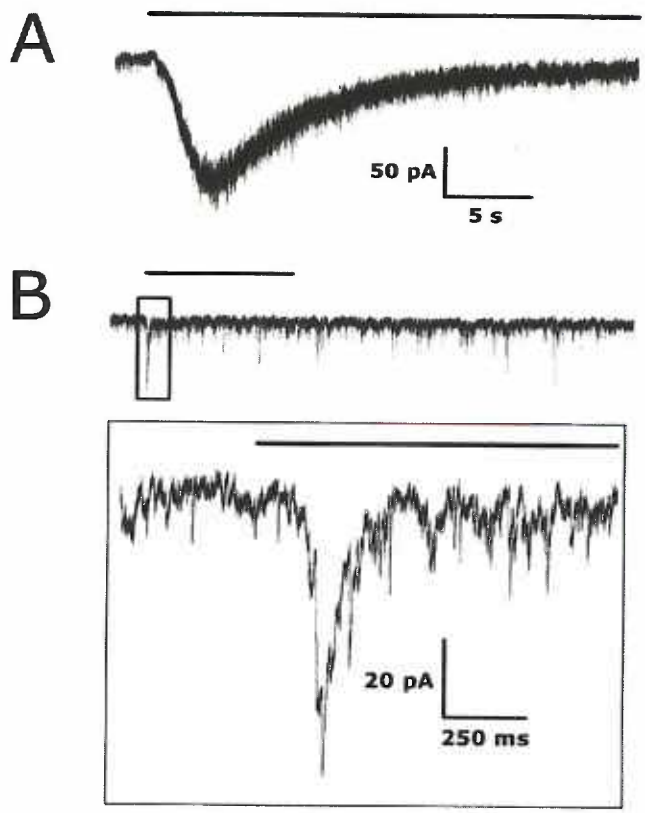

Figure 1: Intrinsic and synaptically-driven light responses from RGCs held at –60 mV.

(A) Whole-cell voltage-clamp recording of an intrinsic light response recorded from an SCN-projecting RGC (B) Upper panel depicts a synaptic light response from a non-SCN-projecting Type I RGC. The box is expanded in lower panel to show an increase in synaptic currents following the onset of light.

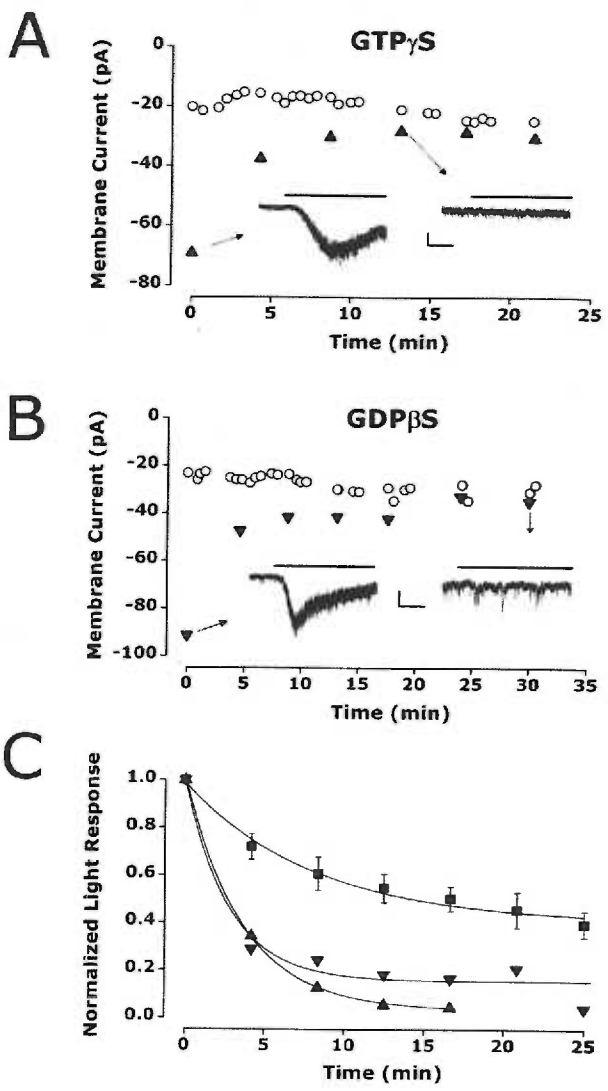

Figure 2: The intrinsic light response is G-protein dependent.

Whole-cell baseline currents were sampled throughout the recordings (○). Triangles represent the peak of the light-activated currents. Inset traces show light responses before (left) and after (right) block of response. Scale bars: 2s, 20 pA. (A) 300 μM GTPγS (▲) in the recording pipette blocks the light response. (B) 300 μM GDPβS (▼) in the recording pipette blocks the light response. (C) Normalized group data from 7 control cells containing 300 μM GTP (■) is plotted alongside normalized data from cells containing GTPγS (▲; n=4) and GDPβS (▼; n=4).

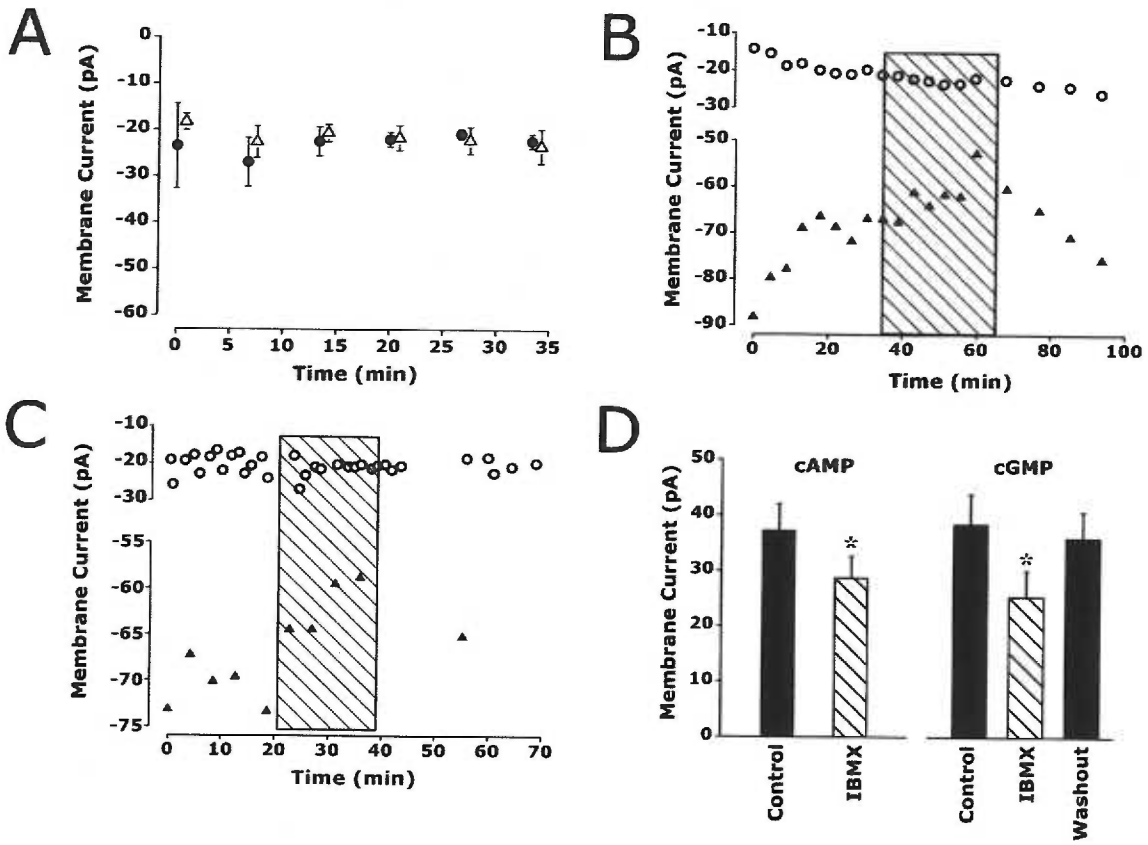

Figure 3: Cyclic nucleotides modulate the light response but do not gate the light-activated channel.

(A) Average whole-cell baseline currents were plotted from cells with pipette solutions containing either 500 μM cAMP (●) or 500 μM cGMP (Δ). One-way ANOVA detected no significant change in baseline currents of either population over the 33 min recording period. (B and C) Baseline currents (○) and peak light-activated currents (▲) from 2 SCN-projecting RGCs with pipette solutions containing either 500 μM cAMP (B) or 500 μM cGMP (C). 500 μM IBMX application is represented by hatched box. (D) Coapplication of IBMX with cAMP or with cGMP significantly reduced the light response.

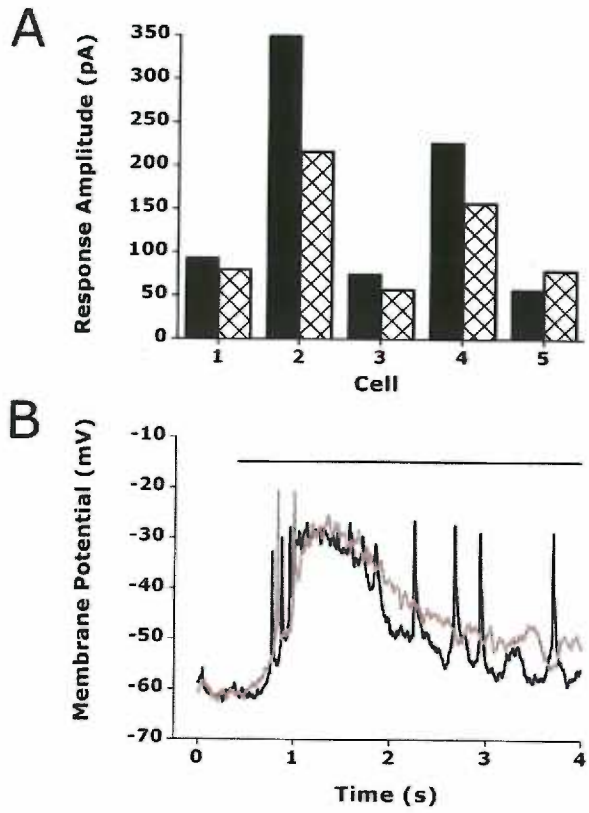

Figure 4: CNG channel blockers do not block the light-activated channel.

(A) Bath application of 50 μM pimozide did not significantly affect the amplitude of the light-activated current in whole-cell voltage-clamp recordings of 5 SCN-projecting RGCs. (B) A cocktail of CNG channel blockers including pimozide (50 μM), l-cis-diltiazem (30 μM), and 3'4'-dichlorobenzamil (30 μM) did not attenuate the light-induced depolarization during a perforated patch current-clamp recording of an SCN-projecting RGC. (Black, control; gray, cocktail).

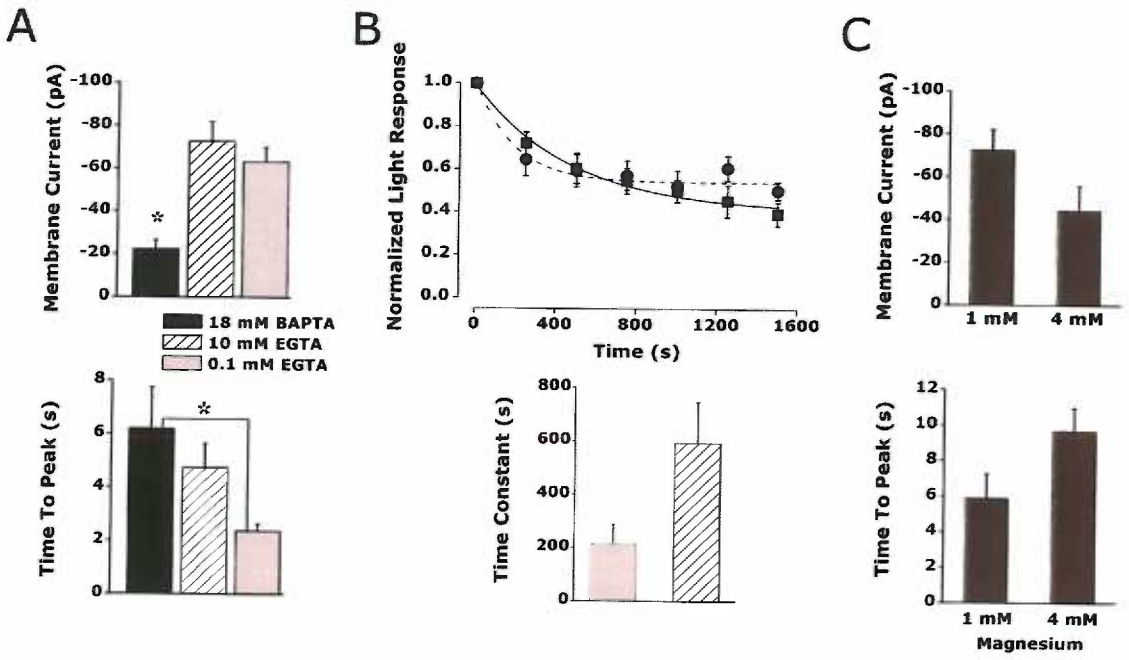

Figure 5: Divalent ions modulate the light-activated current

(A) Upper: The average light response amplitude is significantly smaller when 18 mM BAPTA (black) is included in the pipette compared to 10 mM EGTA (hatched) and 0.1 mm (gray). Lower: The rate of the response is significantly longer in 18 mM BAPTA than in 0.1 mM EGTA. (B) Upper: Light responses were normalized to the first maximal light response and the averages for each group plotted over 1600 s. Both cells with 0.1 mM EGTA (●) and cells with 10 mM EGTA (■) in the pipette solution reached a steady state light response amplitude around 50% of initial amplitude. Lower: The time constants of rundown were calculated by fitting data from each cell to a single exponential decay and averaging within a group. (C) Upper: Increasing internal magnesium from 1 mM to 4 mM reduced the amplitude of the light response. Lower: The increase in magnesium also slowed the development of the light activated inward current. Neither of these findings were significant by student's T-test.

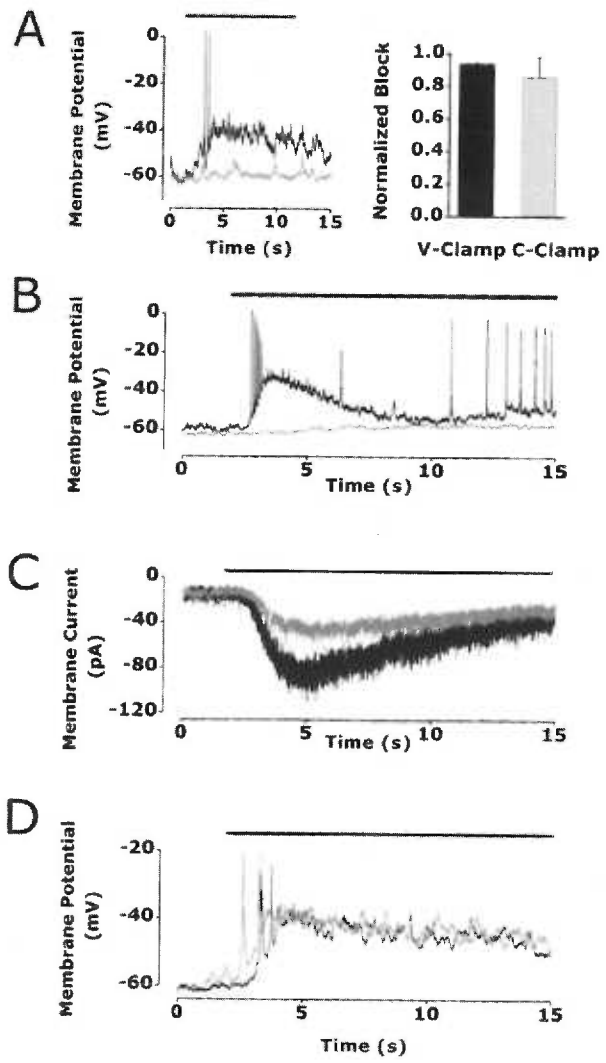

Figure 6: TRP channel antagonists block the intrinsic light response.

(A) Left: 20 μM ruthenium red blocked the intrinsic light response in an SCN-projecting RGC during a perforated-patch current clamp recording. Right: Summary data showing percent block by ruthenium red in 3 voltage-clamp and 3 perforated-patch current-clamp recordings. (B) 100 μM $LaCl_3$ blocked the intrinsic light response in a perforated-patch current-clamp recording. (C) 200 μM $GdCl_3$ reduced the whole-cell light-activated current in this SCN-projecting RGC by 57%. (D) 250 μM flufenamic acid, a TRPC3 and TRPC7 channel blocker, did not block the light response in SCN-projecting RGCs.

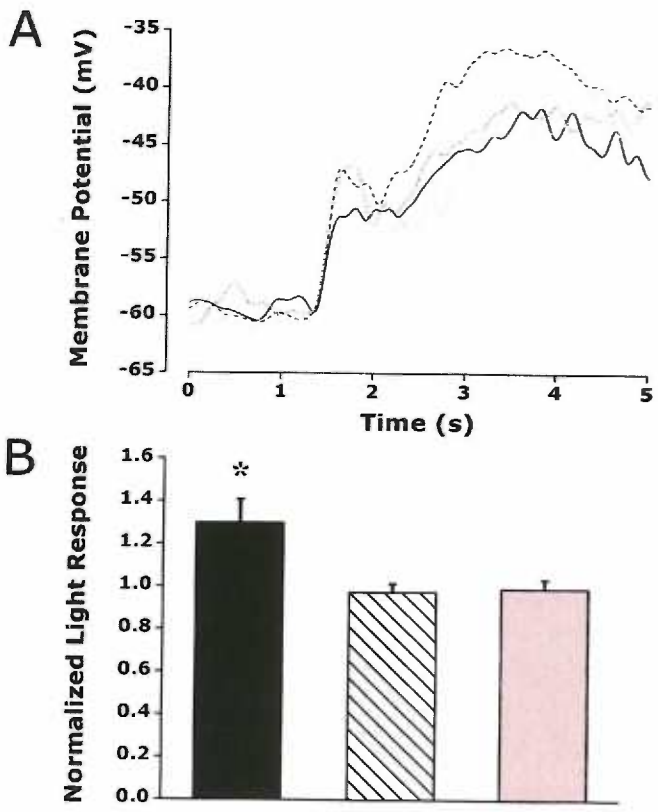

Figure 7: 1-oleoyl-2-acetyl-*sn*-glycerol (OAG) potentiated the intrinsic light response in a PKC dependent manner.

(A) Data taken from one SCN-projecting neuron, low-pass filtered at 2Hz. In order of applications: Control, black; sphingosine, dotted; OAG, dashed; OAG and sphingosine, gray. (B) OAG significantly potentiated the intrinsic light response in 18 SCN-projecting RGCs during perforated-patch current-clamp recordings (black). The PKC antagonist sphingosine had no effect on the light response when applied alone to 5 cells (hatched). Coapplication of OAG and sphingosine blocked the OAG induced potentiation (n=4, gray).

CHAPTER 4

CONCLUSIONS

CONCLUSIONS

A Unique Class of RGC

In the first part of this work, the intrinsic membrane properties and anatomical features of SCN-projecting neurons were examined to determine if they comprise a novel class of RGC. To date, SCN-projecting RGCs have been described as similar to rat type III RGCs and cat γ RGCs based on several morphological criteria (Boycott and Wassle 1974; Perry 1979). First, SCN-projecting RGCs in the rat and cat have a small number of primary dendrites compared to other RGC subtypes. Second, the elaboration of their dendritic trees is simple with few branch points. Third, their dendrites span a large area of the retina. And finally, their cell bodies are typically small to medium in diameter and oval in shape. My observations of SCN-projecting RGCs in the rat were consistent with this type III-like classification as we found that the average number of primary dendrites was 2.6 ± 0.6 (range 2-4), and that the dendritic fields were simple in structure with few branch points (14 ± 8.8). The dendritic extents in these neurons were large, spanning several hundred microns. I measured medium sized cell bodies that were more often oval or irregularly shaped than circular. Considering their morphology alone, the SCN-projecting RGCs from which I recorded appear to fall into the type III category of rat RGCs.

Historically, RGCs fitting this morphological description were classified in the cat as "W" cells, exhibiting physiological properties that distinguished them from "X" and "Y" type RGCs (Stone and Hoffmann 1972). X type RGCs respond to illumination with sustained firing, propagate action potentials at intermediate conduction velocities, and are

best suited for the detection of small objects in the visual field. Y type RGCs respond to light with transient firing, conduct action potentials at fast conduction velocities, and are therefore well-suited for the detection of motion across the visual field. Both X and Y cells have receptive fields organized in a center-surround arrangement and send a large projection to the ventral LGN (Cleland et al., 1971; Cleland and Levick 1974; Fukuda and Stone 1974).

In contrast, W cells display a wide array of response properties, have thin axons with slow conduction velocities, and project primarily to the pretectum and superior colliculus (Cleland and Levick 1974; Stone and Fukuda 1974; Stone and Hoffmann 1972). The W-cell class is thought to contain many functional subtypes of RGCs as reflected by the variety of receptive field properties observed. One type of response is the ON-tonic response characterized by a persistent discharge of spikes in response to light incident on the center of the receptive field (Stone and Fukuda 1974). W cells displaying this type of light response were hypothesized to monitor background illumination. Fukuda and Stone postulated that ON-tonic W cells were the rare ganglion cells first described as "luminance detectors" by Barlow and Levick in the cat retina. These luminance detectors that comprised only 1% of the RGCs sampled responded to light monotonically, showing an increase in spike discharge with increasing illumination (Barlow and Levick 1969). Barlow and Levick suggested that the luminance detectors from which they recorded were ideally suited to mediate the pupillary light reflex in the cat. It is quite likely that the luminance detectors described by Barlow et al. and perhaps some ON-tonic cells later categorized as W cells were indeed SCN-projecting RGCs (Cleland and Levick 1974).

Physiology Of SCN-Projecting RGCs

My experiments demonstrate that the physiology of SCN-projecting RGCs is different from that of RGCs projecting to central visual targets. The most striking difference is that SCN-projecting RGCs exhibit an intrinsic sensitivity to light in the absence of photoreceptor-driven input. The intrinsic light response recorded in current-clamp has several stereotyped features, including a long latency between the light simulus and response, low spike frequency even at the peak of the depolarization, a sustained response lasting for minutes after the offset of light, and an increase in membrane noise that persists throughout and after the response.

The intrinsic light response arises from the activation of an inward current with a long latency (hundreds of milleseconds to seconds) between the light presentation and current activation. This is in sharp contrast to rod and cone light responses which are mediated by a fast G-protein cascade, and exhibit latencies of tens of milliseconds. The long latency of SCN-projecting RGCs suggests that channel activation relies on a slow second messenger signaling pathway, which I later confirmed to be G-protein dependent (Chapter 3). The sluggish light responses of SCN-projecting RGCs are not ill-suited for the purposes of the circadian system. For example, day to night transitions occur on a significantly longer time scale than events captured by the visual system. such as motion across the visual field.

SCN-projecting RGCs fail to exhibit a monotonic increase in action potential firing frequency with sequentically higher current injections and are unable to fire high frequency spike trains that are typical of RGCs projecting to the visual system. During depolarizing current injection, very few SCN-projecting RGCs exhibited fast-activating

and fast-inactivating outward currents resembling I_A (potassium) currents. I_A currents can shorten the refractory window for spike trains by repolarizing the membrane quickly and permitting rapid recovery from sodium channel inactivation. Their absence in the majority of SCN-projecting RGCs may explain the low firing frequency seen in these neurons. It is also possible that the voltage-gated sodium channels expressed in SCN-projecting RGCs are slow to recover from inactivation.

As a luminance detector, the SCN must monitor slow and long changes in background illumination, while ignoring disruptions during the subjective night that do not represent a change in the period of the solar cycle, but rather an anomalous environmental event. One possible advantage of an upper limit on spiking frequency is that sudden and short-lived stimuli (such as lightning during the night) are less likely to be seen by a system that does not have a wide range of temporal responses. Even in the case of nighttime lightning, a short burst of EPSPs reaching the SCN-projecting RGC by way of a rod or cone pathway would not elicit a fast or long train of action potentials in the efferent signal to the SCN.

To date, the salient feature(s) of the intrinsic light response used by SCN to decode luminance is unknown. Preliminary work in our lab using cell-attached patch-clamp recordings did not yield a clear relationship between light intensity and spike number. All intrinsic light responses, regardless of stimulus intensity, showed similar spike trains (usually 5 spikes) in current-clamp at the peak of the depolarization. The amplitude of the light-induced depolarization in whole-cell recordings was the only parameter that consistently increased with increasing light intensities in the majority of

cells. However the spiking pattern at the peak of the response, which is presumably the only signal visible to the SCN, did not necessarily change with intensity.

It would seem then that luminance is coded by the sustained component of the light response. Some SCN-projecting RGCs in cell-attached current-clamp recordings continue to fire action potentials for up to two minutes after the offset of light. Others show transient responses in which spiking does not persist past the initial burst, or persists only until the light is turned off. In two cases, OFF responses were recorded. The heterogeneity of SCN-projecting RGCs responses might be explained if they subserved the visual system as well as the circadian system. This scenario seems likely as they project beyond the SCN and PON to terminate in the ventral LGN. SCN-projecting RGCs might comprise several functional cell groups for the visual system, while constituting a single class of luminance detecting photoreceptors for the circadian system.

An interesting feature of the intrinsic light response is a dramatic increase in noise that persists throughout and after the decay of the response to baseline. The noise resembles fluctuations caused by the opening and closing of ion channels. However, the noise does not decrease, and in some cases becomes larger in amplitude, when the light response terminates. Fourier analysis to identify component frequencies of these oscillations did not reveal a peak frequency that was consistent with ion channels opening and closing. One possible explanation for the observed noise is that it arises from gap junctional coupling of SCN-projecting RGCs. Whole-cell recordings performed with Lucifer yellow in the pipette solution often labeled multiple cell bodies within the vicinity of the labeled SCN-projecting RGC. I have not yet quantified or classified the cells to which SCN-projecting RGCs are coupled, but the frequency at which I observed

dye coupling with other cells in the ganglion cell layer suggests that gap junctional connectivity may play a significant role in the physiological responses of these neurons. If the membrane noise during the intrinsic light response arises from currents though gap junctions, the gap junction de-coupler dopamine should eliminate the persistent membrane noise. Including the gap junction blocker carbonoxalone in the recording pipette should have a similar effect.

Gap junctional coupling would permit SCN-projecting neurons to function as a network and might, despite their heterogeneous light responses, average the signal conveyed to the SCN. While individual SCN-projecting RGCs would not convey luminance information to the SCN, it might be the case that the network would. There are several ways in which to test the role of gap junctions between SCN-projecting RGCs. First, multi-electrode arrays can detect synchronous firing among SCN projecting RGCs in retinal whole mounts. If gap junctions underlie synchronous firing, dopamine application should cause the firing to become asynchronous. Behavioral tests might also determine if photoentrainment or phase-shifting are affected when retinal gap junctions are blocked. For example, one could examine the phase-shifting ability of rats that have undergone chronic intraocular dopamine injections. If SCN-projecting RGCs convey their signal to the SCN as a network, decoupling these neurons should attenuate, or perhaps block, the expected phase-shift.

Finally, SCN-projecting RGCs exhibit extraordinarily few miniature events at rest and receive significantly fewer synaptic inputs than other RGCs. Smaller than average currents elicited by direct application of NMDA and GABA suggest that SCN-projecting RGCs express fewer postsynaptic GABA and NMDA receptors compared to visually

projecting RGCs. The relative quiescence of SCN-projecting RGCs, both in terms of firing frequency and number of synaptic events suggests that the signal to noise ratio seen by the SCN is quite high. Takahashi's work demonstrated that long (5 minute) light pulses optimally phase-shift hamster locomotor rhythms, showing that low frequency sustained RGC input is sufficient for the SCN to extract luminance information for photoentrainment. The SCN is essentially counting photons over extended periods of time based on RHT afferent input. The fidelity of the SCN-projecting RGCs long lasting, low frequency signal would be lost if it were contaminated by excessive spontaneous EPSCs or action potentials. Therefore proper circadian function may depend on the high signal to noise ratio of the afferent SCN signal.

In summary, based on the physiological properties of SCN-projecting RGCs, it seems likely that (1) they comprise a heterogeneous population cells that bear intrinsic light sensitivity as their common feature and (2) the ensemble response of the network of SCN-projecting RGCs is the relevant signal to the SCN.

A Role for TRP Channels

When these studies were begun, it was unknown whether melanopsin was a functional photopigment. Recent work in other labs has established that melanopsin expression by SCN-projecting RGCs is required for normal photoentrainment. Several properties of the intrinsic light response are well-predicted from the involvement of an invertebrate-like opsin, such as melanopsin. First, invertebrate opsins exhibit a resistance to bleaching conferred upon them by their bistability. Light of one wavelength catalyzes conversion of all-*trans* retinal to 11-cis-*retinal*, while light of a second wavelength catalyses the reverse reaction. The intrinsic light response is similarly resistant to

photobleaching. While current rundown was a persistent problem in these studies, the light response did not vanish with repeated exposures to light. Moreover, cell-attached current-clamp recordings demonstrated that the spike trains elicited by light were stable for many sequential trials. It has been a subject of debate whether melanopsin is a bistable opsin, whether there is an additional system contained within the SCN-projecting RGCs allowing regeneration of the chromophore, or whether melanopsin itself is a photoisomerase that catalyzes the regeneration of chromophore for an unidentified photopigment. Recent work from King-Wai Yau's lab indicates that melanopsin is required for the pupillary light reflex in KO mice missing a protein required for rod and cone rhodopsin regeneration, even when exogenous chromophore is supplied to the retina. These findings lend further support to a model in which melanopsin is not simply acting as a photoisomerase, but is required for phototransduction (Fu et al., 2005).

Melanopsin bears similarity in sequence and structure to invertebrate opsins which are coupled to TRP channel activation in invertebrate photoreceptors. We considered members of the TRPC family specifically because they share the most sequence with TRP channels in the *Drosophila* photoreceptor. Establishing that TRP channels mediate the intrinsic light response has been difficult for a number of technical reasons. The first is a lack of specific pharmacological tools with which to probe the role of specific TRPC channel subtypes in the light response. Many TRP channels can form heteromultimers with other TRPC channel subtypes. For example, TRPC4 and TRPC5 combine to form channels with different properties than channels consisting of TRPC4 or TRPC5 subunits alone. The same is true for the TRPC3/6/7 subfamily. One approach to address the many permutations of possible TRPC channel subtype combinations is to

introduce antibodies made against channels into the cell during recording to block conductance. Having narrowed our focus to the TRP3/6/7 subfamily, I will employ this technique in subsequent experiments.

One of the most effective TRP channel blockers, SK&F, was not effective at blocking the light response. A potential explanation for the incomplete block of the light response by lanthanum and gadolinium as well as the failure of SK&F is the preparation used in these studies. Access of the bath solution to the majority of the melanopsin-expressing dendritic arbor was questionable as the inner limiting membrane was only removed directly above the cell body. Attempts to record from dissociated labeled neurons were made virtually impossible due to the small number of labeled neurons in any given retina.

Future plans to circumvent these technical challenges are already underway in the laboratory. R.Van Gelder has generously offered founder mice containing a GFP gene driven by the melanopsin promoter. The benefit to using mouse retina with GFP- labeled melanopsin will be a high yield of SCN-projecting cells from which to record in every experiment. We also anticipate that the neurons will be healthier without a high concentration of dextran in their cytoplasm. Another strategy to increase labeling is to apply fluorescently tagged primary antibodies made against melanopsin (α-MEL) to live floating retina prior to recording. Preliminary attempts indicate that the retina will bind α-MEL in a timely fashion for subsequent recording. Finally, intraocular injections of fluorescently tagged α-MEL might adequately label SCN-projecting RGCs. I have yet to determine if the binding of α-MEL to melanopsin interferes with cell viability or the intrinsic light response.

Complete labeling of SCN-projecting RGCs will permit recordings to be made from dissociated neurons, as the chance of finding a viable labeled cell will increase about 100 fold. Dissociated cell recordings will ensure ideal voltage clamp and optimal control of the extracellular bathing solution. It is our expectation that the LAC in the dissociated SCN-projecting RGC will be blocked by concentrations of lanthanides that are reported elsewhere in heterologous systems.

Another question that has yet to be addressed is whether the SCN-projecting RGCs themselves display a circadian rhythmicity in their light sensitivity. The light required to evoke intrinsic light responses in these studies was very bright. The retinas were intentionally light adapted to reduce any photoreceptor-driven synaptic input, and it is not known whether this light exposure similarly reduces the pool of available melanopsin photopigment. Considering that melanopsin might be a bistable photopigment, it is possible that exposure to the bright white unfiltered light used in our experiments drives the melanopsin *cis-trans* equilibrium more strongly in one direction. To explore whether the intrinsic light response echoes the putative bistability of melanopsin, one could pre-expose cells to different monochromatic wavelengths of light and compare their response amplitudes to a test pulse of 480 nm light. The wavelengths of light which best enhanced the subsequent light response to a 480 nm test pulse could then be used to enhance phase-shifting to light in behavioral studies.

In my studies, the rats were sacrificed between CT 4 and CT 7 when one would expect the SCN to be insensitive to light input. Studies by Ding et al. in which it was determined that the SCN slice is insensitive to direct glutamate application during the daytime indicate that a gate exists at the level of the SCN blocking glutamatergic

signaling during the subjective day. However, work by Sakamoto et al. (2004) revealed that melanopsin mRNA and protein levels in the retina itself also oscillate, peaking in the early subjective night (Sakamoto et al., 2004). The possibility remains that there is redundant gating of the light signal in both the RGC and the SCN, and that the SCN-projecting RGC may display a higher sensitivity to light during the subjective night due to elevated expression of the photopigment melanopsin.

Perhaps the set of experiments most relevant to the field of circadian biology and mammalian photoentrainment will be those addressing how these RGCs code luminance for the SCN. As mentioned before, the limited ability of the SCN-projecting RGC to generate spike trains suggests that the salient feature of the response is the long lasting train of low frequency action potentials that follow a light flash. In these studies the light stimuli ranged between 10 and 30 seconds and were considered excessively long compared to the duration of light flashes capable of activating rods and cones. However given that the circadian system phase shifts best to 300 second stimuli, it will be important to increase the range of stimulation durations used on SCN-projecting RGCs. As discussed above, it is also imperative to examine the response properties of these neurons as a population to determine what form the averaged signal reaching the SCN takes. Techniques to examine SCN-projecting RGC network properties include injecting calcium indicator dyes into the SCN and recording calcium transients during intrinsic light responses in isolated wholemount retina. Another approach is to record extracellular spikes from retinas resting on multi-electrode arrays. By using GFP labeled retinas, spiking patterns can be correlated with individually labeled SCN-projecting RGCs. These

techniques should estimate the signal propagated to the SCN by the network of SCN-projecting RGCs.

To understand how the SCN decodes light information from the retina, it is essential to study the signal itself. The work described in this thesis has provided insight into the retinal photoreceptors that bear the responsibility of synchronizing the circadian clock with the solar cycle. While they comprise only a small percentage of retinal neurons, SCN-projecting RGCs convey information to the SCN which is appropriately transduced to almost every system in the organism. Their intrinsic light sensitivity highlights the unique role that SCN-projecting RGCs play in the retina, and the important, and probably ancient, place they occupy in the circadian system. The anatomical, passive, and excitable membrane properties of SCN-projecting RGCs, described in this study, shed light on their responses properties. Additionally, the characterization of the intrinsic light response in these neurons suggests how SCN-projecting RGCs might filter out irrelevant photic information to the SCN, and what form relevant information about luminance might take. Future work will focus on the transduction machinery within these neurons conferring their intrinsic sensitivity, how their network properties might contribute to their function, and ultimately how the signal they send to the SCN codes photon number or luminance.

1. Aggelopoulos NC and Meissl H (2000) Responses of neurones of the rat suprachiasmatic nucleus to retinal illumination under photopic and scotopic conditions. J. Physiol 523 Pt 1: 211-222.

2. Allada R, White NE, So WV, Hall JC, and Rosbash M (1998) A mutant Drosophila homolog of mammalian Clock disrupts circadian rhythms and transcription of period and timeless. Cell 93: 791-804.

3. Aronin N, Sagar SM, Sharp FR, and Schwartz WJ (1990) Light regulates expression of a Fos-related protein in rat suprachiasmatic nuclei. Proc. Natl. Acad. Sci. U. S. A 87: 5959-5962.

4. Azmitia EC and Segal M (1978) An autoradiographic analysis of the differential ascending projections of the dorsal and median raphe nuclei in the rat. J. Comp Neurol. 179: 641-667.

5. Bae K, Jin X, Maywood ES, Hastings MH, Reppert SM, and Weaver DR (2001) Differential functions of mPer1, mPer2, and mPer3 in the SCN circadian clock. Neuron 30: 525-536.

6. Bandyopadhyay BC and Payne R (2004) Variants of TRP ion channel mRNA present in horseshoe crab ventral eye and brain. J. Neurochem. 91: 825-835.

7. Barlow HB and Levick WR (1969) Changes in the maintained discharge with adaptation level in the cat retina. J. Physiol 202: 699-718.

8. Baylor DA (1987) Photoreceptor signals and vision. Proctor lecture. Invest Ophthalmol. Vis. Sci. 28: 34-49.

9. Berson DM, Dunn FA, and Takao M (2002) Phototransduction by retinal ganglion cells that set the circadian clock. Science 295: 1070-1073.

10. Bertolucci C and Foa A (2004) Extraocular photoreception and circadian entrainment in nonmammalian vertebrates. Chronobiol. Int. 21: 501-519.

11. Boycott BB and Wassle H (1974) The morphological types of ganglion cells of the domestic cat's retina. J. Physiol 240: 397-419.

12. Card JP and Moore RY (1982) Ventral lateral geniculate nucleus efferents to the rat suprachiasmatic nucleus exhibit avian pancreatic polypeptide-like immunoreactivity. J. Comp Neurol. 206: 390-396.

13. Card JP and Moore RY (1989) Organization of lateral geniculate-hypothalamic connections in the rat. J. Comp Neurol. 284: 135-147.

14. Chang DC and Reppert SM (2003) A novel C-terminal domain of drosophila PERIOD inhibits dCLOCK:CYCLE-mediated transcription. Curr. Biol. 13: 758-762.

15. Chen D, Buchanan GF, Ding JM, Hannibal J, and Gillette MU (1999) Pituitary adenylyl cyclase-activating peptide: a pivotal modulator of glutamatergic regulation of the suprachiasmatic circadian clock. Proc. Natl. Acad. Sci. U. S. A 96: 13468-13473.

16. Cleland BG, Dubin MW, and Levick WR (1971) Sustained and transient neurones in the cat's retina and lateral geniculate nucleus. J. Physiol 217: 473-496.

17. Cleland BG and Levick WR (1974) Brisk and sluggish concentrically organized ganglion cells in the cat's retina. J. Physiol 240: 421-456.

18. Colwell CS, Foster RG, and Menaker M (1991) NMDA receptor antagonists block the effects of light on circadian behavior in the mouse. Brain Res. 554: 105-110.

19. Cyran SA, Buchsbaum AM, Reddy KL, Lin MC, Glossop NR, Hardin PE, Young MW, Storti RV, and Blau J (2003) vrille, Pdp1, and dClock form a second feedback loop in the Drosophila circadian clock. Cell 112: 329-341.

20. Czeisler CA, Shanahan TL, Klerman EB, Martens H, Brotman DJ, Emens JS, Klein T, and Rizzo JF, III (1995) Suppression of melatonin secretion in some blind patients by exposure to bright light. N. Engl. J. Med. 332: 6-11.

21. Ding JM, Chen D, Weber ET, Faiman LE, Rea MA, and Gillette MU (1994) Resetting the biological clock: mediation of nocturnal circadian shifts by glutamate and NO. Science 266: 1713-1717.

22. Drucker-Colin R, Aguilar-Roblero R, Garcia-Hernandez F, Fernandez-Cancino F, and Bermudez RF (1984) Fetal suprachiasmatic nucleus transplants: diurnal rhythm recovery of lesioned rats. Brain Res. 311: 353-357.

23. Dunlap JC (1999) Molecular bases for circadian clocks. Cell 96: 271-290.

24. Dunn FA and Berson DM (2002) Are Intrinisically Photosensitive Retinal Ganglion Cells Influenced by Rods and Cones? [abstract]. 2002 Annual Meeting Abstract and Program Planner accessed at www. arvo. org. Association for Research in Vision and Ophthamology. Abstract 2982:

25. Dziema H and Obrietan K (2002) PACAP potentiates L-type calcium channel conductance in suprachiasmatic nucleus neurons by activating the MAPK pathway. J. Neurophysiol. 88: 1374-1386.

26. Edery I, Zwiebel LJ, Dembinska ME, and Rosbash M (1994) Temporal phosphorylation of the Drosophila period protein. Proc. Natl. Acad. Sci. U. S. A 91: 2260-2264.

27. Estacion M, Li S, Sinkins WG, Gosling M, Bahra P, Poll C, Westwick J, and Schilling WP (2004) Activation of human TRPC6 channels by receptor stimulation. J. Biol. Chem. 279: 22047-22056.

28. Fesenko EE, Kolesnikov SS, and Lyubarsky AL (1985) Induction by cyclic GMP of cationic conductance in plasma membrane of retinal rod outer segment. Nature 313: 310-313.

29. Foster RG, Provencio I, Hudson D, Fiske S, De Grip W, and Menaker M (1991) Circadian photoreception in the retinally degenerate mouse (rd/rd). J. Comp Physiol [A] 169: 39-50.

30. Freedman MS, Lucas RJ, Soni B, von Schantz M, Munoz M, David-Gray Z, and Foster R (1999) Regulation of mammalian circadian behavior by non-rod, non-cone, ocular photoreceptors. Science 284: 502-504.

31. Freichel M, Suh SH, Pfeifer A, Schweig U, Trost C, Weissgerber P, Biel M, Philipp S, Freise D, Droogmans G, Hofmann F, Flockerzi V, and Nilius B (2001) Lack of an endothelial store-operated Ca2+ current impairs agonist- dependent vasorelaxation in TRP4-/- mice. Nat. Cell Biol. 3: 121-127.

32. Fu Y, Zhong H, Wang MH, Luo DG, Liao HW, Maeda H, Hattar S, Frishman LJ, and Yau KW (2005) Intrinsically photosensitive retinal ganglion cells detect light with a vitamin A-based photopigment, melanopsin. Proc. Natl. Acad. Sci. U. S. A 102: 10339-10344.

33. Fukuda Y and Stone J (1974) Retinal distribution and central projections of Y-, X-, and W-cells of the cat's retina. J. Neurophysiol. 37: 749-772.

34. Gastel JA, Roseboom PH, Rinaldi PA, Weller JL, and Klein DC (1998) Melatonin production: proteasomal proteolysis in serotonin N-acetyltransferase regulation. Science 279: 1358-1360.

35. Gekakis N, Staknis D, Nguyen HB, Davis FC, Wilsbacher LD, King DP, Takahashi JS, and Weitz CJ (1998) Role of the CLOCK protein in the mammalian circadian mechanism. Science 280: 1564-1569.

36. Gooley JJ, Lu J, Chou TC, Scammell TE, and Saper CB (2001) Melanopsin in cells of origin of the retinohypothalamic tract. Nat. Neurosci. 4: 1165-

37. Gray P and Attwell D (1985) Kinetics of light-sensitive channels in vertebrate photoreceptors. Proc. R. Soc. Lond B Biol. Sci. 223: 379-388.

38. Green DJ and Gillette R (1982) Circadian rhythm of firing rate recorded from single cells in the rat suprachiasmatic brain slice. Brain Res. 245: 198-200.

39. Guldner FH (1983) Numbers of neurons and astroglial cells in the suprachiasmatic nucleus of male and female rats. Exp. Brain Res. 50: 373-376.

40. Halaszovich CR, Zitt C, Jungling E, and Luckhoff A (2000) Inhibition of TRP3 channels by lanthanides. Block from the cytosolic side of the plasma membrane. J. Biol. Chem. 275: 37423-37428.

41. Hannibal J, Ding JM, Chen D, Fahrenkrug J, Larsen PJ, Gillette MU, and Mikkelsen JD (1997) Pituitary adenylate cyclase-activating peptide (PACAP) in the retinohypothalamic tract: a potential daytime regulator of the biological clock. J. Neurosci. 17: 2637-2644.

42. Hannibal J, Hindersson P, Knudsen SM, Georg B, and Fahrenkrug J (2002a) The photopigment melanopsin is exclusively present in pituitary adenylate cyclase-activating polypeptide-containing retinal ganglion cells of the retinohypothalamic tract. J. Neurosci. 22: RC191-

43. Hannibal J, Hindersson P, Nevo E, and Fahrenkrug J (2002b) The circadian photopigment melanopsin is expressed in the blind subterranean mole rat, Spalax. Neuroreport 13: 1411-1414.

44. Hannibal J, Moller M, Ottersen OP, and Fahrenkrug J (2000) PACAP and glutamate are co-stored in the retinohypothalamic tract. J. Comp Neurol. 418: 147-155.

45. Hannun YA, Merrill AH, Jr., and Bell RM (1991) Use of sphingosine as inhibitor of protein kinase C. Methods Enzymol. 201: 316-328.

46. Hao H, Allen DL, and Hardin PE (1997) A circadian enhancer mediates PER-dependent mRNA cycling in Drosophila melanogaster. Mol. Cell Biol. 17: 3687-3693.

47. Hardie RC (2001) Phototransduction in Drosophila melanogaster. J. Exp. Biol. 204: 3403-3409.

48. Hardie RC and Minke B (1992) The trp gene is essential for a light-activated Ca2+ channel in Drosophila photoreceptors. Neuron 8: 643-651.

49. Hardin PE, Hall JC, and Rosbash M (1990) Feedback of the Drosophila period gene product on circadian cycling of its messenger RNA levels. Nature 343: 536-540.

50. Hardin PE, Hall JC, and Rosbash M (1992) Circadian oscillations in period gene mRNA levels are transcriptionally regulated. Proc. Natl. Acad. Sci. U. S. A 89: 11711-11715.

51. Hassock SR, Zhu MX, Trost C, Flockerzi V, and Authi KS (2002) Expression and role of TRPC proteins in human platelets: evidence that TRPC6 forms the store-independent calcium entry channel. Blood 100: 2801-2811.

52. Hattar S, Liao HW, Takao M, Berson DM, and Yau KW (2002) Melanopsin-containing retinal ganglion cells: architecture, projections, and intrinsic photosensitivity. Science 295: 1065-1070.

53. Hattar S, Lucas RJ, Mrosovsky N, Thompson S, Douglas RH, Hankins MW, Lem J, Biel M, Hofmann F, Foster RG, and Yau KW (2003) Melanopsin and rod-cone photoreceptive systems account for all major accessory visual functions in mice. Nature 424: 76-81.

54. Haynes LW (1992) Block of the cyclic GMP-gated channel of vertebrate rod and cone photoreceptors by l-cis-diltiazem. J. Gen. Physiol 100: 783-801.

55. Haynes LW (1995) Permeation and block by internal and external divalent cations of the catfish cone photoreceptor cGMP-gated channel. J. Gen. Physiol 106: 507-523.

56. Hickey TL and Spear PD (1976) Retinogeniculate projections in hooded and albino rats: an autoradiographic study. Exp. Brain Res. 24: 523-529.

57. Hofmann T, Obukhov AG, Schaefer M, Harteneck C, Gudermann T, and Schultz G (1999) Direct activation of human TRPC6 and TRPC3 channels by diacylglycerol. Nature 397: 259-263.

58. Hsu YT and Molday RS (1993) Modulation of the cGMP-gated channel of rod photoreceptor cells by calmodulin. Nature 361: 76-79.

59. Huang ZJ, Edery I, and Rosbash M (1993) PAS is a dimerization domain common to Drosophila period and several transcription factors. Nature 364: 259-262.

60. Ibuka N, Inouye SI, and Kawamura H (1977) Analysis of sleep-wakefulness rhythms in male rats after suprachiasmatic nucleus lesions and ocular enucleation. Brain Res. 122: 33-47.

61. Inoue R, Okada T, Onoue H, Hara Y, Shimizu S, Naitoh S, Ito Y, and Mori Y (2001) The transient receptor potential protein homologue TRP6 is the essential component of vascular alpha(1)-adrenoceptor-activated Ca(2+)- permeable cation channel. Circ. Res. 88: 325-332.

62. Inouye ST and Kawamura H (1979) Persistence of circadian rhythmicity in a mammalian hypothalamic "island" containing the suprachiasmatic nucleus. Proc. Natl. Acad. Sci. U. S. A 76: 5962-5966.

63. Isoldi MC, Rollag MD, Lauro Castrucci AM, and Provencio I (2005) Rhabdomeric phototransduction initiated by the vertebrate photopigment melanopsin. Proc. Natl. Acad. Sci. U. S. A 102: 1217-1221.

64. Johnson CH, Elliott J, Foster R, Honma K, and Kronauer R (2004) The Fundamental Properties of Circadian Rhythms. 67-105.

65. Johnson CH, Elliott JA, and Foster R (2003) Entrainment of circadian programs. Chronobiol. Int. 20: 741-774.

66. Johnson RF, Moore RY, and Morin LP (1988) Loss of entrainment and anatomical plasticity after lesions of the hamster retinohypothalamic tract. Brain Res. 460: 297-313.

67. Jung S, Muhle A, Schaefer M, Strotmann R, Schultz G, and Plant TD (2003) Lanthanides potentiate TRPC5 currents by an action at extracellular sites close to the pore mouth. J. Biol. Chem. 278: 3562-3571.

68. Jung S, Strotmann R, Schultz G, and Plant TD (2002) TRPC6 is a candidate channel involved in receptor-stimulated cation currents in A7r5 smooth muscle cells. Am. J. Physiol Cell Physiol 282: C347-C359.

69. Kalsbeek A, Buijs RM, Engelmann M, Wotjak CT, and Landgraf R (1995) In vivo measurement of a diurnal variation in vasopressin release in the rat suprachiasmatic nucleus. Brain Res. 682: 75-82.

70. Kalsbeek A, van d, V, and Buijs RM (1996) Decrease of endogenous vasopressin release necessary for expression of the circadian rise in plasma corticosterone: a reverse microdialysis study. J. Neuroendocrinol. 8: 299-307.

71. Kaupp UB and Seifert R (2002) Cyclic nucleotide-gated ion channels. Physiol Rev. 82: 769-824.

72. Kleene SJ (1995) Block by external calcium and magnesium of the cyclic-nucleotide-activated current in olfactory cilia. Neuroscience 66: 1001-1008.

73. Konopka RJ and Benzer S (1971) Clock mutants of Drosophila melanogaster. Proc. Natl. Acad. Sci. U. S. A 68: 2112-2116.

74. Kornhauser JM, Nelson DE, Mayo KE, and Takahashi JS (1990) Photic and circadian regulation of c-fos gene expression in the hamster suprachiasmatic nucleus. Neuron 5: 127-134.

75. Kwan HY, Huang Y, and Yao X (2004) Regulation of canonical transient receptor potential isoform 3 (TRPC3) channel by protein kinase G. Proc. Natl. Acad. Sci. U. S. A

76. Lee C, Etchegaray JP, Cagampang FR, Loudon AS, and Reppert SM (2001) Posttranslational mechanisms regulate the mammalian circadian clock. Cell 107: 855-867.

77. Lowrey PL, Shimomura K, Antoch MP, Yamazaki S, Zemenides PD, Ralph MR, Menaker M, and Takahashi JS (2000) Positional syntenic cloning and functional characterization of the mammalian circadian mutation tau. Science 288: 483-492.

78. Lucas RJ, Hattar S, Takao M, Berson DM, Foster RG, and Yau KW (2003) Diminished pupillary light reflex at high irradiances in melanopsin- knockout mice. Science 299: 245-247.

79. Masubuchi S, Kataoka N, Sassone-Corsi P, and Okamura H (2005) Mouse Period1 (mPER1) acts as a circadian adaptor to entrain the oscillator to environmental light/dark cycles by regulating mPER2 protein. J. Neurosci. 25: 4719-4724.

80. McArthur AJ, Gillette MU, and Prosser RA (1991) Melatonin directly resets the rat suprachiasmatic circadian clock in vitro. Brain Res. 565: 158-161.

81. McNaughton PA (1990) Light response of vertebrate photoreceptors. Physiol Rev. 70: 847-883.

82. Medanic M and Gillette MU (1992) Serotonin regulates the phase of the rat suprachiasmatic circadian pacemaker in vitro only during the subjective day. J. Physiol 450: 629-642.

83. Melyan Z, Tarttelin EE, Bellingham J, Lucas RJ, and Hankins MW (2005) Addition of human melanopsin renders mammalian cells photoresponsive. Nature 433: 741-745.

84. Minke B and Cook B (2002) TRP channel proteins and signal transduction. Physiol Rev. 82: 429-472.

85. Montell C (2003) The venerable inveterate invertebrate TRP channels. Cell Calcium 33: 409-417.

86. Montell C and Rubin GM (1989) Molecular characterization of the Drosophila trp locus: a putative integral membrane protein required for phototransduction. Neuron 2: 1313-1323.

87. Moore RY (1983) Organization and function of a central nervous system circadian oscillator: the suprachiasmatic hypothalamic nucleus. Fed. Proc. 42: 2783-2789.

88. Moore RY and Eichler VB (1972) Loss of a circadian adrenal corticosterone rhythm following suprachiasmatic lesions in the rat. Brain Res. 42: 201-206.

89. Moore RY and Lenn NJ (1972a) A retinohypothalamic projection in the rat. J. Comp. Neurol. 146: 1-14.

90. Moore RY and Lenn NJ (1972b) A retinohypothalamic projection in the rat. J. Comp Neurol. 146: 1-14.

91. Moore RY, Speh JC, and Card JP (1995b) The retinohypothalamic tract originates from a distinct subset of retinal ganglion cells. J. Comp. Neurol. 352: 351-366.

92. Moore RY, Speh JC, and Card JP (1995a) The retinohypothalamic tract originates from a distinct subset of retinal ganglion cells. J. Comp Neurol. 352: 351-366.

93. Nawathean P and Rosbash M (2004) The doubletime and CKII kinases collaborate to potentiate Drosophila PER transcriptional repressor activity. Mol. Cell 13: 213-223.

94. Nelson DE and Takahashi JS (1991) Sensitivity and integration in a visual pathway for circadian entrainment in the hamster (Mesocricetus auratus). J. Physiol 439: 115-145.

95. Newman LA, Walker MT, Brown RL, Cronin TW, and Robinson PR (2003) Melanopsin forms a functional short-wavelength photopigment. Biochemistry 42: 12734-12738.

96. Nicol GD (1993) The calcium channel antagonist, pimozide, blocks the cyclic GMP- activated current in rod photoreceptors. J. Pharmacol. Exp. Ther. 265: 626-632.

97. Nicol GD, Schnetkamp PP, Saimi Y, Cragoe EJ, Jr., and Bownds MD (1987) A derivative of amiloride blocks both the light-regulated and cyclic GMP-regulated conductances in rod photoreceptors. J. Gen. Physiol 90: 651-669.

98. Okada T, Inoue R, Yamazaki K, Maeda A, Kurosaki T, Yamakuni T, Tanaka I, Shimizu S, Ikenaka K, Imoto K, and Mori Y (1999) Molecular and functional characterization of a novel mouse transient receptor potential protein homologue TRP7. Ca(2+)-permeable cation channel that is constitutively activated and enhanced by stimulation of G protein-coupled receptor. J. Biol. Chem. 274: 27359-27370.

99. Oshima N (2001) Direct reception of light by chromatophores of lower vertebrates. Pigment Cell Res. 14: 312-319.

100. Panda S, Nayak SK, Campo B, Walker JR, Hogenesch JB, and Jegla T (2005) Illumination of the melanopsin signaling pathway. Science 307: 600-604.

101. Panda S, Provencio I, Tu DC, Pires SS, Rollag MD, Castrucci AM, Pletcher MT, Sato TK, Wiltshire T, Andahazy M, Kay SA, Van Gelder RN, and Hogenesch JB

(2003) Melanopsin Is Required for Non-Image-Forming Photic Responses in Blind Mice. Science

102. Panda S, Sato TK, Castrucci AM, Rollag MD, DeGrip WJ, Hogenesch JB, Provencio I, and Kay SA (2002) Melanopsin (Opn4) requirement for normal light-induced circadian phase shifting. Science 298: 2213-2216.

103. Pasqualetti M, Bertolucci C, Ori M, Innocenti A, Magnone MC, De Grip WJ, Nardi I, and Foa A (2003) Identification of circadian brain photoreceptors mediating photic entrainment of behavioural rhythms in lizards. Eur. J. Neurosci. 18: 364-372.

104. Pennartz CM, de Jeu MT, Bos NP, Schaap J, and Geurtsen AM (2002) Diurnal modulation of pacemaker potentials and calcium current in the mammalian circadian clock. Nature 416: 286-290.

105. Perry VH (1979) The ganglion cell layer of the retina of the rat: a Golgi study. Proc. R. Soc. Lond B Biol. Sci. 204: 363-375.

106. Pickard GE (1980) Morphological characteristics of retinal ganglion cells projecting to the suprachiasmatic nucleus: a horseradish peroxidase study. Brain Res. 183: 458-465.

107. Pickard GE (1982) The afferent connections of the suprachiasmatic nucleus of the golden hamster with emphasis on the retinohypothalamic projection. J. Comp Neurol. 211: 65-83.

108. Preitner N, Damiola F, Lopez-Molina L, Zakany J, Duboule D, Albrecht U, and Schibler U (2002) The orphan nuclear receptor REV-ERBalpha controls circadian transcription within the positive limb of the mammalian circadian oscillator. Cell 110: 251-260.

109. Provencio I, Berson DM, Richardson RC, Rollag MD, and Castrucci AM (2002a) Melanopsin Immunoreactivity in Retinal Ganglion Cells [abstract]. 2002 Annual Meeting Abstract and Program Planner accessed at www. arvo. org. Association for Research in Vision and Ophthamology. Abstract 1363:

110. Provencio I and Foster RG (1995) Circadian rhythms in mice can be regulated by photoreceptors with cone- like characteristics. Brain Res. 694: 183-190.

111. Provencio I, Jiang G, De Grip WJ, Hayes WP, and Rollag MD (1998) Melanopsin: An opsin in melanophores, brain, and eye. Proc. Natl. Acad. Sci. U. S. A 95: 340-345.

112. Provencio I, Rodriguez IR, Jiang G, Hayes WP, Moreira EF, and Rollag MD (2000) A novel human opsin in the inner retina. J. Neurosci. 20: 600-605.

113. Provencio I, Rollag MD, and Castrucci AM (2002b) Photoreceptive net in the mammalian retina. This mesh of cells may explain how some blind mice can still tell day from night. Nature 415: 493-

114. Provencio I, Wong S, Lederman AB, Argamaso SM, and Foster RG (1994) Visual and circadian responses to light in aged retinally degenerate mice. Vision Res. 34: 1799-1806.

115. Pu M (1999) Dendritic morphology of cat retinal ganglion cells projecting to suprachiasmatic nucleus. J. Comp Neurol. 414: 267-274.

116. Pu M (2000) Physiological response properties of cat retinal ganglion cells projecting to suprachiasmatic nucleus. J. Biol. Rhythms 15: 31-36.

117. Qiu X, Kumbalasiri T, Carlson SM, Wong KY, Krishna V, Provencio I, and Berson DM (2005) Induction of photosensitivity by heterologous expression of melanopsin. Nature 433: 745-749.

118. Ralph MR (1991) Suprachiasmatic Nucleaus Transplant Studies Using the Tau Mutation in Golden Hamsters. 341-348.

119. Ralph MR, Foster RG, Davis FC, and Menaker M (1990) Transplanted suprachiasmatic nucleus determines circadian period. Science 247: 975-978.

120. Refinetti R (1995) Effects of suprachiasmatic lesions on temperature regulation in the golden hamster. Brain Res. Bull. 36: 81-84.

121. Reppert SM and Weaver DR (2002) Coordination of circadian timing in mammals. Nature 418: 935-941.

122. Rusak B, Robertson HA, Wisden W, and Hunt SP (1990) Light pulses that shift rhythms induce gene expression in the suprachiasmatic nucleus. Science 248: 1237-1240.

123. Rutila JE, Suri V, Le M, So WV, Rosbash M, and Hall JC (1998) CYCLE is a second bHLH-PAS clock protein essential for circadian rhythmicity and transcription of Drosophila period and timeless. Cell 93: 805-814.

124. Sakamoto K, Liu C, and Tosini G (2004) Classical photoreceptors regulate melanopsin mRNA levels in the rat retina. J. Neurosci. 24: 9693-9697.

125. Saper CB, Lu J, Chou TC, and Gooley J (2005) The hypothalamic integrator for circadian rhythms. Trends Neurosci. 28: 152-157.

126. Sehgal A, Price JL, Man B, and Young MW (1994) Loss of circadian behavioral rhythms and per RNA oscillations in the Drosophila mutant timeless. Science 263: 1603-1606.

127. Sehgal A, Rothenfluh-Hilfiker A, Hunter-Ensor M, Chen Y, Myers MP, and Young MW (1995) Rhythmic expression of timeless: a basis for promoting circadian cycles in period gene autoregulation. Science 270: 808-810.

128. Shafer OT, Rosbash M, and Truman JW (2002) Sequential nuclear accumulation of the clock proteins period and timeless in the pacemaker neurons of Drosophila melanogaster. J. Neurosci. 22: 5946-5954.

129. Shi J, Mori E, Mori Y, Mori M, Li J, Ito Y, and Inoue R (2004) Multiple regulation by calcium of murine homologues of transient receptor potential proteins TRPC6 and TRPC7 expressed in HEK293 cells. J. Physiol 561: 415-432.

130. Shibata S and Moore RY (1993) Neuropeptide Y and optic chiasm stimulation affect suprachiasmatic nucleus circadian function in vitro. Brain Res. 615: 95-100.

131. Shibata S, Tominaga K, Hamada T, and Watanabe S (1992) Excitatory effect of N-methyl-D-aspartate and kainate receptor on the 2-deoxyglucose uptake in the rat suprachiasmatic nucleus in vitro. Neurosci. Lett. 139: 83-86.

132. Shigeyoshi Y, Taguchi K, Yamamoto S, Takekida S, Yan L, Tei H, Moriya T, Shibata S, Loros JJ, Dunlap JC, and Okamura H (1997) Light-induced resetting of a mammalian circadian clock is associated with rapid induction of the mPer1 transcript. Cell 91: 1043-1053.

133. Simonneaux V and Ribelayga C (2003) Generation of the melatonin endocrine message in mammals: a review of the complex regulation of melatonin synthesis by norepinephrine, peptides, and other pineal transmitters. Pharmacol. Rev. 55: 325-395.

134. Skaliora I, Scobey RP, and Chalupa LM (1993) Prenatal development of excitability in cat retinal ganglion cells: action potentials and sodium currents. J. Neurosci. 13: 313-323.

135. Sollars PJ, Smeraski CA, Kaufman JD, Ogilvie MD, Provencio I, and Pickard GE (2003) Melanopsin and non-melanopsin expressing retinal ganglion cells innervate the hypothalamic suprachiasmatic nucleus. Vis. Neurosci. 20: 601-610.

136. Stephan FK and Zucker I (1972) Circadian rhythms in drinking behavior and locomotor activity of rats are eliminated by hypothalamic lesions. Proc. Natl. Acad. Sci. U. S. A 69: 1583-1586.

137. Stone J and Fukuda Y (1974) Properties of cat retinal ganglion cells: a comparison of W-cells with X- and Y-cells. J. Neurophysiol. 37: 722-748.

138. Stone J and Hoffmann KP (1972) Very slow-conducting ganglion cells in the cat's retina: a major, new functional type? Brain Res. 43: 610-616.

139. Takahashi JS, DeCoursey PJ, Bauman L, and Menaker M (1984) Spectral sensitivity of a novel photoreceptive system mediating entrainment of mammalian circadian rhythms. Nature 308: 186-188.

140. Tang J, Lin Y, Zhang Z, Tikunova S, Birnbaumer L, and Zhu MX (2001) Identification of common binding sites for calmodulin and inositol 1,4,5-trisphosphate receptors on the carboxyl termini of trp channels. J. Biol. Chem. 276: 21303-21310.

141. Trebak M, Bird GS, McKay RR, and Putney JW, Jr. (2002) Comparison of human TRPC3 channels in receptor-activated and store-operated modes. Differential sensitivity to channel blockers suggests fundamental differences in channel composition. J. Biol. Chem. 277: 21617-21623.

142. Trebak M, Hempel N, Wedel BJ, Smyth JT, Bird GS, and Putney JW, Jr. (2005) Negative regulation of TRPC3 channels by protein kinase C-mediated phosphorylation of serine 712. Mol. Pharmacol. 67: 558-563.

143. Ueda HR, Chen W, Adachi A, Wakamatsu H, Hayashi S, Takasugi T, Nagano M, Nakahama K, Suzuki Y, Sugano S, Iino M, Shigeyoshi Y, and Hashimoto S (2002) A transcription factor response element for gene expression during circadian night. Nature 418: 534-539.

144. van den Pol AN (1980) The hypothalamic suprachiasmatic nucleus of rat: intrinsic anatomy. J. Comp Neurol. 191: 661-702.

145. Venkatachalam K, Zheng F, and Gill DL (2003) Regulation of canonical transient receptor potential (TRPC) channel function by diacylglycerol and protein kinase C. J. Biol. Chem. 278: 29031-29040.

146. Vindlacheruvu RR, Ebling FJ, Maywood ES, and Hastings MH (1992) Blockade of Glutamatergic Neurotransmission in the Suprachiasmatic Nucleus Prevents Cellular and Behavioural Responses of the Circadian System to Light. Eur. J. Neurosci. 4: 673-679.

147. Vitaterna MH, King DP, Chang AM, Kornhauser JM, Lowrey PL, McDonald JD, Dove WF, Pinto LH, Turek FW, and Takahashi JS (1994) Mutagenesis and mapping of a mouse gene, Clock, essential for circadian behavior. Science 264: 719-725.

148. Vosshall LB, Price JL, Sehgal A, Saez L, and Young MW (1994) Block in nuclear localization of period protein by a second clock mutation, timeless. Science 263: 1606-1609.

149. Wang GY, Ratto G, Bisti S, and Chalupa LM (1997) Functional development of intrinsic properties in ganglion cells of the mammalian retina. J. Neurophysiol. 78: 2895-2903.

150. Warren EJ, Allen CN, Brown RL, and Robinson DW (2003) Intrinsic light responses of retinal ganglion cells projecting to the circadian system. Eur. J. Neurosci. 17: 1727-1735.

151. Wei JY, Roy DS, Leconte L, and Barnstable CJ (1998) Molecular and pharmacological analysis of cyclic nucleotide-gated channel function in the central nervous system. Prog. Neurobiol. 56: 37-64.

152. Wilson MM, Rice RW, and Critchlow V (1976) Evidence for a free-running circadian rhythm in pituitary-adrenal function in blinded adult female rats. Neuroendocrinology 20: 289-295.

153. Woodfill CJ, Wayne NL, Moenter SM, and Karsch FJ (1994) Photoperiodic synchronization of a circannual reproductive rhythm in sheep: identification of season-specific time cues. Biol. Reprod. 50: 965-976.

154. Yamazaki S, Numano R, Abe M, Hida A, Takahashi R, Ueda M, Block GD, Sakaki Y, Menaker M, and Tei H (2000) Resetting central and peripheral circadian oscillators in transgenic rats. Science 288: 682-685.

155. Yoshimura T and Ebihara S (1996) Spectral sensitivity of photoreceptors mediating phase-shifts of circadian rhythms in retinally degenerate CBA/J (rd/rd) and normal CBA/N (+/+)mice. J. Comp Physiol [A] 178: 797-802.

156. Zerr DM, Hall JC, Rosbash M, and Siwicki KK (1990) Circadian fluctuations of period protein immunoreactivity in the CNS and the visual system of Drosophila. J. Neurosci. 10: 2749-2762.

157. Zhu X, Jiang M, and Birnbaumer L (1998) Receptor-activated Ca2+ influx via human Trp3 stably expressed in human embryonic kidney (HEK)293 cells. Evidence for a non-capacitative Ca2+ entry. J. Biol. Chem. 273: 133-142.

158. Zimmerman AL and Baylor DA (1992) Cation interactions within the cyclic GMP-activated channel of retinal rods from the tiger salamander. J. Physiol 449: 759-783.

159. Zordan MA, Rosato E, Piccin A, and Foster R (2001) Photic entrainment of the circadian clock: from Drosophila to mammals. Semin. Cell Dev. Biol. 12: 317-328.

160. Zufall F and Firestein S (1993) Divalent cations block the cyclic nucleotide-gated channel of olfactory receptor neurons. J. Neurophysiol. 69: 1758-1768.